Materially Efficient Structural Floor Systems for Housing in India

By

Mohamed A. Ismail

B.S.E. Civil Engineering
Duke University, 2009

M.Arch Architecture
University of Virginia, 2016

Submitted to the
Department of Architecture
in partial fulfillment of the requirements for the degree of

MASTER OF SCIENCE IN ARCHITECTURE STUDIES
AT THE
MASSACHUSETTS INSTITUTE OF TECHNOLOGY
JUNE 2019

Signature of Author .....
Department of Architecture
May 23, 2019

Certified by .....
Caitlin Mueller
Associate Professor of Architecture and Civil and Environmental Engineering
Thesis Supervisor

Accepted by .....
Nasser Rabbat
Aga Khan Professor
Chair of the Department Committee on Graduate Students

THESIS COMMITTEE

Caitlin T. Mueller, PhD
Ford International Career Development Professor
Associate Professor of Architecture
Associate Professor of Civil and Environmental Engineering
Thesis Supervisor

Leslie Keith Norford, PhD
George Macomber Professor in Construction Management
Professor of Building Technology
Associate Head, Department of Architecture
Thesis Reader

Materially Efficient Structural Floor Systems for Housing in India

By

Mohamed A. Ismail

Submitted to the Department of Architecture

on May 23, 2019 in partial fulfillment of the requirements for the degree of

Master of Science in Architecture Studies

ABSTRACT

In 2015, the government of India launched the "Housing for All by 2022" initiative to build 20 million units of affordable urban housing for lower income groups. Thus far, they have built fewer than two million units. In India, it is estimated that material costs can constitute 60 to 80% of the total cost of residential construction. Nonetheless, their construction mimics the materially inefficient practices of developed countries, practices developed to reduce labor over material costs. As a result, prismatic beams and flat slabs are frequently used despite their structural inefficiency. In its current state, the construction industry is resource intensive and unsustainable.

The mounting use of steel-reinforced concrete structures in Indian cities has also garnered concern for the environmental costs of construction; construction accounts for 22% of India's carbon emissions. The impact of structural systems on a building's embodied energy are immediately apparent: cement and steel are responsible for nearly 90% of a multistory concrete frame building's total embodied energy, and at least 50% of that is in the horizontally-spanning elements alone. With no end to construction in sight, new practices are needed to curb the environmental and economic costs of India's construction.

This thesis explores the design of materially efficient floor systems that can reduce the economic and environmental costs of construction. Utilizing computational structural design, this thesis presents several strategies for the structural optimization of one-way concrete floor systems. Designed for the constraints of India, the structural elements are optimized to reduce the necessary volume of concrete and steel while resisting the same loads of an equivalent solid prismatic beam or slab. While structural optimization for material efficiency is not a new practice, it is technically challenging and often reserved for large-scale and exclusive architectural projects. Conversely, this research applies these principles to common residential construction.

Thesis Supervisor: Caitlin Mueller

Title: Associate Professor of Architecture and Civil and Environmental Engineering

ACKNOWLEDGEMENTS

This thesis is the culmination of two years of research at MIT, exploring India's construction practices–both historic and present–to inform the practices of the future. It would not have been possible without the guidance and support of many people. First, I am exceedingly grateful to my thesis and academic advisor, Professor Caitlin Mueller, who has been a constant source of wisdom and inspiration. Professor Mueller not only guided me throughout my time at MIT, she also gave me the freedom to develop along my own path and explore what I found interesting and noteworthy along the way. I thank Professor Mueller for her open-mindedness, honesty, understanding, trust, and enthusiasm at every stage of my time here.

Beginning with my first semester in the Building Technology seminar, I have learned how rare and invaluable the Building Technology family is. The questions, comments, and feedback from Professors Leon Glicksman, Christoph Reinhart, Josephine Carstensen, and Les Norford redefined how I understood and communicated my work, reframing it within a larger discourse on performance-oriented design and technology. Professor Oral Buyukozturk was crucial in my understanding of concrete mechanics and its applicability to structural optimization. My classmates and colleagues have been an unceasing source of motivation, never shy of offering their own time and expertise whenever I was in need. I am grateful for the assistance of undergraduate researchers Eric Wong and Claire Holley. It is also clear to me that I would not have accomplished much of this research without the help of my engineering colleagues and friends, Jackson Jewett and Abigail Anderson. I would like to thank the members of the MIT Digital Structures group for enthusiastically sharing their skills and expertise and encouraging me to expand my own horizons.

I must thank the faculty and staff of the MIT School of Architecture and Planning for their enduring patience and support. The members of CRON were always accessible and quick to respond to any of my computing needs. Jen O'Brien and Chris Dewart provided support in and out of the architecture shops, sharing their experience and giving me numerous opportunities to explore new modes of designing and making. I have had the steadfast support of an exceptional staff that includes the enthusiastic Kathleen Ross, Erin Buckley, Alan Reyes, and Denita Washington of the Building Technology group, and Cynthia Stewart, who kept us all on track and moving forward.

I am enormously grateful to the MIT Tata Center for their generous financial support and guidance. This thesis would not have happened without the belief and sage input of Dr. Angeliki Diane Rigos, Dr. Robert Stoner, Dr. Jason Prapas, and Dr. Chintan Vaishnav.

Through the help of the Tata Center and the Tata Trusts, I had the opportunity to travel to India and meet with an assortment of designers, researchers, and stakeholders in India's affordable housing sector. It was through these trips that I met our local partner, Technology and Action for Rural Advancement (TARA), and their excellent team led by Dr. Soumen Maity, Shrashtant Patara, and Biswajit Swain. I am indebted to all of the people that took the time to meet with me during my travels including Harsh Vardhan Jain of HVJ Architects, Siva Kandasami of Larsen and Toubro, Lara Davis of the Auroville Earth Institute, Professor BV Venkatarama Reddy of the India Institute of Science, R. Sundaram of Sundaram Architects, Alpa Sheth of VMS Consultants, and Anupama Kundoo of Anupama Kundoo Architect.

Finally, and perhaps most importantly, I would like to thank my friends and family beyond the MIT community. They have provided an endless stream of encouragement and reminders that I am worthy of my opportunities here. Without my family's patience, support, and understanding, I would not be at MIT doing work I find both fulfilling and meaningful. Furthermore, I am blessed with an extension to my family within walking distance of where I live and work, giving me reprieve and relief when I need it most. Due to all of these people and their belief in my potential, I am thrilled to continue my work as a doctoral candidate in MIT's Building Technology Program under the tutelage of Professor Caitlin Mueller.

CONTENTS

LIST OF FIGURES

LIST OF TABLES

NOTATION

a $=$ depth of Whitney stress block, mm

a_{vx} $=$ shear span, mm

A_c $=$ compression area of concrete, mm^2

A_s $=$ area of longitudinal steel, mm^2

A_v $=$ area of transverse steel, mm^2

b $=$ overall width of section, mm

b_w $=$ minimum width of section, mm

c_{max} $=$ max. depth of neutral axis, mm

d $=$ effective depth of section, mm

D_L $=$ dead load, $\frac{N}{m^2}$

Δ_{max} $=$ maximum deflection, mm

EE $=$ total embodied energy, MJ

EEC $=$ embodied energy coefficient, $\frac{MJ}{kg}$

E_s $=$ young'smodulus of steel, $\frac{N}{mm^2}$

ϵ_u $=$ ultimate strain of concrete, $\frac{mm}{mm}$

$\epsilon_{t,min}$ $=$ min. strain of steel, $\frac{mm}{mm}$

f $=$ flexural stress, $\frac{N}{mm^2}$

f_c' $=$ unixial strength of concrete, MPa

f_y $=$ yield stess of steel, MPa

γ $=$ material density, $\frac{kg}{m^3}$

h $=$ overall height of section, mm

I_x $=$ moment of inertia about x axis, mm^4

L_L $=$ live load, $\frac{N}{m^2}$

M_n $=$ design moment capacity, Nmm

M_u $=$ factored applied moment, Nmm

N_c $=$ concrete compressive force, N

N_T $=$ steel tensile force, N

$P(\boldsymbol{x})$ $=$ penalty, function of $\boldsymbol{x}$

ϕ $=$ strength reduction factor

Q $=$ $first$ moment of area, mm^3

ρ $=$ reinforcement ratio $= \frac{A_s}{b_w d}$

ρ_{min} $=$ min. reinforcement ratio

ρ_{max} $=$ max. reinforcement ratio

ρ_n $=$ design reinforcement ratio

s $=$ spacing of transverse steel, mm

τ $=$ shear stress, $\frac{N}{mm^2}$

τ_c $=$ shear strength of concrete, $\frac{N}{mm^2}$

θ $=$ angle of inclination, rad

V_c $=$ shear capacity of concrete section, N

V_s $=$ shear capacity of transverse steel, N

V_n $=$ design shear capacity, N

V_u $=$ factored applied shear force, N

$Vol(\boldsymbol{x})$ $=$ volume, function of $\boldsymbol{x}$

W_{IN} $=$ internal strain energy, Nm

w_u $=$ factored applied load, $\frac{N}{m^2}$

$\boldsymbol{x}$ $=$ design vector

y $=$ distance from neutral axis, mm

z $=$ internal moment arm, mm

CHAPTER 1 INTRODUCTION

1.1. Motivation

In India, steel-reinforced concrete frames dominate the skylines of rapidly growing cities. In Less Economically Developed Countries (LEDCs), such as India, material costs can constitute the bulk of the total cost of building construction [1]. Nonetheless, construction in these regions mimics the materially inefficient practices of More Economically Developed Countries (MEDCs), developed to reduce labor over material costs (Figure 1). As a result, prismatic beams and flat slabs are commonly used despite their structural inefficiency.

Figure 1 Informal survey of common construction practices in Indian cities

This thesis explores the design of an alternative structural system to the prismatic beams and slabs of Indian concrete construction. This research has three key motivations: the increasing demand for urban housing, the economic cost of residential buildings, and the environmental costs of concrete construction in India. The following sections will discuss these motivations in further detail.

1.1.1. Demand for Housing

In 2017, India had an urban population growth rate of 2.4 percent, which will result in an urban population of 590 million by the year 2030 [2]. As a result, the country needs to build 700 to 900 million square meters of urban space—the equivalent of a new Chicago—every year. This demand for construction makes India one of the largest building markets in the world, growing at an annual rate of 6.4 percent, 30 percent of which is due to affordable housing construction [3].

"Housing for all by 2022" – also known as Pradhan Mantri Awaas Yojana – was announced by Indian Prime Minister Modhi to abate the escalating national housing deficit. According to the Ministry of Rural Development and the Ministry of Housing and Urban Poverty Alleviation, nearly a quarter of Indian households lack adequate facilities [4]. To meet this need, it was established that 20 million urban housing units would be built by 2022. As of March, 2019, only 1.8 million homes have been built [5].

Many reasons for the lack of progress are cited: high gestation periods for construction projects in India, limited capital, high taxation and fees, rising land and construction fees, and the low affordability by what is termed the Economically Weaker Sector (EWS) and Lower Income Group (LIG) households. It is estimated that 99 percent of the housing demand is attributed to the EWS and LIG sectors alone [6]. Steps have been suggested, and taken, to alleviate the political and economic obstructions to progress including a resolution to reclassify affordable housing construction as infrastructure, simplifying the government approval process for construction projects, and increasing financing options for EWS and LIG households – but more can be done. This thesis looks at the technology of construction itself, and asks what improvements can be made to a system mostly learned by rote and largely reliant upon rules-of-thumb.

1.1.2. Economic motivation

In More Economically Developed Countries (MEDCs), affordable construction is constrained by the cost of labor. Due to a prioritization of reduced labor costs, designers in MEDCs tend to rely on consistent profiles and nominal sizing for structural members (see Figure 2), decreasing structural complexity and time needed for assembly.

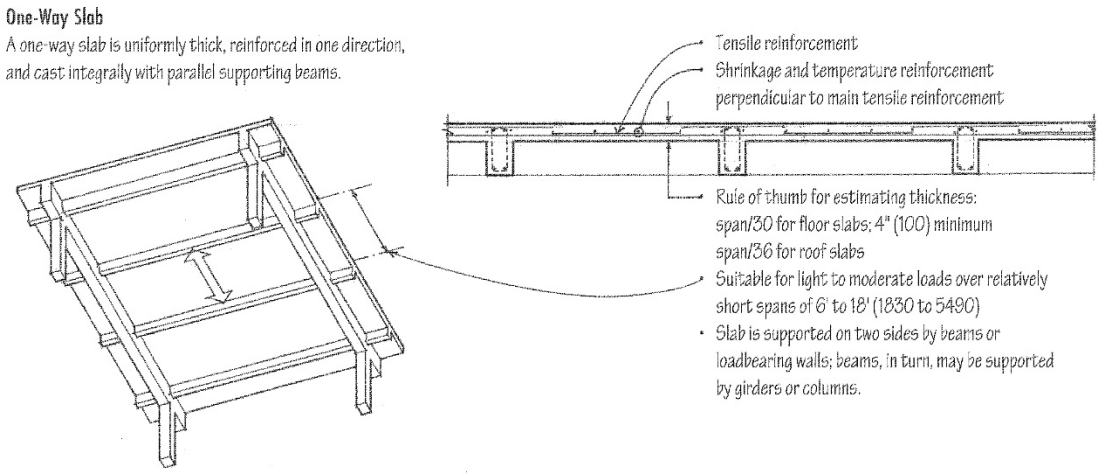

Figure 2 Typical one-way reinforced concrete slab system, courtesy of [7]

Conversely, in Less Economically Developed Countries (LEDCs) material costs, rather than labor, inhibit affordable construction (see Figure 3).

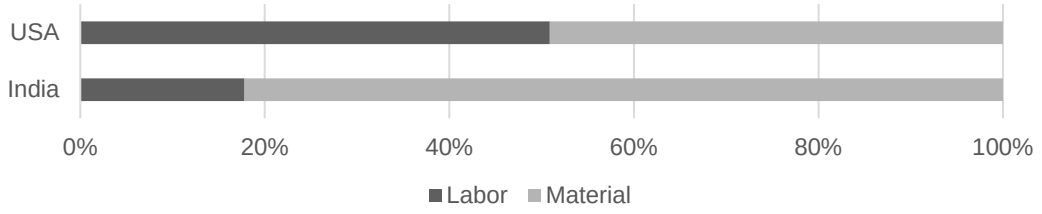

Figure 3 Comparative costs of material and labor for construction in the USA [8] and India [9]

Nonetheless, the construction practices of MEDCs are echoed in LEDCs despite a context that demands material savings over labor reduction. These standardized practices are inherently over-structured and inefficient in their material usage. This incongruity highlights an opportunity for structural components that are optimized for material efficiency and suit the context of a developing LEDC like India.

1.1.3. Environmental motivation

As the construction industry continues to expand, so too do the ecological costs of building. Governing bodies are constantly implementing policies and technologies to reduce the lifetime operational emissions of buildings, but they often neglect the embodied carbon of buildings. These are the emissions from material extraction, transportation, construction, and demolition [10]. With global efforts to reduce the lifetime operational energy of buildings through energy efficiency and passive design solutions, it is increasingly necessary to address the remaining embodied energy of buildings. The construction industry's

embodied emissions contribute up to 11 percent of global carbon emissions [11]. In India, the construction sector accounts for 22 percent of India's carbon emissions [12] and that figure is expected to rise.

While concrete and steel are often the materials of choice in LEDCs, they are habitually poorly utilized and energy-intensive in their production. The most basic components of concrete – cement and steel – are the result of industrial processes that require massive capital investment, skilled labor, and functional infrastructure. Today, the production of cement creates 5-8 percent of global carbon emissions, and that figure will only rise as concrete continues to be the most produced synthetic material in the world [13]. Reinforced concrete has an embodied energy of 1.0 MJ/Kg, while steel has about 42 MJ/Kg of embodied energy – in contrast to wood and solid masonry which average about 3.0 MJ/kg [12].

Additionally, there are ecological costs to concrete construction that go beyond carbon emissions. Concrete construction makes up nearly one-tenth of global industrial water use, 75 percent of which is in drought and water-stressed regions. The use of cement contributes to 10 percent of Delhi's airborne particulate matter due to wind-blown cement stocks and mixers, contributing to a number of respiratory illnesses and increasing the air pollution index near construction sites [14]. The intense demand for fine aggregate has caused irreparable damage to natural ecosystems and to the criminalization of sand mining worldwide. This, in turn, restricts the supply of sand to certain regions of the world or requires industrial-scale pulverization of materials like basalt as a substitute.

Consequently, the mounting use of concrete structures in India's cities has led to a developing concern for the environmental costs of construction. The impact of these materials on a building's embodied energy are immediately apparent: cement and steel are responsible for nearly 90 percent of a multistory concrete frame building's total embodied energy [15] and at least 50 percent is in the horizontally-spanning elements alone (see Figure 4 and Figure 5) [16]. In high-rise buildings, between 60-80 percent of the mass and embodied energy of the structure can be found in the floors [17], suggesting a strong opportunity for material efficient floor systems.

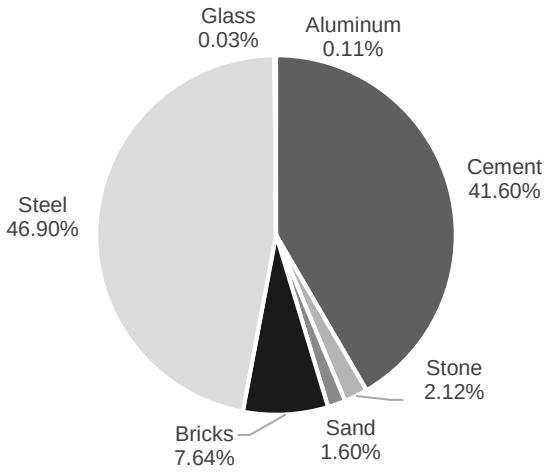

Figure 4 Embodied energy as a percent of the total of a multi-story Indian house [15]

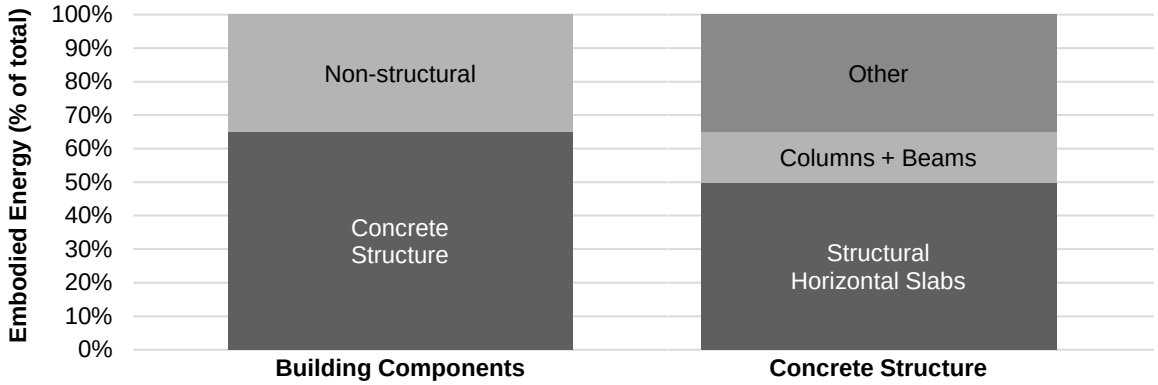

Figure 5 Embodied energy as a percent of the total of a multi-story concrete building [16]

1.2. Historic concrete in India

Material efficient concrete construction is not new to India. Historically, designers worked towards material efficiency by developing novel solutions never before seen in India. In his design for the India International Center in New Delhi (IIC, 1962), Joseph Allen Stein utilized ferrocement panels and modular blocks to reduce the amount of concrete in long-spanning roof and floor systems [18]. The IIC was designed in close coordination with in-house engineer and partner, Binoy Chatterjee, and local building contractors, Stein used a material palette of handmade tiles to support local craftspeople, local quartzite for cladding, and concrete for the structural frames, domes, vaults, “jali" screens, and floors. Precast elements were used in newly-introduced horizontal spanning systems like vaults and domes, reducing construction time and keeping the project within budget (Figure 6). Lightweight elements were designed to be carried by local builders.

Figure 6 The India International Center by J. A. Stein, New Delhi, 1962

The architect Laurie Baker pioneered techniques for low-cost housing design in India, constructing homes for one-fifth the cost of competing designers. His techniques included filler slabs (Figure 7) and vaulted systems that utilized clay brick and reduced the need for steel reinforcing [19].

Figure 7 Filler slab inspired by Laurie Baker, Indian Institute of Science, Bangalore

Post-independence, Indian architects and engineers like BV Doshi, Raj Rewal, Charles Correa, and Mahendra Raj introduced efficient and long-spanning concrete systems such as thin shells, folded-plates (see Figure 8), and space frames in developing a modern vernacular for the newly independent nation [20].

Figure 8 20m span folded-plate roof; Municipal Stadium, Charles Correa and Mahendra Raj, Ahmedabad, 1966

Nonetheless, once the cost of labor in MEDCs became the controlling factor in building construction the appetite for materially-efficient structures gave way to an interest in easily erected, modular systems. These same systems became the norm in LEDCs through industrial standardization and increasingly conservative design practices led by developers.

1.3. Emerging opportunities

Structural optimization is not new, but it is uncommon. Post-World War II, materials constrained construction costs while labor was plentiful and inexpensive. Consequently, architects and engineers developed innovative material efficient structures that elevated engineering to a form of art. As the cost of labor rose, however, interest in efficient structures gave way to standardized systems.

Today, new tools are emerging that allow practitioners to increasingly engage in performance-based design. Structural optimization is a process of efficiently configuring building materials based upon an understanding of structural mechanics and material behavior. Contemporary digital fabrication involves computer numerical controlled (CNC) devices such as routers and mills, laser cutters, fused-deposition modeling, powder printing, and more. Digital fabrication connects the complex result of structural optimization to the machinery that builds it, making traditionally difficult structures far more attainable.

A concern for the environmental costs of construction and a growing selection of digital tools have revived interest in structural efficiency by incorporating computational optimization into the design and fabrication process [21], [22]. Traditionally, structural optimization is reserved for large-scale and exclusive projects, neglecting the scalable potential of improving the standardized systems of construction. This thesis builds upon—and augments—historic practices of material efficient construction using digital fabrication and computational structural analysis.

1.4. Research question and scope

There is an opportunity for material efficient structural elements that can reduce the economic and environmental costs of construction. Utilizing computational structural design, this research explores the material optimization of concrete horizontal spanning components through a platform of design strategies. The scope will be limited to the design of one-way reinforced concrete slab designed for residential use under static loading conditions as defined by the Indian National Building Code. The ambition of this thesis is the development of a platform of strategies that range in complexity and efficiency depending on skill and fabrication constraints (Figure 9). Designed for the material constraints of India, floor elements are optimized and fabricated to reduce their volume of concrete and steel while resisting the required loads of an equivalent solid rectangular prismatic beam or slab.

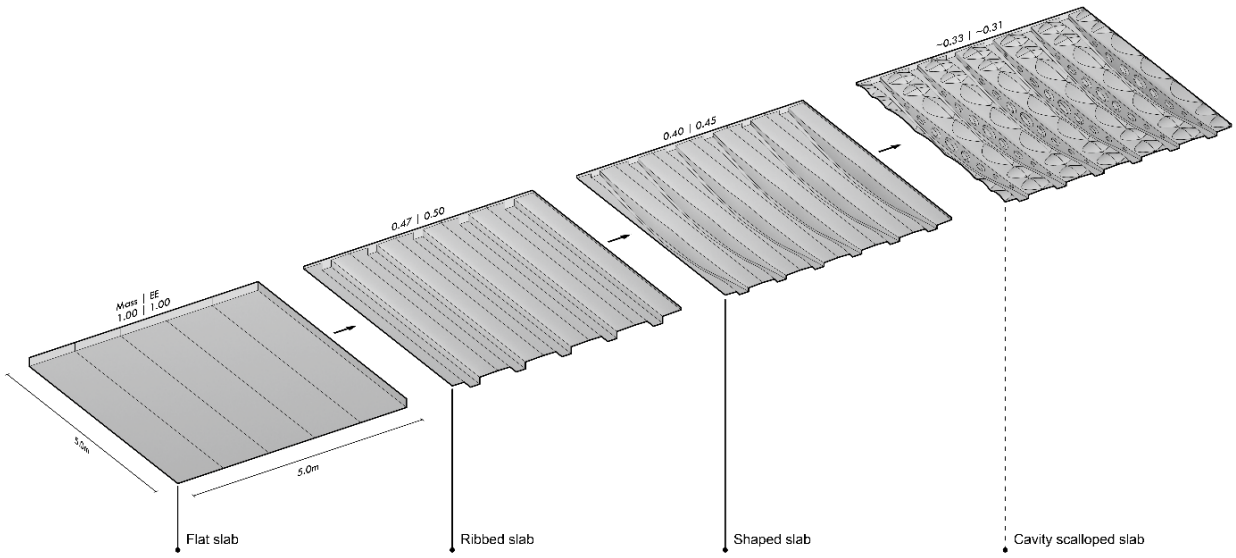

Figure 9 A platform of material efficient elements for residential construction in India

CHAPTER 2 STATE OF THE ART

2.1. Mechanics and shape optimization

Textbooks often credit Galileo Galilee's (1564-1642) study of a cantilever beam as the beginning of both elastic theory and beam theory. In his 1638 text, "Two New Sciences", Galileo's analytical attempt to understand the load carrying capacity of a cantilever beam soon led to his attempt at discovering the "solids of equal resistance" [23]. Galileo determines that a constant-width cantilevering beam loaded at its tip could change in depth and have an equal resistance to the load at all sections along its length. Galileo may have made the first known attempt at designing a uniform strength beam, also known as a shaped beam.

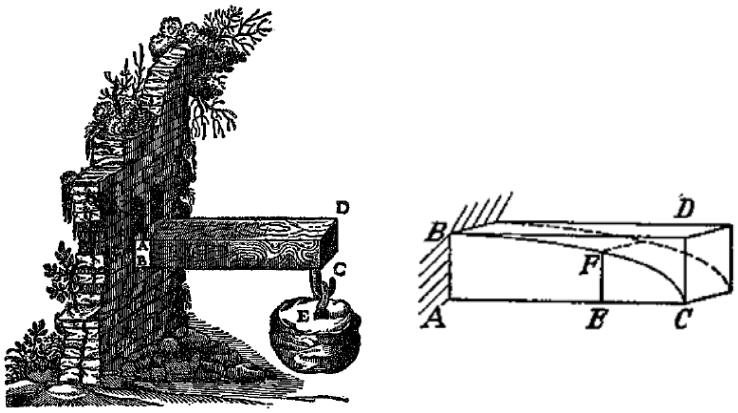

Figure 10 Galileo Galilea's design of a uniform strength beam, 1638 [23]

As shown in Figure 10 above, the result of Galileo's analytical method was the design of a cantilever beam with a parabolic reduction in depth along its length. His incorrect assumption of a constant stress distribution caused his derivation of a beam's strength to be off by a factor of three, but his attempt to design a uniform strength beam was ahead of its time. Galileo also correctly observed that a beam with a

hollow section could be relatively stronger than a beam of similar mass but solid in section, preempting the use of hollow-core extruded sections in modern construction.

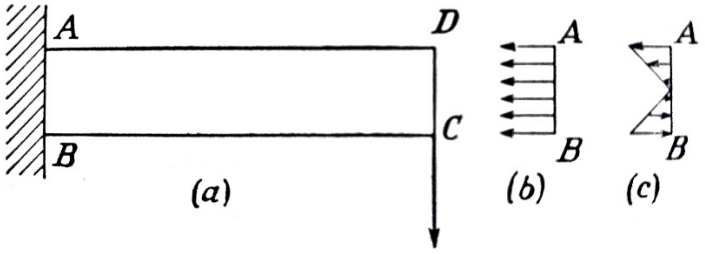

Figure 11 Stress distribution in a cantilever beam b) assumed by Galileo and c) correctly determined by Parent

Scientists continued to expand and correct Galileo's theorems over the following two centuries. Robert Hooke's (1635-1703) studies in elasticity and the linear relationship between stress and strain helped him determine that an elastic and homogenous beam undergoing flexural loading was in tension on one face and compression on the other. Antoine Parent (1666-1716) was the first to determine the appropriate stress distribution within the section of a homogenous rectangular beam as shown in Figure 11, correcting the work of his predecessors and leading to the well-known formula relating a beam's flexural strength to its sectional geometry. To this day, this formula informs how designers choose and analyze horizontal spanning elements according to flexural stresses:

$$f = \frac{M_u \mathrm{y}}{I_x} \tag{1}$$

For a long while it was assumed that shear strength was unimportant in the design of beams, that is, until Dmitrii Ivanovich Zhuravskii (1821-1891) found that it was vital to the design of deep or brittle beams. While designing bridges for the St. Petersburg to Moscow railway Zhuravskii derived the missing formula relating a beam's geometry to its shear stress in 1855. This formula is named in his honor and still in use today:

$$\tau = \frac{V_u Q}{I_x b_w} \tag{2}$$

Galileo's problem of shaped beam design reappears in early to mid- 20th century scientific literature. Early engineering handbooks describe the design of a statically-determinate shaped beam, neglecting its self-weight, as an elementary application of the flexural and shear strength formulas. Later literature explores increasingly complex methods for the design of shaped beams. In the seminal 1930 text, *Strength of Materials*, Timoshenko outlines a method for designing variable section beams. He suggests that a beam

be designed as a series of beams with different carrying capacities according to their strength requirements, leading to a segmented—rather than continuous—form [24].

In *The Art of Structures*, Muttoni discusses the relationship between a beam's geometry and its structural performance using similar methods to the early engineering handbooks [25]. Muttoni illustrates a series of uniform strength beams for a point load and compares various forms of shaped beams for a range of depth-to-span ratios. These illustrations demonstrate a number of ways that shaped beams could be designed with varying efficiencies and stiffnesses (Figure 12).

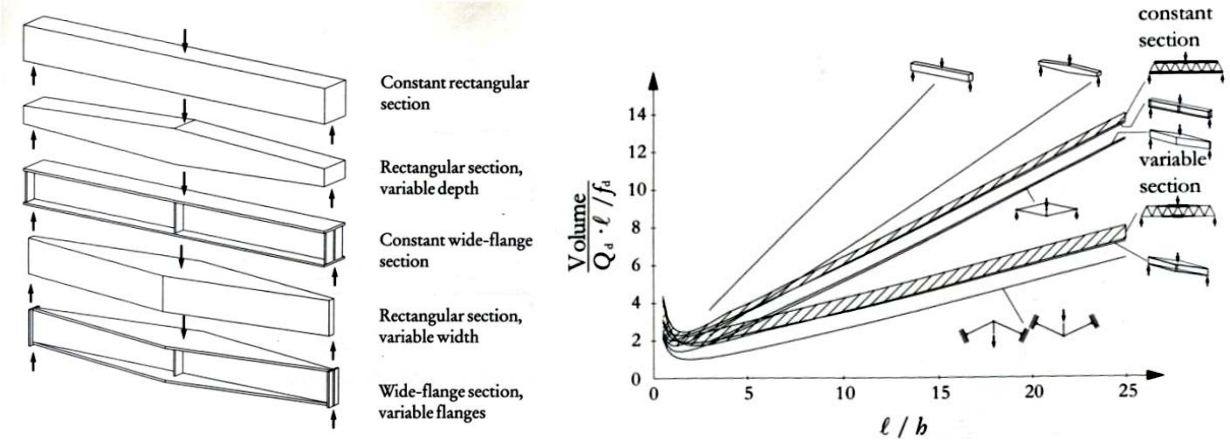

Figure 12 Shaped beams for a point load and volume of material needed for ranging slenderness ratios [25]

Later advances in computation allows designers to revisit the problem of shaped structures with improved precision and acuity. Opatowski [26] discusses the design of a cantilever beam of uniform strength undergoing a point load at its free end. Unlike previous literature, Opatowski includes the self-weight of the beam, requiring advanced integration. Li and Gross [27] discuss the design of uniform strength beams under a uniformly distributed load using Laplace transformations.

Around the 1960s, designers begin to apply the calculus of variation methods developed by Joseph-Louis Lagrange (1736-1813) to optimize the design of a beam subject to constraints. Barnett uses the calculus of variations to minimize the amount of steel needed in a statically-determinate steel I-beam [28]. Haftka, with reference to Barnett, outlines the procedure for designing a simply-supported beam subject to a deflection constraint [29]. Haug and Dupuis expand upon this method by including stress constraints [30].

Nearly all of these explorations looked at the shape optimization of idealized, elastic, and homogenous beams such as steel I-beams or tubes. As a multi-material system, these methods do not apply directly to

reinforced concrete beams. The following sections will discuss the attempts by designers to develop and construct efficient concrete structures.

2.2. Efficiency in concrete without optimization

Post-World War II, material constrained construction costs in many parts of the world while labor remained relatively abundant and inexpensive. These innovations included, among others, the thin concrete shells of Heinz Isler and Felix Candela, the monumental frames of Pier Luigi Nervi, and the long-spanning vaults of Eduardo Torroja. These designers relied upon an understanding of material, construction, and mechanics coupled with their intuition. For instance, Isler's thin concrete shells were designed using scaled models of hanging fabric, alluding to Robert Hooke's (1635-1703) observation: "As hangs the flexible line, so but inverted will stand the rigid arch." Many of the historic innovations in India's long-spanning concrete systems discussed earlier mirrored the materially efficient construction being done in Europe and the USA.

Nowadays, architects and researchers in India are continuing the legacy of these designers. Most of the ongoing research in India is focused on the material configuration of construction, using waste products or local resources as building materials, and prefabricated systems that are easily assembled yet reliant on imported materials and transportation costs [1]. The construction of Development Alternative's headquarters in New Delhi [31] (Figure 13) and a number of buildings in Auroville, Pondicherry, utilize similar techniques to those of Stein and Baker. Auroville-based architect, Anupama Kundoo, has designed a number of prefabricated housing prototypes to encourage the use of local materials and concrete composites for lightweight and low-energy construction [32] (Figure 14).

Figure 13 Filler slab; Development Alternatives Headquarters, Ashok B. Lall Architects, New Delhi, 2014

Figure 14 Ferrocement panels, vaulted roof, and filler slab in Wall house, Anupama Kundoo, Auroville, 2000

For decades, designers and researchers at the Auroville Earth Institute (AVEI) have contributed to the field of earth-based construction methods, researching old and new technologies and passing them on to communities worldwide (Figure 15). Their research has explored the use of ferrocement channels,

Figure 15 Experiments at AVEI in a) hybrid soil-concrete beams and b) ferrocement channels

compressed stabilized earth blocks (CSEBs), vaulted structures [33], hybrid concrete-CSEB beams, and much more [34]. Research at the Indian Institute of Science shows the potential for low-energy construction materials in rural regions, using local materials, traditional building techniques, and low-energy supplements for cement in construction. This work includes the design of hybrid structural elements such as steel truss and concrete beams and filler slabs.

2.3. Efficiency in concrete with digital fabrication and optimization

Today, researchers are once again exploring efficient horizontal spanning structures, but focus has shifted to the reduction of embodied energy rather than the cost of construction. Largely in academia, newly developed systems utilize digital-fabrication and prefabricated elements that require little to no human labor and relatively complex methods of production. These enable the fabrication of complex forms that are difficult to manage in traditional construction practices.

Methods for the use of adaptive and flexible molds have been developed for the fabrication of doubly-curved concrete shells at Graz University of Technology [35], ETH Zurich [36], and Delft University of Technology [37]. These use forms supported in tension or upon robotic armatures to fabricate thin shell structures that would be difficult or uneconomic to build with traditional means.

Figure 16 Mock-up of robotically fabricated doubly-curved concrete slab, Graz University of Technology

Figure 17 Prototype thin concrete shell fabricated using hybrid cable net and fabric formwork, ETH Zurich

Figure 18 Doubly-curved concrete panel fabricated using adaptive mold system, Delft University of Technology

Led by the C.A.S.T. group at the University of Manitoba, researchers are exploring the potential for structural optimization and lightweight construction through fabric formwork [38]. This research focuses on the ease of construction through lightweight formwork rather than cumbersome and wasteful plywood and metal forms. The availability of high-strength and durable fabrics has bolstered this research and enabled the construction of a variety of fabric-formed structures.

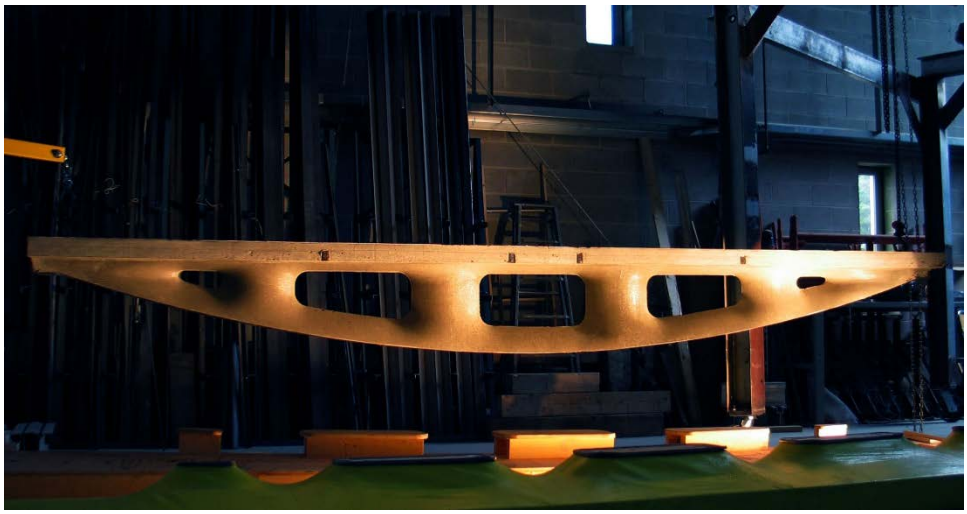

Figure 19 Concrete truss built using flexible fabric formwork, University of Manitoba

Research at the University of Cambridge and University of Bath is exploring the use of fabric formwork to enable lightweight and efficient concrete construction [39]. This research has been combined with computational structural optimization and form finding methods that simulate the hydrostatic conditions of poured concrete. This research has already yielded impressive results, including the construction of a school building in Cambodia by StructureMode [40].

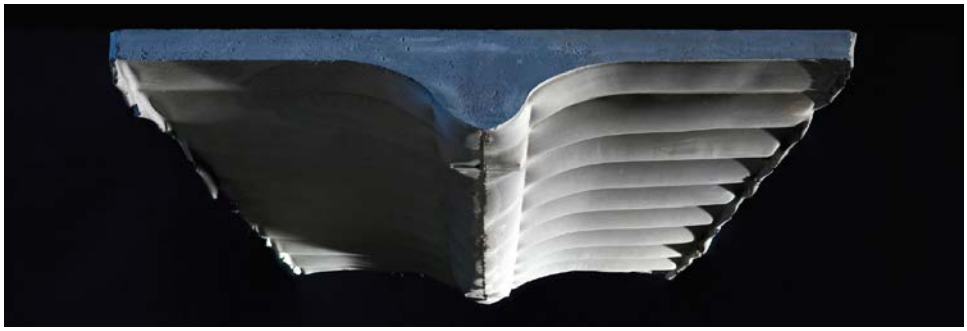

Figure 20 Ribbed slab built using fabric formwork and keel mold, University of Bath

Figure 21 Fabric formwork beams in use at a school in Bomnong L'Or, Cambodia

Researchers at the University of Cambridge are designing a light-weight vaulted floor system with steel ties in place of traditional reinforcement, focusing on formwork constructed from planar materials such as commercial plywood [41]. Similarly, the Block Research Group at ETH Zurich are developing a number of floor systems that are primarily compressive, reducing the need for steel reinforcement through the use of Thrust Network Analysis (TNA) [42]. This work has resulted in the design of a ribbed-slab with steel ties reminiscent of historic vaulting techniques paired with high-technology fabrication and high-strength materials such as Ultra-High Performance Concrete (UHPC) and glass fiber reinforcing.

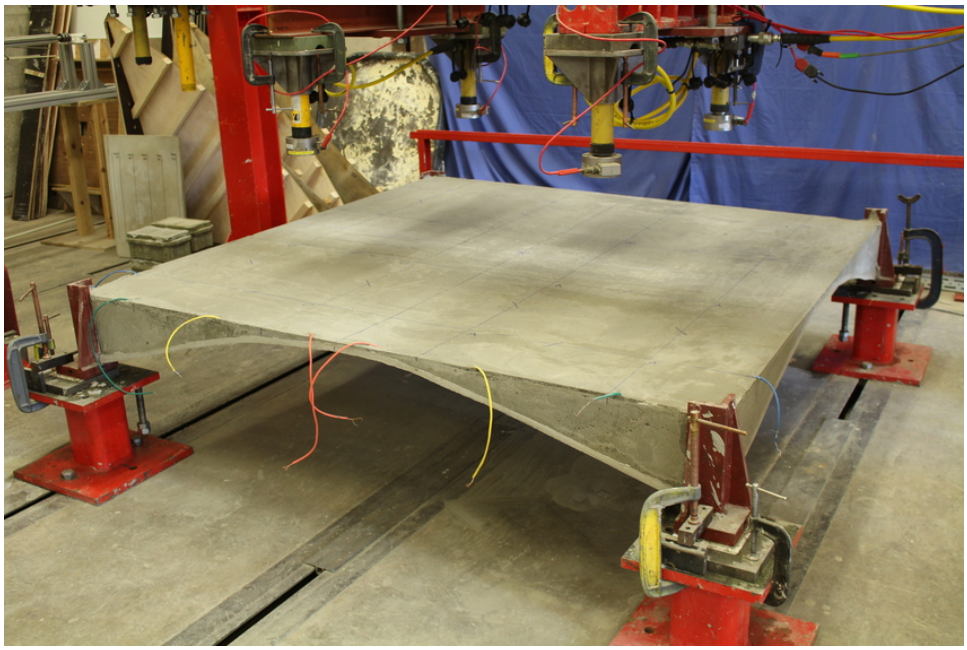

Figure 22 Prototype thin-shell textile-reinforced concrete floor system, University of Cambridge

Figure 23 Prototype ribbed UHPC floor slab, ETH Zurich

The Digital Building Technology group at ETH Zurich is using Topology Optimization—as opposed to shape optimization—to design post-tensioned fiber-reinforced floor slabs. This was most notably used in the Smart Slab project [43], fabricated using particle bed 3D printing for its complex formwork [44].

Figure 24 Topology optimized concrete slab built using particle-bed 3D printed formwork, ETH Zurich

There is increasing interest in additive fabrication methods like 3D printing [45] and dynamic casting [46] for efficient concrete elements. These may help overcome the difficulties of realizing complex forms derived from structural optimization methods like Topology Optimization.

Figure 25 Prototype 3D printed concrete slab, Loughborough University

Figure 26 Concrete pillar built using Smart Dynamic Casting/slip-forming, ETH Zurich

2.4. Research opportunity

Some of the solutions developed in India have the advantage of being designed and tested within their setting, yet they remained isolated case studies. Little study and poor understanding of their behavior leave their design to rules-of-thumb and additional factors of safety out of precaution. Alternatively, new academic precedents in floor system design rely on high-technology fabrication methods, complex procedures, and specialized materials largely unavailable to Indian builders, limiting their use to very few parts of the world.

New tools have bolstered the design of material efficient structures with increased precision and predictability. Yet existing optimization techniques typically neglect the complexity of reinforced concrete as a configuration of various materials – aggregate, steel, cement, water – resulting in excessive material use and uncertain results. This research connects an understanding of concrete mechanics to new methods of structural optimization and fabrication and proposes an application of those same principles to the residential construction of India's growing cities. Through structural optimization and digital fabrication, there is an opportunity to build far more with far less, reducing the economic and environmental costs while meeting the demands of a growing population.

CHAPTER 3 GENERAL METHODOLOGY

This thesis follows a methodology of three parts. First, a structural element is designed using a parametric framework and assessed through digital structural analysis. This framework comes from an intuitive sketch of how material can be removed—or shaped—to suit the given boundary and load conditions. Second, the elements are cast in digitally fabricated formwork, built with methods available in India. Third, the constructed elements are load tested and compared to control elements to verify their structural capacities. The following sections will describe the general theory of concrete beam design, focusing on the concrete mechanics relevant to this thesis.

3.1. Concrete design

Concrete is a mix of cement, aggregates, and water, often combined with reinforcing bars, tendons, or fibers for enhanced performance and safety. It is a system that shifts between solid and liquid, smooth and rough, natural and artificial. It engrosses engineers and architects and involves experimentation and computation while remaining both historical and revolutionary. It is no wonder that Frank Lloyd Wright considered concrete a “mongrel” material [47]. Concrete exists between classifications, refusing to stay in one classification for very long.

It is important to note that while most refer to concrete as a material, it is more accurately a system of construction where the material is coupled with the process of construction and application [13]. Due to its dense structural matrix, plain concrete is exceptionally strong in compression; yet its brittle and porous nature makes it very ineffective against tensile stress. From the late 19th century, industrialists and inventors experimented with methods of embedding metals in plain concrete to overcome this weakness leading to the development of the steel-reinforced concrete system in use today [48].

In the United States, the design and analysis of a concrete element is prepared with reference to the American Concrete Institute's ACI 318-14, also referred to as ultimate strength design, LRFD, ultimate limit state, or ULS [49]. This method assumes that concrete performs in compression near the element's ultimate strength, while tensile stresses are handled solely by longitudinal (flexural) reinforcing steel near the bottom. Unless otherwise stated, this thesis will make use of the ACI 318 method for concrete design. The following sections will discuss the general methods for concrete beam and slab designs.

3.1.1. Flexural design

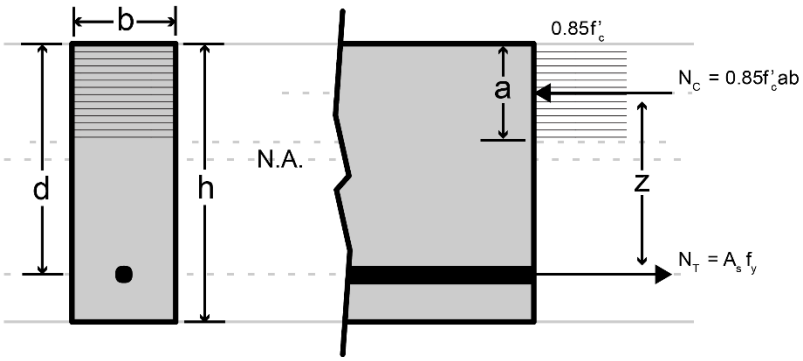

Figure 27 Ultimate strength design method using the Whitney stress block simplification

Within a reinforced concrete beam, the tensile and compressive stresses are equated using the Whitney stress block assumption shown in Figure 27, and the moment capacity is determined using the moment arm between the compressive block and tensile steel as shown in Equation 3:

$$M_N = N_C z \text{ or } N_T z \tag{3}$$

A useful relationship from the above formula is that between the depth of the Whitney stress block in compression, a, and the area of steel in tension, A_s. This is used to determine the internal moment arm, z, and the moment capacity, M_n.

$$N_C \mathrm{z} = N_T z \tag{4}$$

$$N_C = N_T \tag{5}$$

$$0.85 f_c' \mathrm{a} b = f_y A_s \tag{6}$$

$$a = \frac{f_y A_s}{0.85 f_c' b} \tag{7}$$

The moment capacity is compared to the moment envelope—the moment due to applied loads and self-weight, shown in Figure 28—and the element's section is designed to meet the required moment envelope at all points along the element's length. When done by hand, designers make a series of assumptions about the member's dimensions, the amount of steel necessary, and the overall shape.

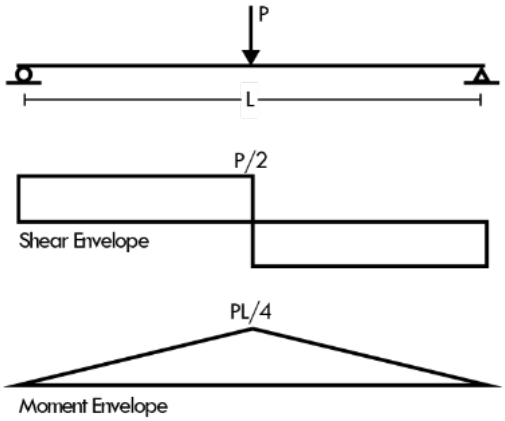

Figure 28 Shear and moment envelope of a simply-supported beam with a concentrated load at mid-span

In the Indian National Building Code (NBC), referencing the Indian Standard 456 (IS 456), a slight variation to the ULS method is used, using an assumed compressive stress distribution rather than the Whitney stress block simplification. This difference is shown in the diagram below:

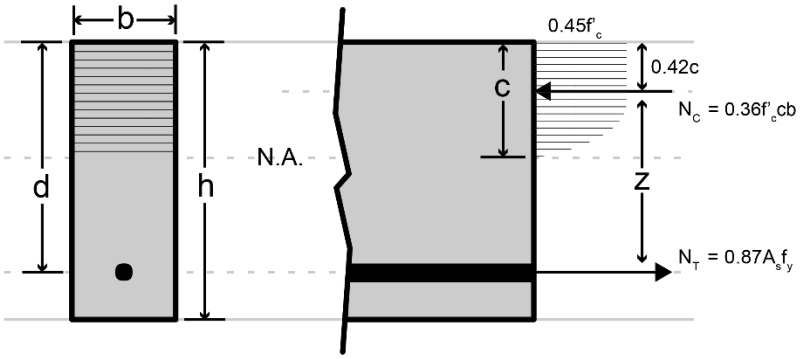

Figure 29 ULS method as outlined by IS 456

Rather than simplifying the compressive stress field into a rectangular block, an estimation of the neutral axis depth, c, is used. Additionally, a constant is applied to the formula for the moment capacity rather than applying a strength reduction factor, ϕ, as is done in the ACI. Nonetheless, this gives a similar result to the ACI method when assessing a concrete beam's flexural capacity.

3.1.2. Shear design

A concrete beam's behavior at failure due to shear is distinctly different from its failure due to flexure. A beam failing in shear fails suddenly and with little warning; the shearing forces cause a single element to fragment into multiple pieces. The difference is highlighted in the diagram below:

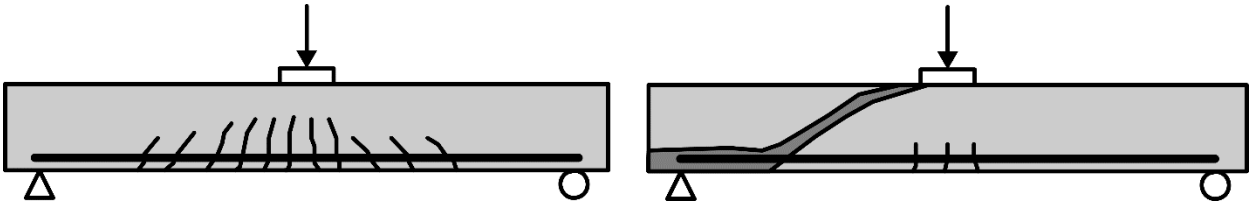

Figure 30 Failure modes of a concrete beam undergoing a) flexural failure and b) shear failure; adapted from [48]

With reference to ACI 318-14, the design and analysis of a concrete element's shear reinforcing begins by assessing the concrete's shear capacity and comparing it to the shear envelope as shown in Equation 8. If the concrete falls short of the required shear capacity, then transverse reinforcing is added. This prevents the sudden failure of concrete by resisting shear stresses—or, diagonal tension—and enables a more gradual and ductile failure due to flexure.

$$V_u = \phi(V_c + V_s) \tag{8}$$

where ϕ is 0.75 for shear. The shear capacity of the transverse reinforcement can be calculated using:

$$V_s = \frac{A_v}{s}\phi f_y d(\sin\theta + \cos\theta) \tag{9}$$

The necessary amount of transverse steel and its spacing is determined by rearranging the above equation:

$$\frac{A_v}{s} = \frac{(V_u - \phi V_c)}{(\phi f_y d(\sin\theta + \cos\theta))} \tag{10}$$

The following section will detail the methods for calculating the concrete's shear capacity, V_c.

3.1.2.1. Concrete shear capacity

The shear design of reinforced concrete beams is largely indirect and empirical because the tensile strength of concrete is highly variable; its ability to carry the diagonal tension component of a shear force cannot be fully predicted. Additionally, a concrete beam's shear capacity will include the resistance from aggregate interlock, the dowel resistance of longitudinal steel, and the resistance of the uncracked concrete. Nonetheless, a number of methods have emerged for the prediction of a plain (unreinforced) concrete beam's shear capacity and the subsequent design of transverse shear reinforcement.

The ACI 318 formulation for a concrete beam's shear capacity is based upon empirical observations and experiments measuring the components described above and has proven mostly conservative for constant section beams. The formula given by the ACI is:

$$V_c = 1.9 b_w d \sqrt{f_c'} + 2500 \rho \frac{V_n d}{M_n} b_w \leq 3.5 b_w d \sqrt{f_c'} \tag{11}$$

For simplicity, designers are permitted to use the even more conservative equation:

$$V_c = 2 b_w d \sqrt{f_c'} \tag{12}$$

Numerous alternatives to the empirical method of the ACI have been proposed, but few have been adopted by national codes. The strut-and-tie method, which uses a truss analogy for the concrete beam, has been adopted by some codes—or reserved for special cases—but it often leads to an overdesign of transverse steel in concrete beams [50].

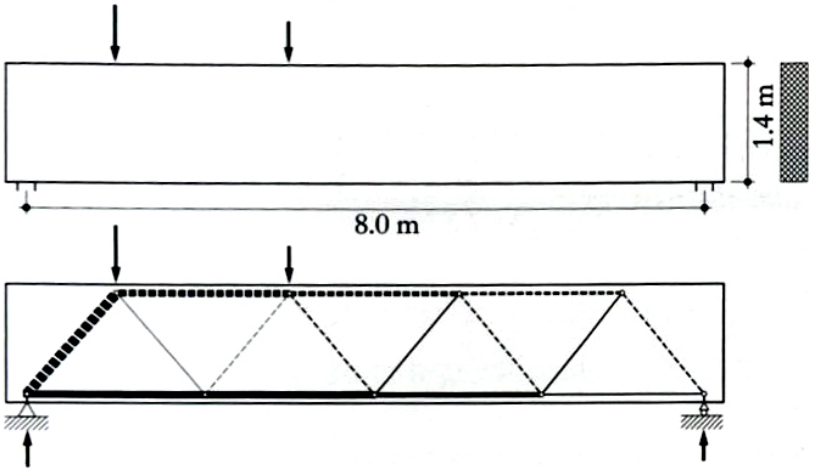

Figure 31 Beam forces idealized using the truss analogy [25]

On the other hand, some designers idealize the cracked concrete beam as a tied arch, disregarding the concrete cracked under tension and assuming the steel has a constant tensile force along its length near the ultimate load.

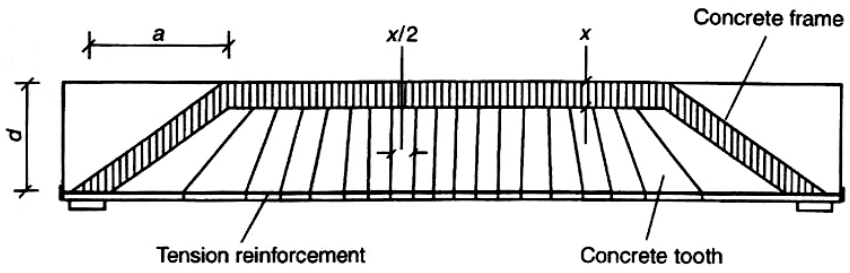

Figure 32 Concrete beam model used by CFP method for concrete shear capacity [51]

In response to this incongruity, Kotsovos developed the Compression Force Path (CFP) method [51], [52]. Kotsovos attributes more strength to the concrete than assumed by the ACI by including the resistance of the concrete "teeth" formed between cracks (see Figure 32) and accounts for geometric conditions of the beam such as the shear-span to depth ratio, a_{vx}.

$$a_{vx} = \frac{M_u}{V_u} \tag{13}$$

$$V_c = 0.875 a_{vx} d \left[0.342 b_w + 0.3 \frac{M_n}{d^2} \sqrt{\frac{z}{a_{vx}}} \right] \sqrt[4]{\frac{16.66}{\rho f_y}} \tag{14}$$

Similar to the ACI formulas, the expressions provided by the CFP method still rely on empirical observations and experimental data. Nonetheless, the CFP method has shown promising results in predicting the shear capacity of variable section concrete beams [53], and often results in less transverse reinforcement due to a higher presumed concrete shear capacity.

In IS 456, a more conservative approach is taken in assessing a concrete section's shear capacity. This is still based on empirical methods, but it only involves the concrete design strength and does not consider any of the geometric or loading conditions. The following equations are used to calculate the nominal shear strength, τ_c, of a concrete mix:

$$\beta = \frac{0.8 f_c'}{689 \rho} \geq 1 \tag{15}$$

$$\tau_c = \frac{0.85 \sqrt{0.8 f_c'} (\sqrt{1 + 5\beta} - 1)}{6\beta} \tag{16}$$

For simplicity's sake, the concrete's nominal shear strength is often provided in a table for a range of concrete compressive strengths. This nominal shear strength is then used to calculate the shear capacity, V_c, through the simple equation:

$$V_c = \tau_c * b_w d \tag{17}$$

3.1.3. Mix design

For this thesis, a custom mix design is needed to maintain workability without forfeiting the structural capacity of the concrete. The mix is designed with reference to the ACI 211.1 code [54], using a recipe of cement, water, fine aggregate, and chemical plasticizer for increased flow. According to this method, the strength is dependent upon the water/cement ratio (w/c); the higher the ratio, the weaker the concrete mix. Table 1 shows the general mix design used in this thesis, with slight variations depending on the experiment. The mix is designed for a 28-day compressive strength of 30MPa.

Table 1 General concrete mix design for 1m^3 of 30MPa concrete

Component	Quantity	% of total weight
Water, kg	265	12%
Cement, kg	491	22%
Fine aggregate, kg	1524	33%
Water for aggregate absorption, kg	23	
Super plasticizer, L	22	
Total fresh concrete, kg	~2300	

Coarse aggregate is not used due to the small scale and relative complexity of the formwork used in this thesis. To verify the strength of the mix, 75mm x 152mm cylinders are cast for uniaxial compressive testing from the same mixes that the elements are cast from.

3.2. Load testing

Each element is subjected to a loading test with simply supported bending. Load is applied with a central hydraulic jack, and the test is displacement-controlled. Additionally, concrete cylinders are load-controlled tested for compressive strength in order to verify the quality and strength of the mix design.

3.3. General digital design

The designs in this thesis are realized through digital shape optimization and structural analysis, using the 3D modelling software Rhinoceros 5.0, the visual programmer Grasshopper for Rhino5. Grasshopper is a

visual algorithm editor tightly integrated with Rhino's modelling tools, allowing for real-time parametric design and analysis. Several plugins for Grasshopper are used including Karamba 3D [55] for structural analysis, the optimization solver, Goat [56], and the optimization toolkit, Design Space Exploration [57].

Unless otherwise state, the assumed material properties used in the structural design process are summarized in the table below.

Table 2 Material properties used in structural design

Property	Value	Unit
$clear\ cover$	15	mm
$\gamma_{concrete}$	2400	kg/m3
γ_{steel}	8050	kg/m3
$EEC_{concrete}$	1	MJ/kg
EEC_{steel}	42	MJ/kg
f_c'	40	N/mm2
f_y	415	N/mm2
E_s	205000	N/mm2
ϵ_u	0.0035	
$\epsilon_{t,min}$	0.0038	
ρ_{max}	1.92E-02	
ρ_{min}	3.81E-03	

3.4. Design strategies

As suggested in Chapter 2, there is a number of strategies for the design of material efficient concrete elements. The following sections will detail the methodologies and results of three different strategies, discussing their limitations and viability for large-scale implementation. The strategies are: 1) cavity beams using consumer waste for material displacement, 2) variable-width beams with efficient steel reinforcing layouts, and 3) shape optimized floor slabs.

CHAPTER 4 STRATEGY 1

Variable-Width Beams

Similar to the uniform strength beam designs of Galileo and Timoshenko, this strategy explores potential material savings through single-dimension beam shaping. This begins with an analytical procedure that dimensions concrete beams in one dimension according to their moment envelope. This involves code written in Grasshopper 3D; a diagram of the design algorithm is attached in Appendix A. The resultant design achieves a material reduction of 36 percent for a beam spanning 1m with a concentrated load of 24.2kN at mid-span.

Analysis shows that failure through shear becomes critical so this strategy explores two methods of digitally fabricating transverse reinforcing. Two variable-width beams are designed and constructed with transverse reinforcing, and then load-tested in comparison to a variable-width beam without transverse reinforcing and a standard prismatic beam.

4.1. Methodology

4.1.1. Flexural design

As shown in Section 3.1.1, the moment capacity of a concrete beam is a function of the beam's cross-sectional areas of concrete and steel and the moment arm between them. The derivation of the beam's flexural capacity can be rearranged to determine the necessary depth for a given width, or the necessary width for a given depth, in response to the flexural load. It should be noted that this is not optimization,

but a similar approach to the uniform strength beam designs discussed in Section 2.1 adapted to the design of a concrete beam.

The following equations can be used to design a shaped concrete beam with a rectangular section according to its flexural capacity, beginning by relating the factored applied moment, M_u, to the section geometry.

$$M_u = \phi M_n = \phi N_T z = \phi A_s f_y z = \phi A_s f_y \left(d - \frac{a}{2}\right) \tag{18}$$

Using Equation 7 as discussed in Section 3.1.1:

$$A_s = \rho_n * b_w d \tag{19}$$

$$a = \frac{f_y A_s}{0.85 f_c' b} = \frac{\rho_n f_y d}{0.85 f_c'} \tag{20}$$

Equation 18 can then be rewritten as:

$$M_u = \phi \rho_n f_y b d^2 \left(1 - 0.59 \frac{\rho_n f_y}{f_c'}\right) \tag{21}$$

With a simple rearrangement, a beam's depth or width can be determined as a function of the applied moment, a desired reinforcement ratio, and one fixed dimension.

$$bd^2 = \frac{M_u}{\phi \rho_n f_y \left(1 - 0.59 \frac{\rho_n f_y}{f_c'}\right)} \tag{22}$$

$$\therefore b = \frac{M_u}{\phi \rho_n f_y \left(1 - 0.59 \frac{\rho_n f_y}{f_c'}\right) * d^2} \tag{23}$$

$$\therefore d = \sqrt{\frac{M_u}{\phi \rho_n f_y \left(1 - 0.59 \frac{\rho_n f_y}{f_c'}\right) * b}} \tag{24}$$

For this thesis, the reinforcement ratio was set for ease of fabrication and small-scale load testing. The beam's maximum cross-section was set to 152mm x 100mm with two longitudinal bars of 9.5mm diameter and a clear span of 1m. The maximum cross-section is used as the control design for a prismatic beam,

giving a baseline volume to compare against. This results in a design reinforcement ratio, ρ_n, of 0.011 and a maximum applied moment, M_u, of 6.04kN-m at mid-span.

If the beam's width is kept constant, there can be a material reduction of nearly 30 percent while meeting the necessary moment capacity for a simply-supported beam with a concentrated load at mid-span. A larger material reduction of nearly 40 percent can be achieved by varying the beam's width rather than its depth (Figure 33). For this strategy, the variable-width beam is chosen for its potential material reduction.

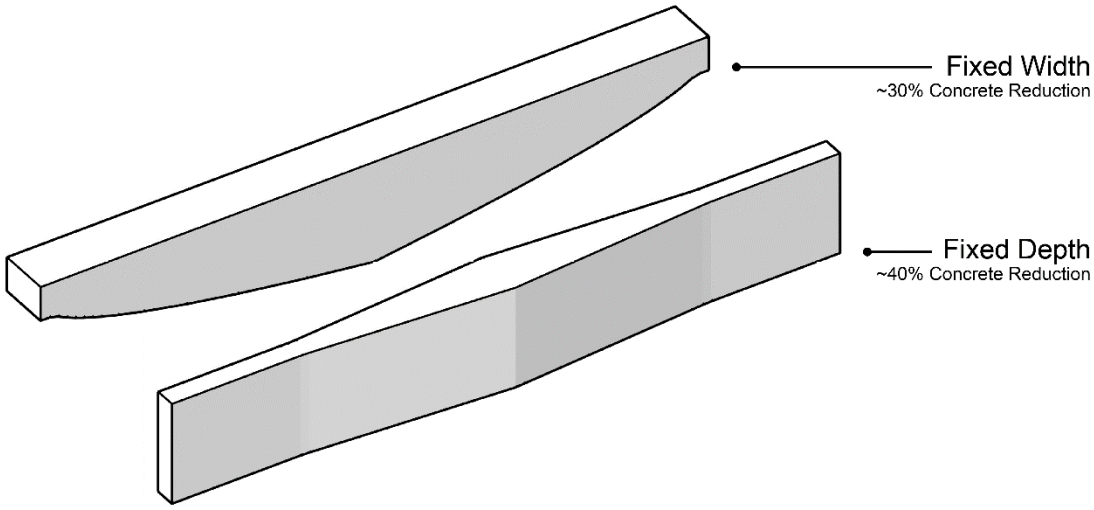

Figure 33 Comparison of material reduction achieved in two forms of uniform strength concrete beams

4.1.2. Shear design

The resultant shaped beam is analyzed along its length for its shear capacity without transverse reinforcing. Through this analysis it becomes clear that there is a deficit in the concrete shear capacity (see Figure 34) as the section area diminishes to meet a decreasing flexural demand along its length. This deficit in shear capacity is used to design the transverse steel reinforcement.

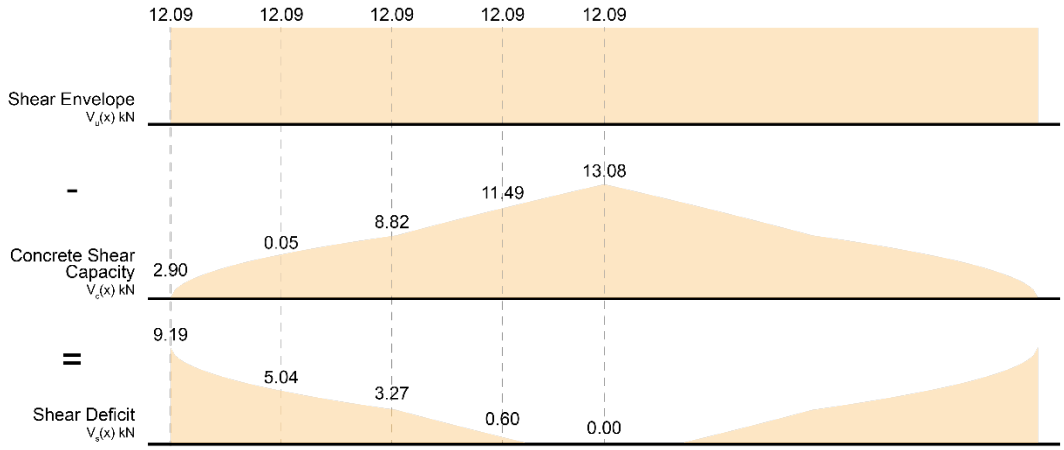

Figure 34 Magnitudes of applied shear, concrete capacity, and shear deficit requiring transverse reinforcement

The amount of steel necessary for transverse reinforcement is determined using Equation 10 as discussed in Section 3.1.2.

4.1.3. Fabrication

To meet the shear deficit, two forms of digital fabrication are used for efficient transverse steel layouts. The first is a combination of two bars of 9.5mm longitudinal steel reinforcing and CNC-bent transverse reinforcing made from 3.2mm mild-steel wire with a yield stress of 345MPa (Figure 35a). The stirrups are bent using a desktop DI Wire Plus from Pensa Labs. The second is a bespoke steel-plate reinforcing fabricated by CNC waterjet 6.35mm mild-steel plate with a yield stress of 372MPa (Figure 35b). The steel plate reinforcing also allowed for the longitudinal steel to change in area, showing that further reductions in steel are possible by keeping the design reinforcement ratio constant along the length of the beam. Numerous tests were required to find the tolerance for interlocking joints and identify the necessary irregularity along the steel-plate profiles to ensure sufficient engagement with the concrete.

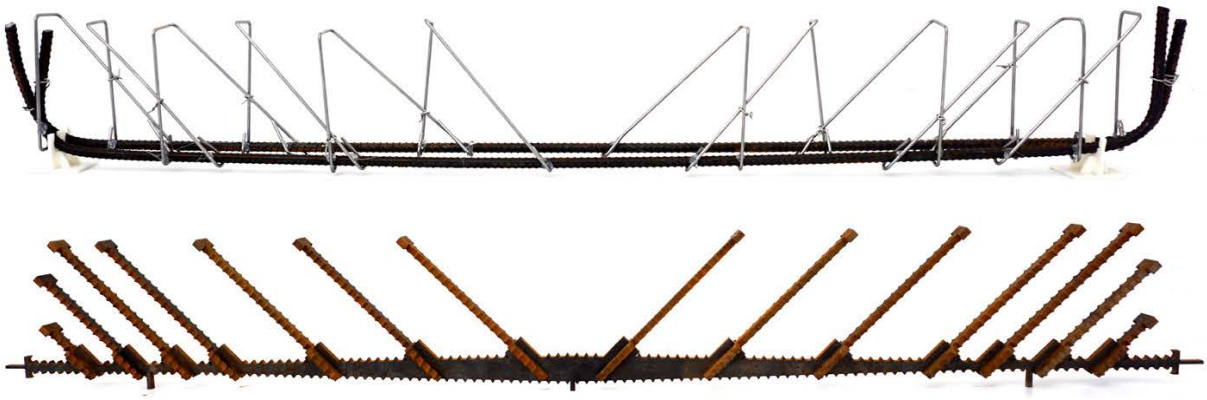

Figure 35 Shear reinforcement with a) CNC-bent wire and b) waterjet-cut plate-steel

At the given scale, it is difficult to use traditional rebar chairs to hold the reinforcing in place. Therefore, custom rebar chairs were 3D printed to ensure a clear cover of 25mm and hold the reinforcement in position during casting (see Figure 36). In contrast, the plate reinforcement was designed with notches in the formwork to hold it in place.

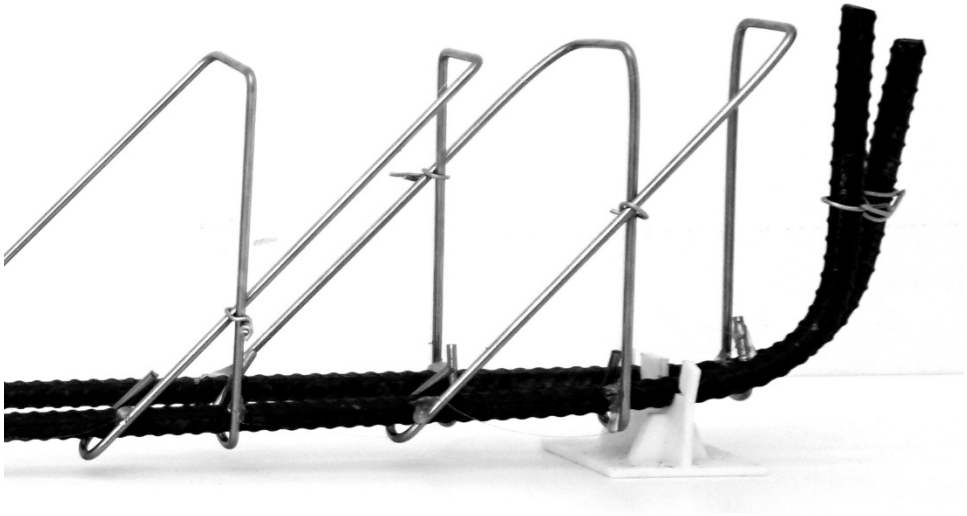

Figure 36 Detail view of 3D printed rebar chair supporting steel reinforcement

The formwork is fabricated with plywood boxes and CNC-milled extruded polystyrene foam inserts, as seen below. Two variable-width beams are cast with the shear reinforcing shown above, and a control beam is cast with only longitudinal steel and no transverse reinforcing.

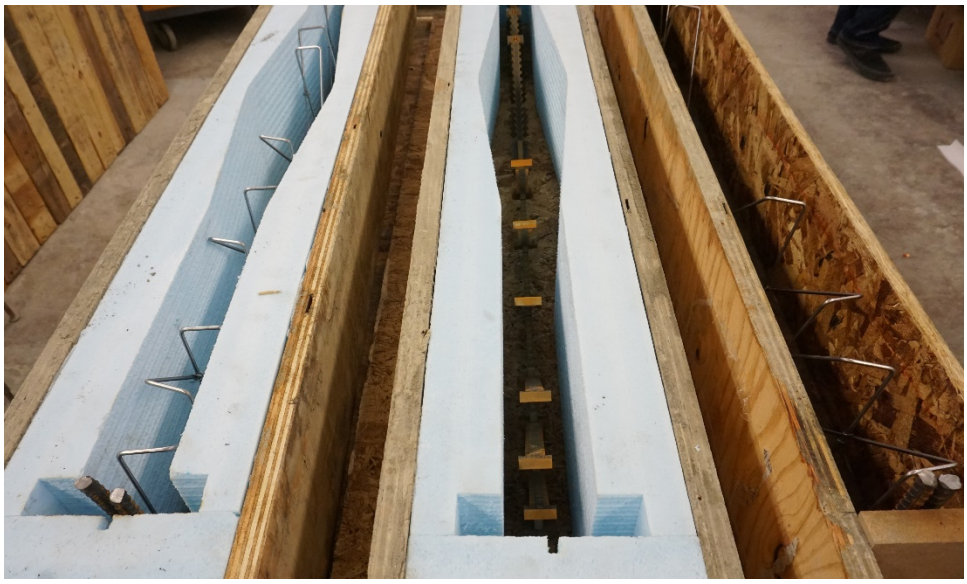

Figure 37 Shaped beam formwork and reinforcement

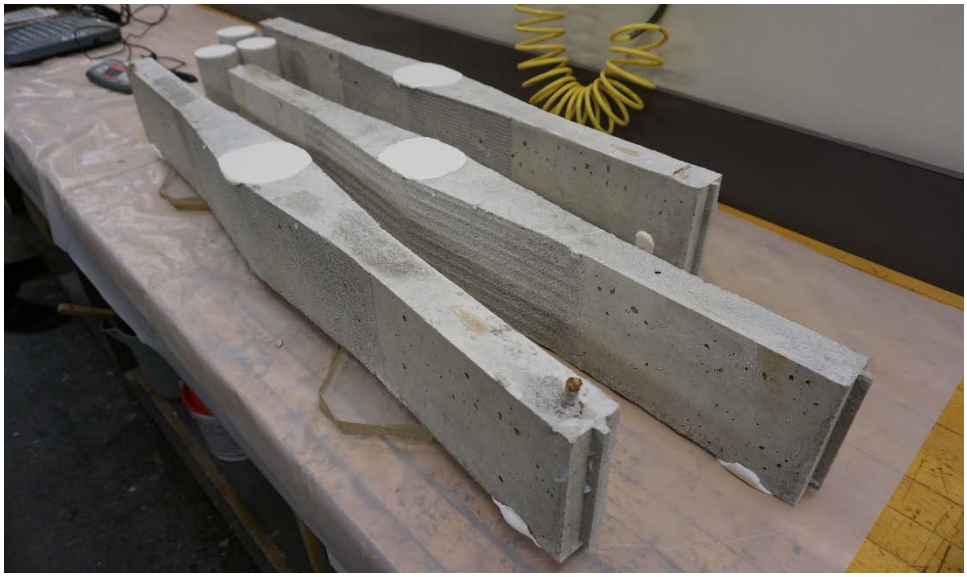

Figure 38 Resultant cast shaped beams in preparation for load testing

4.2. Results and discussion

This strategy results in the design of a variable-width concrete beam that requires 36 percent less material than a prismatic beam of equivalent strength. As shear becomes more of an issue for an element designed in this manner, this strategy applies digital fabrication to material efficient transverse reinforcing that ensures ductile failure at its ultimate strength.

Three variable-width beams with both transverse reinforcing methods and no transverse reinforcing were tested against a control prismatic beam; the results are shown in Figure 39. Additionally, the results of the concrete mix compression test are summarized in Table 3 below.

Table 3 Uniaxial compression test results

Cylinder	Stress (MPa)
1	26.8
2	26.7
3	26.1
Average	26.6

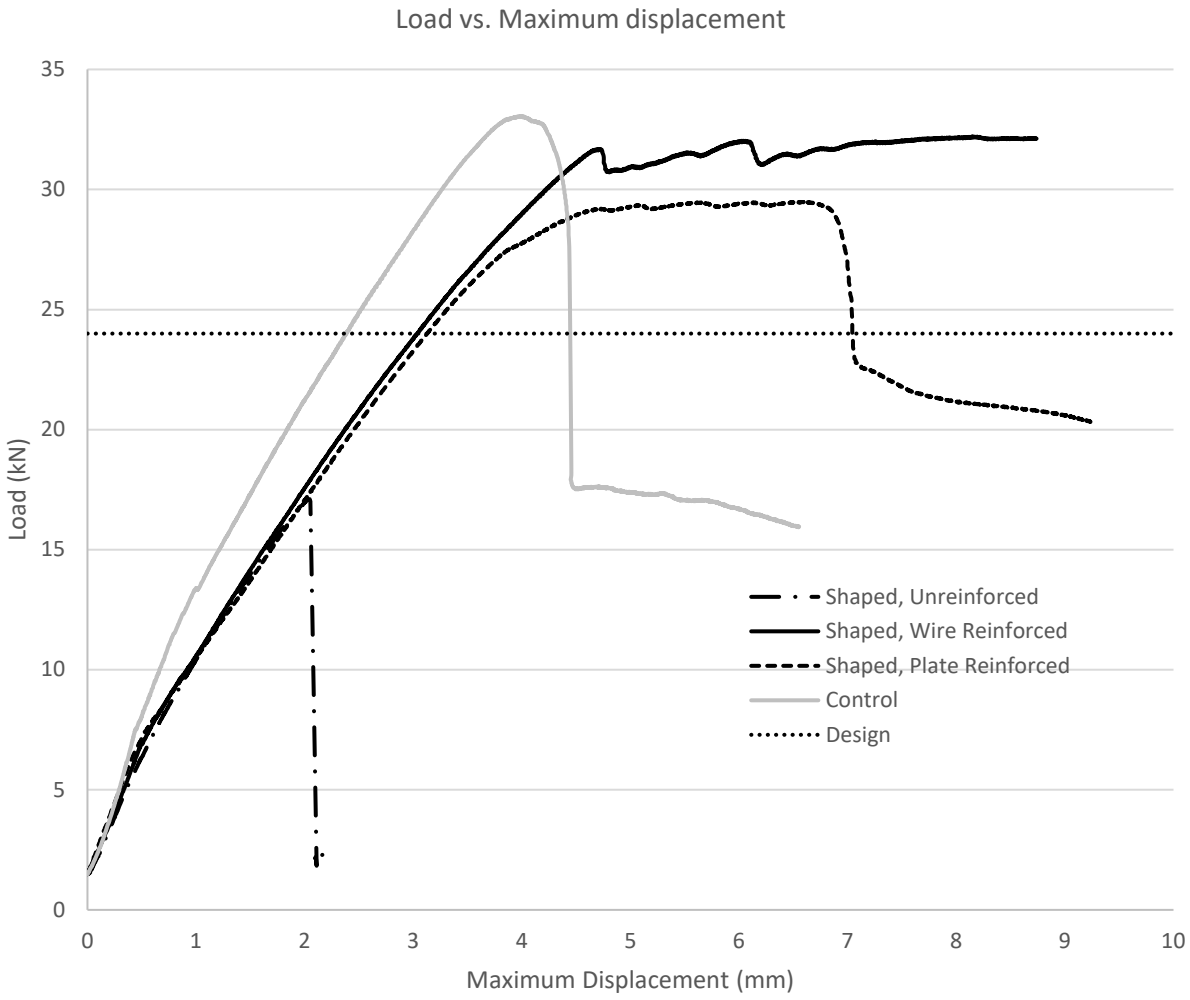

Figure 39 Variable-width beam three-point bending test results

As seen in the plot above, the control beam without shear reinforcing fails suddenly at a load of 17.1kN while the two beams reinforced against shear failure reach an average peak load of 30.8kN. The CNC wire-reinforced beam reached an ultimate strength of 32.2kN, 3 percent weaker than the control beam but surpassing the design strength of 24.2kN. Similarly, the CNC waterjet steel plate-reinforced beam surpassed the design strength but was weaker than the control beam by 11 percent. As would be expected, though, both beams lose stiffness by removing material. The CNC wire-reinforced beam has a 23 percent reduction in stiffness while the waterjet beam has a 15 percent reduction in stiffness when compared to the prismatic control beam.

The result shows that both forms of transverse reinforcing nearly double the ultimate strength of the unreinforced (against shear) variable-width beam and enables a desirable ductile failure mode. While not immediately appropriate for Indian construction, the steel plate reinforcing allows for precise control of steel volumes and these findings could translate to a precise design of reinforcement and further economic and environmental cost reductions at full-scale. Images of the CNC wire-reinforced beam after testing are shown in Figure 40.

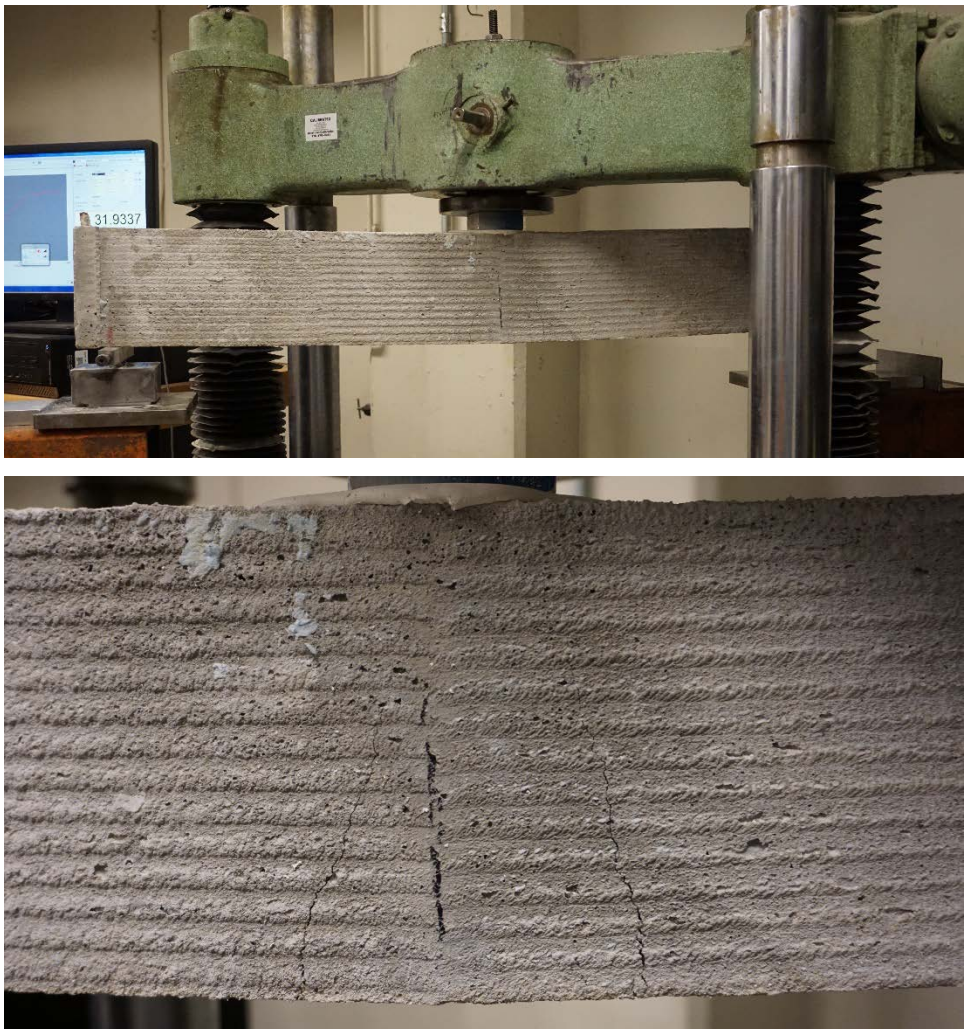

Figure 40 CNC wire-reinforced beam shows ideal ductile failure after loading, closeup of flexural cracks

CHAPTER 5 STRATEGY 2

Cavity Beams

This strategy involves the design of cavity beams with consumer waste for material displacement. An optimization algorithm determines the location and rotation of empty plastic water bottles within a prismatic reinforced concrete beam in order to reduce material usage without reducing strength. The design is realized through digital shape optimization and structural analysis, using Rhinoceros 5.0, Grasshopper for Rhino5, and the plugins Karamba 3D for structural analysis and the optimization solver, Goat. A diagram of the design algorithm can be found in Appendix B. The designed beam results in a potential material reduction of 16 percent for a span of 1.1m and ultimate concentrated point load of 12.5kN at mid-span.

5.1. Methodology

5.1.1. Computational design and analysis

First, a control beam is designed with the cross section shown in Figure 41 and an unsupported span of 1.1m. The longitudinal reinforcing consists of one reinforcing bar of steel with a yield stress of 415MPa and a diameter of 9.5mm. This simply-supported beam is designed to resist a 12.5kN concentrated load at mid-span using the flexural design method outlined in Section 3.1.1.

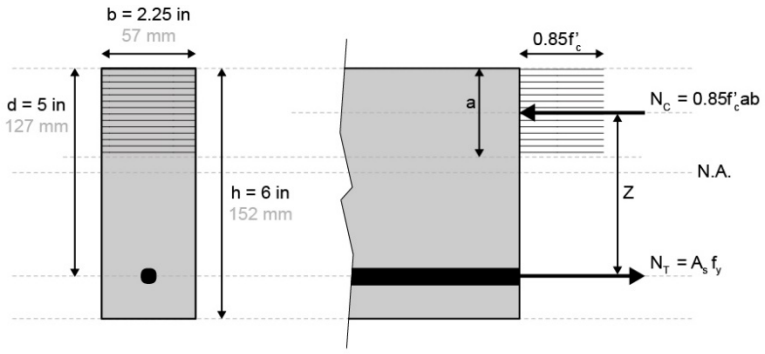

Figure 41 Control beam designed using ACI 318

Subsequently, a cavity beam is designed within the dimensions of the control beam with voids cast around empty plastic water bottles as “lost formwork”. An assumption is made that the strength of the beam can be preserved as long as the bottles remain between the compression zone and longitudinal steel of the concrete beam. Bottles are chosen as a viable enclosed volume, but other waste products may be substituted. A Grasshopper definition locates distinct bottle silhouettes inside a representative model of the control beam and then analyzes it using Karamba 3D’s finite element analysis as a 2D plate, assessing it for structural utilization and total strain energy. The objective of the optimization is the minimization of the strain energy in an attempt to keep the beam as stiff as possible.

There are three discrete variables defined for optimization: the type of bottle, its location within the beam, and its rotation about its centroid (see Figure 42). Additionally, a number of constraints are placed on the solver to keep the bottles outside of the compressive stress path, the region of longitudinal steel, and to prevent bottles from intersecting. To reduce processing times, the bottles are located symmetrically about the mid-span axis and aligned at the same depth.

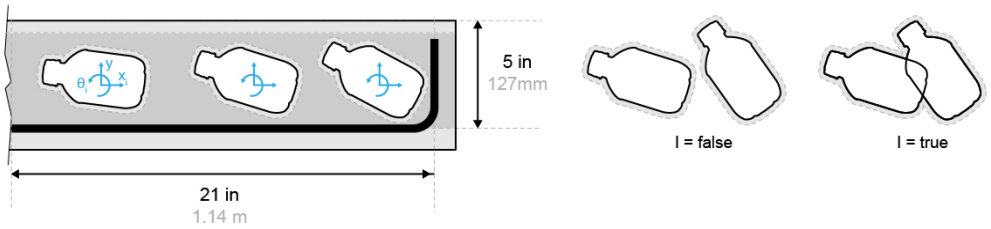

Symbol	Variable	Range
$\boldsymbol{x_i}$	horizontal location of bottle i	$0 < x < 21$ in (533 mm)
$\boldsymbol{y}$	vertical location of all bottles	$0 < y < 5$ in (127 mm)
$\boldsymbol{\theta_i}$	rotation of bottle i	$-\pi/2 < \theta < \pi/2$ rad

Figure 42 Bottle optimization variables and constraints, light grey areas result in a penalty when crossed

In summary, the objective problem is defined below:

$$\boldsymbol{x} = \begin{bmatrix} x_i \\ y \\ \theta_i \end{bmatrix} \tag{25}$$

$$\min W_{IN}(\boldsymbol{x})\big(1 + P(\boldsymbol{x})\big) \tag{26}$$

where $\boldsymbol{x}$ is the design vector containing all design variables while the objective, W_{IN}, is the internal strain energy of the beam as calculated by Karamba 3D, and $P(\boldsymbol{x})$ is the penalty jump function defined below.

$$P(\boldsymbol{x}) = \begin{cases} 10^6 \text{ if } I = \text{true} \\ 0 \text{ if } I = \text{false} \end{cases} \tag{27}$$

where I is the boolean expression for object intersection defined in Figure 42 above.

$$\min Vol(\boldsymbol{x})\,\big(1 + P_1(\boldsymbol{x}) + P_2(\boldsymbol{x})\big) \tag{28}$$

$Vol(\boldsymbol{x})$ is the total volume of the beam estimated by Grasshopper, and $P_1(\boldsymbol{x})$ and $P_2(\boldsymbol{x})$ are the penalty jump functions defined below:

$$P_1(\boldsymbol{x}) = \begin{cases} 10^6 \text{ if } \Delta_{max} \geq \frac{L}{360} \\ 0 \text{ if } \Delta_{max} < \frac{L}{360} \end{cases} \tag{29}$$

$$P_2(\boldsymbol{x}) = \begin{cases} 10^6 \text{ if Utilization} > 100\% \\ 0 \text{ if Utilization} \leq 100\% \end{cases} \tag{30}$$

The variable Δ_{max} is the maximum deflection of the beam calculated by Karamba 3D.

An initial optimization is run using Goat's local, quadratic algorithm—appropriate for smooth and continuous problems—in order to minimize the strain energy by manipulating the bottles' locations and rotations. A second optimization is run using Goat's global, deterministic algorithm—suitable for a combinatorial problem—to minimize the beam's volume by changing the type of bottles. The design used for testing is shown below.

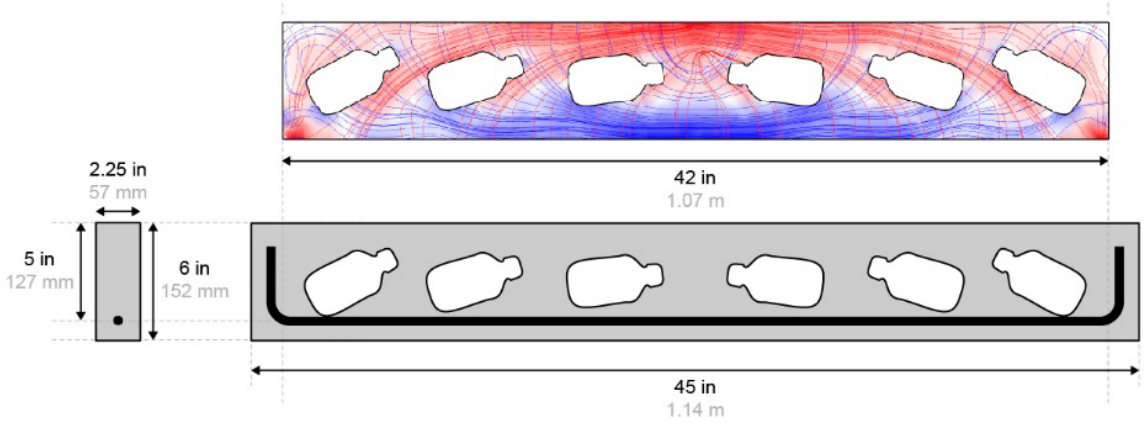

Figure 43 Final design of optimized cavity beams

5.1.2. Fabrication

A plywood box form is used to fabricate each of the control beams while CNC-milled formwork is used as inserts for the cavity beams. To precisely locate the bottles within the formwork, impressions of the bottles' surfaces are milled into rigid insulation sheathing panels using a three-axis CNC router (see Figure 44). The bottles are adhered to the milled impressions and longitudinal reinforcing is cut and bent to fit the formwork. Due to the scale of the beams, custom rebar chairs are once again 3D printed to hold the longitudinal steel in place. The width of the beams is controlled by the diameter of the bottles, giving them surface-to-surface contact with the formwork. For this exploration, four total beams are cast: two control beams and two cavity beams.

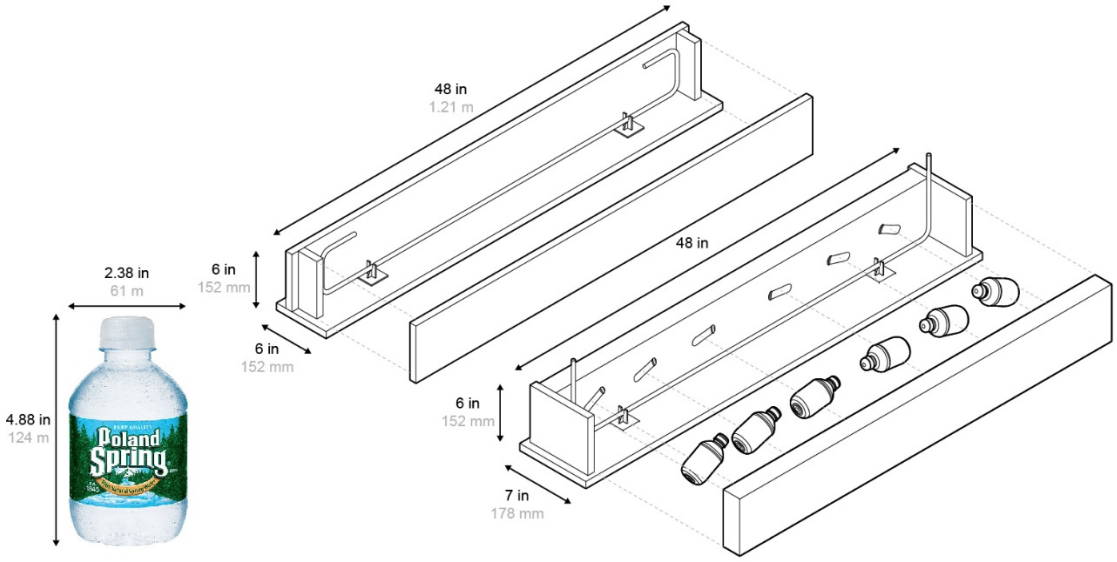

Figure 44 Diagram of formwork construction for control and cavity beams and bottle dimensions

5.2. Results and discussion

The strategy presented here reduces the volume of concrete needed by 16 percent to resist a similar load to a solid reinforced concrete beam with a span of 1.1m. The example presented in this thesis is designed to resist an ultimate load of 12.5kN. This is accomplished through the two-step optimization of a cavity beam, optimizing the location, rotation, and size of plastic bottle that minimize the strain energy and volume of concrete. The results of the cylinder compression tests are summarized in the table below.

Table 4 Uniaxial compression test results

Cylinder	Stress (MPa)
1	23.4
2	23.9
3	24.6
Average	24.0

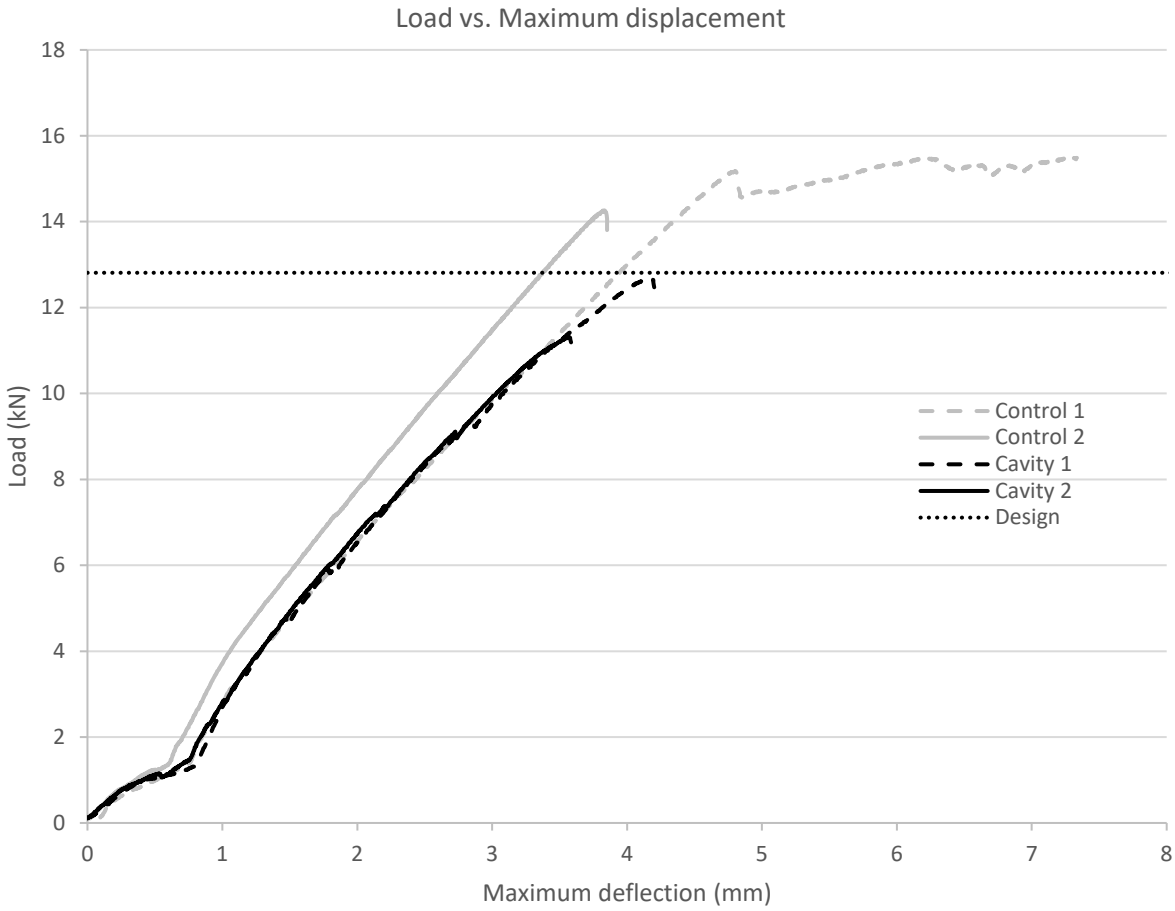

Figure 45 Cavity beam three-point bending test results

Due to the scale and complexity of the initial prototypes, transverse reinforcing was neglected. All but one control beam failed in a sudden manner due to shear (see Figure 46), highlighting the need for said reinforcing. The cavity beams failed at an average ultimate load of 12.0kN while the control beams failed at 14.9kN. On average, the cavity beams were 6 percent weaker than the design strength, and 19 percent weaker than the control beams. They were also 7 percent less stiff than the average of the control beams.

While the ultimate load of the cavity beam did not reach the intended strength, the results are promising. If precautions are taken against shear failure, such as transverse or fiber reinforcing, it may be possible to design cavity beams with a flexural strength exceeding the design strength while displacing unnecessary material. Further study is required to design appropriate shear reinforcing. Additionally, a study of the potential savings at larger spans can be undertaken to assess the viability of this strategy in full-scale structures where shear is no longer the controlling failure mode.

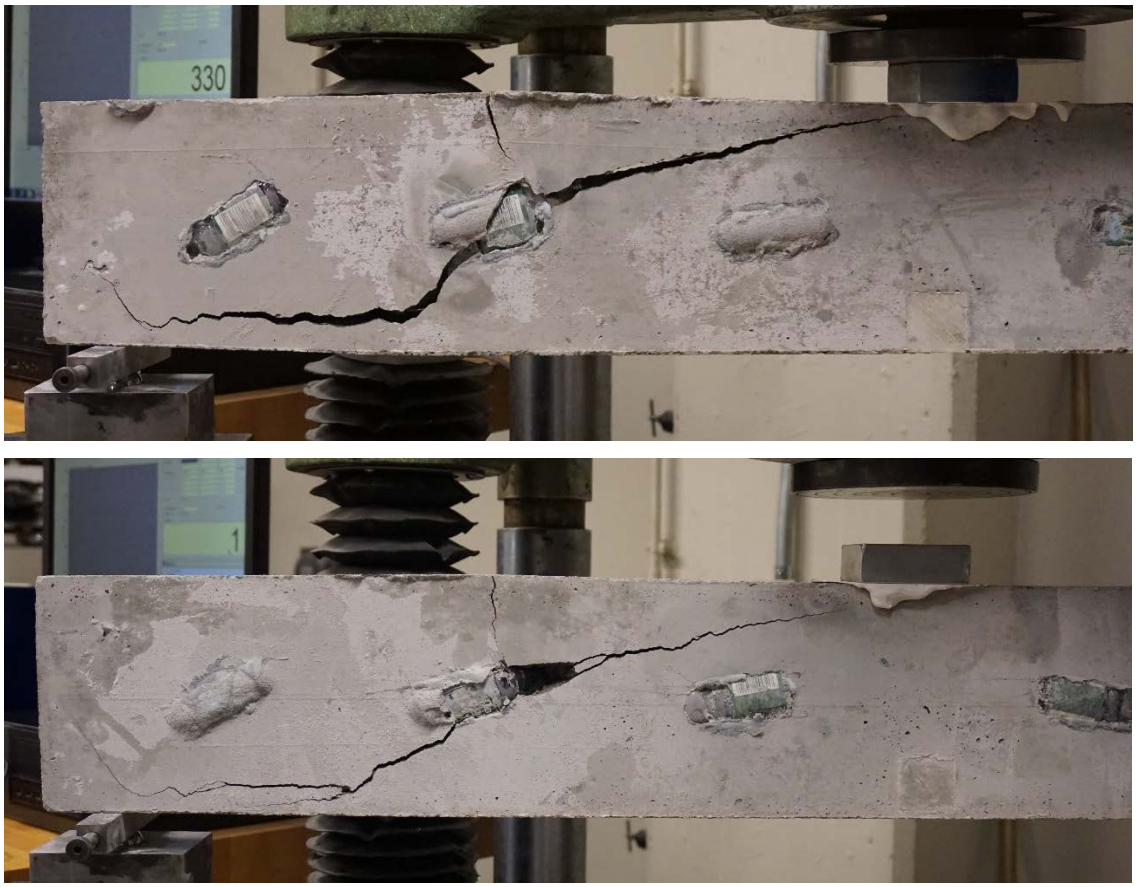

Figure 46 Beams after testing show shear cracks passing from point of loading to supports

CHAPTER 6 STRATEGY 3

Shaped Slabs

This strategy extends the procedure introduces in Chapter 4 to the design of shaped reinforced concrete slabs through the constrained optimization of its geometry. In practice, a one-way concrete slab is designed as a wide beam, making the general design method discussed in Chapter 3 applicable to this strategy. A constrained optimization minimizes or maximizes an objective function by manipulating its variables subject to constraints. Since this strategy approaches a design for implementation in India, this strategy references the National Building Code (NBC) of India, specifically the Indian Standard 456-2000: Plain and Reinforced Concrete Code of Practice (IS 456). While similar to the procedures outlined by ACI 318, there are a few changes to safety factors and constants as discussed in Chapter 3.

This involves code written in Grasshopper 3D using the plug-ins Karamba 3D and Design Space Exploration; a diagram of the design algorithm can be found in Appendix C. Unlike previous strategies, this strategy looks at the minimization of an element's embodied energy rather than just the concrete component. This gives a more comprehensive approach to material efficiency, and could be extended to include economic costs with sufficient financial data. The result of this strategy is a material efficient ribbed slab with a potential 55-70 percent reduction in embodied energy, and a similar reduction in material and mass, when compared to a typical flat slab of 5m span. This span was chosen as representative of multi-story concrete residential construction in Indian cities, which are typically built with slabs spanning three to five meters.

6.1. Geometry and performance

6.1.1. One-dimensional shaping

Exploration of the shape optimization of concrete slabs begins with a one-dimensional shaping exercise for existing structural systems: flat slabs, and ribbed slabs or t-beams (see Figure 47). When all other dimensions are fixed, the embodied energy can be formulated as a function of the element's depth.

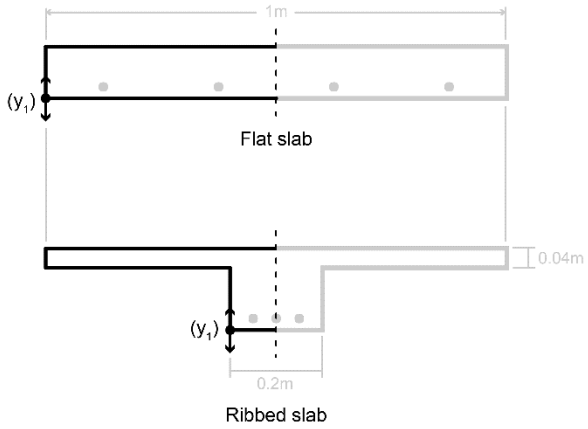

Figure 47 Typical design process for a flat slab or ribbed slab

The following chart shows the resultant embodied energy for a flat slab of varying depth, and a ribbed slab with varying depth, a flange depth of 40mm, and a rib width of 200mm. Each element is designed to carry the live load of 200kg/m^2 and its own self-weight. The minimum embodied energies—and their associated depths—are highlighted in the chart below.

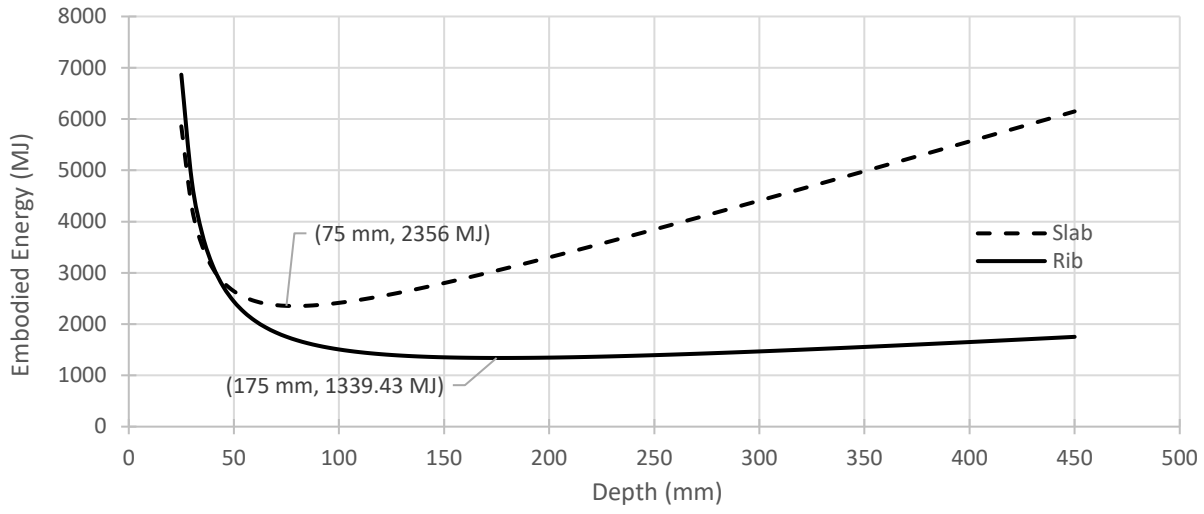

Figure 48 Embodied energy of one-way slabs, 5m span and 1m wide

6.1.2. Three-dimensional shaping

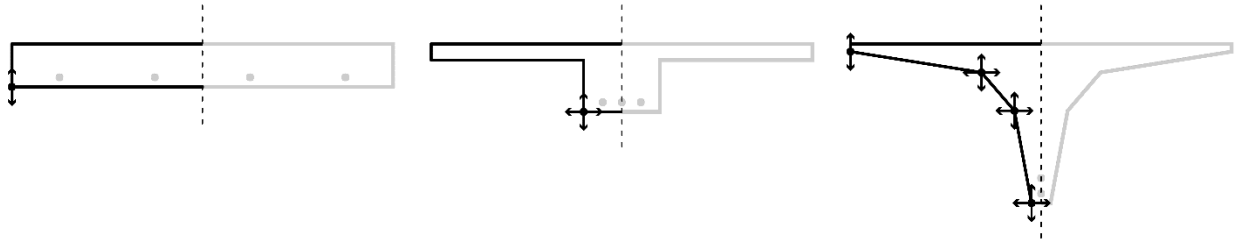

Figure 49 Potential design process of a slab with increasing degrees of freedom and complexity

This process of geometric manipulation to minimize a concrete element's embodied energy can go further when applied to the three-dimensional manipulation of variables along its length. Increasing the degrees of freedom, as in Figure 49 above, along a slab's length could lead to designs that are nearly impossible to determine through traditional design methods. A potential procedure for the constrained optimization of a concrete element's geometry is described in Figure 50. Once again, the objective of this optimization is to reduce the embodied energy, but the objective could be changed to cost or mass depending on the designer's priorities.

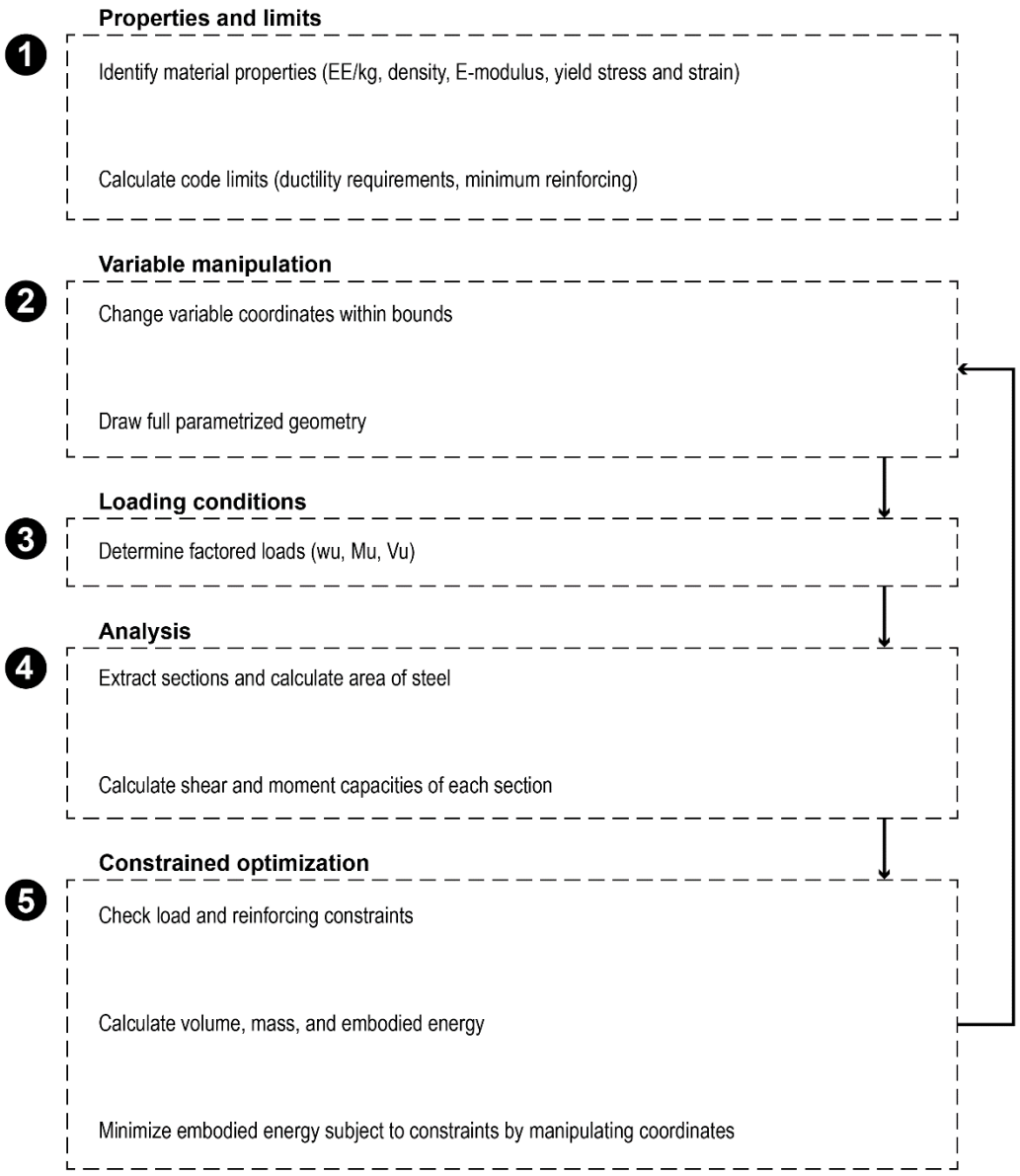

Figure 50 Optimization procedure for a shaped concrete slab

6.2. Structural analysis and performance

A definition is developed in Grasshopper to design a concrete slab with an adaptable geometry that could be analyzed and adjusted by a constrained optimization algorithm. The optimization is done using Design Space Exploration's Radical tool, developed to run constrained optimization within Grasshopper's coding environment. The following sections lay out a method to assess the structural capacity and performance of a shaped slab.

6.2.1. Structural analysis and constraints

In contrast to the time-consuming process of numerically analyzing an arbitrary concrete slab design through methods such as Finite Element Analysis (FEA), analytical methods of structural design enable the rapid assessment and subsequent optimization of a shaped slab. In this strategy, a shaped element is assessed along its length by cutting a series of sections as shown in Figure 51. The analysis is simplified by assuming symmetry and assessing only half of the element with each iteration. The structural analysis results in three main constraints for the optimization: ductility, flexural capacity, and shear capacity. Additional constraints on flange thickness, clear cover, and effective flange width will also be discussed. The following sections detail how these constraints are checked in each iteration of the optimization process.

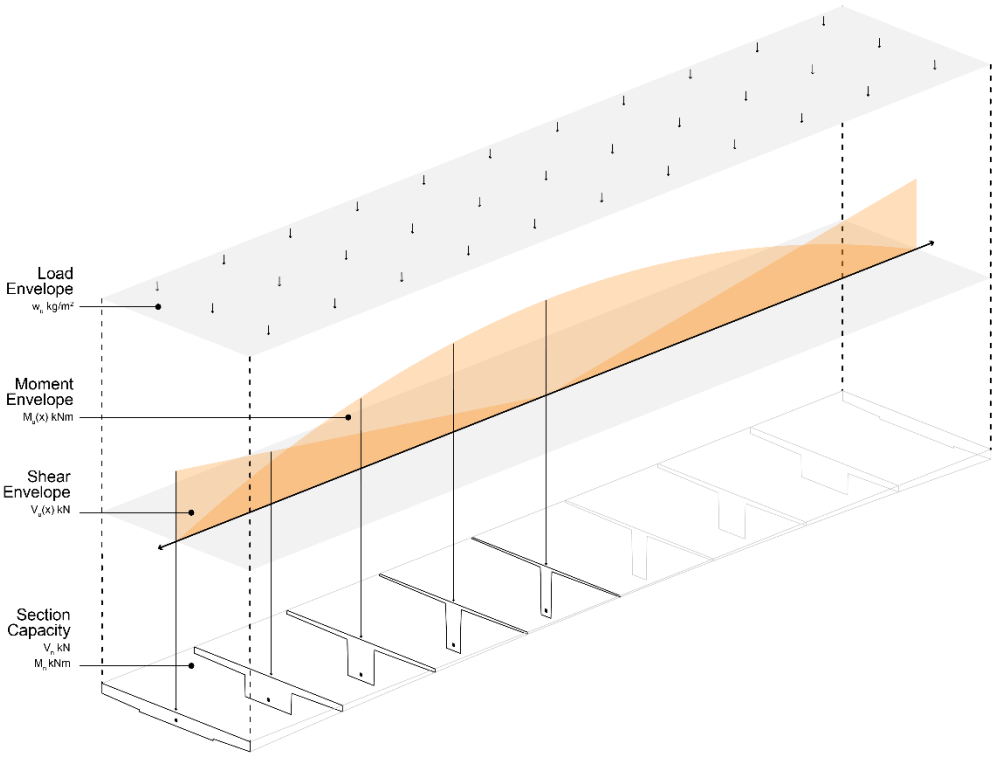

Figure 51 Structural analysis of a shaped slab

6.2.1.1. Loading envelope

The first thing that must be determined is the loading envelope of the shaped slab, as shown in the figure above. With reference to the Indian NBC, the element undergoes a residential live load, L_L, of 200kg/m^2 (1.96kN/ m^2) and the average dead load, D_L, of its self-weight. The loads are applied using the equations

below, provided by the NBC, where material volume is calculated using a built-in component of Grasshopper:

$$w_u = 1.2L_L + 1.6D_L \tag{31}$$

$$D_L = \gamma_{concrete} * volume_{concrete} + \gamma_{steel} * volume_{steel} \tag{32}$$

The dead load is an average of the slab's weight smeared across its length. This is done for simplicity and appears to have little impact on the final result as long as the span is kept within a residential scale of three to five meters. As the span increases, the dead weight distribution of the beam becomes increasingly important, as seen in long-spanning structures like bridges. The following sections will detail the structural analysis of an arbitrary concrete section.

6.2.1.2. Constraint 1 | Ductility requirement

The variable ρ_{max} is an upper bound to the reinforcement ratio required by IS 456 to ensure an under-reinforced concrete section, enabling ductile failure. This is done by guaranteeing that the ultimate strain in the steel is reached before the ultimate strain of the concrete in compression, avoiding a crushing failure mode.

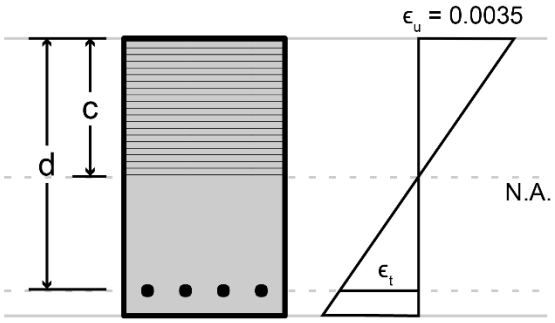

Figure 52 Relationship between a reinforced concrete beam's geometry and the steel tensile strain, ϵ_t

As shown in the figure above, the maximum reinforcement ratio is calculated using the ratio of the maximum neutral axis depth, c_{max}, to the total depth, d. This results in the following relationship between the section's geometry and material properties.

$$\frac{c_{max}}{d} = \frac{\epsilon_u}{\epsilon_u + \epsilon_t} = \frac{0.0035}{0.0055\frac{f_y}{E_s}} \tag{33}$$

$$\rho_{max} = \frac{0.36 f_c'}{0.87 f_y}\left(\frac{c_{max}}{d}\right) \tag{34}$$

An additional limit is placed on the minimum amount of reinforcing required, ρ_{min}, to ensure that the slab does not fail as soon as the concrete cracks:

$$\rho_{min} = \frac{0.25\sqrt{f_c'}}{f_y} \tag{35}$$

If the design reinforcement ratio, ρ_n, lies between these two values then the section should not fail through compressive crushing or tensile cracking of the concrete. Nonetheless, an additional constraint is necessary to ensure that the section will not undergo a brittle shear failure, as discussed later in Section 6.2.1.4.

6.2.1.3. Constraint 2 | Flexural capacity

As mentioned in Chapter 3, ULS assumes that concrete performs only in compression near the element's ultimate strength, while tensile stresses are handled solely by longitudinal reinforcing steel near the bottom. The tensile and compressive stresses in the section are equated and the moment capacity is determined using the moment arm between the compressive block and tensile steel as shown in the following equations, adapted from IS 456:

$$M_N = N_C z \text{ or } N_T z \tag{3}$$

$$N_C = 0.36 A_c f_c' \tag{36}$$

$$N_T = 0.87 A_s f_y \tag{37}$$

In this strategy, the moment capacity is compared to the moment envelope—the moment due to applied loads and self-weight—and the element's section is designed to meet the required moment envelope at all points along the element's length.

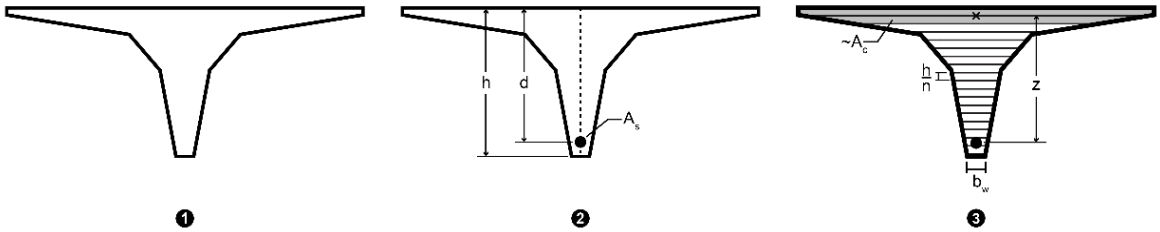

Figure 53 Arbitrary section assessed for moment capacity

To assess the moment capacity of an arbitrary section, the unknown dimensions $\{z,\ d, A_{c,} A_s\}$ must be determined (see Figure 53). The effective depth, d, is found by subtracting the clear cover (15mm for interior floor slabs) from the given height, h. The area of steel is then determined using a similar approach to the Portland Cement Association's Simplified Design method [58], which relates the area of steel to the section's effective depth, d, and the applied moment envelope, M_u. This relationship is shown in the equation below:

$$A_s = \frac{M_u}{0.87 f_y d \left(1 - 1.005 \rho_n \frac{f_y}{f_c'}\right)} \tag{38}$$

where the design reinforcement ratio, ρ_n, is selected to be $0.66\rho_{max}$ based upon common practice.

Once the area of steel is found, an approximation of the compressive area of concrete, A_c, is determined by balancing the tensile force of the steel and the compressive force in the concrete at ultimate strength:

$$N_C = N_T \tag{39}$$

$$0.36 A_c f_c' = 0.87 A_s f_y \tag{40}$$

$$\therefore \text{desired } A_c \geq \frac{0.87 A_s f_y}{0.36 f_c'} \tag{41}$$

Each section is divided into a predetermined number of subsections, n, and integrated from the top compressive face downwards until an approximate area of concrete is found that meets the requirement shown in Equation 41. The distance between the centroid of this newfound area of concrete in compression and the area of steel gives the moment arm, z. Finally, the moment capacity is compared to the applied moment envelope and the area of steel is checked against the reinforcement ratio limits discussed earlier. It should be noted that this method will result in different areas of steel along the slab's length; for this thesis, the maximum area of steel is chosen and used along the slab's entire length for constructability.

As the subdivision of the section and subsequent integration is computationally demanding, it is necessary to identify the minimum number of subsections, n, required for an accurate calculation of the moment capacity. This can be done by incrementally increasing the number of subsections for a sample design, calculating the resultant ratio, M_n/M_u, and identifying the minimum number of subsections that gives a nearly consistent result.

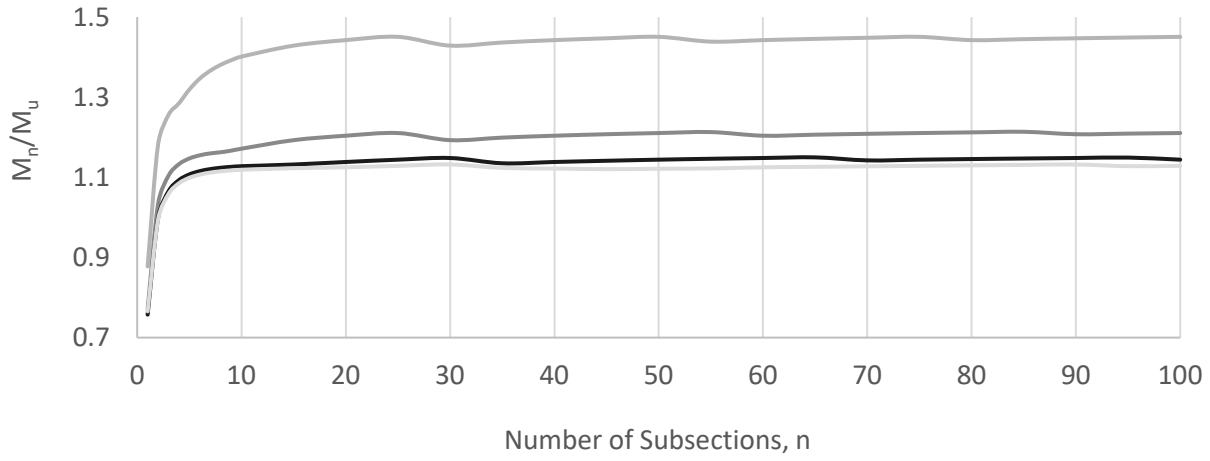

Figure 54 Ratio of moment capacity to applied moment for different numbers of subsections, n

The result of this process is shown in the chart above, and suggests that a value of 10 is appropriate for n. It should be noted that the values of M_n/M_u are higher than 1.0 at certain sections because the area of steel is kept at the maximum required along the element's length, resulting in a conservative design for flexure at numerous points along its length.

6.2.1.4. Constraint 3 | Shear capacity

As discussed in Section 3.1.2, the shear capacity of a shaped section can be determined in a number of ways. This method utilizes three different methods for calculating the shear capacity of the concrete section and compares their results: ACI 318 method, the Compressive Fore Path Method (CFP), and the IS 456 method.

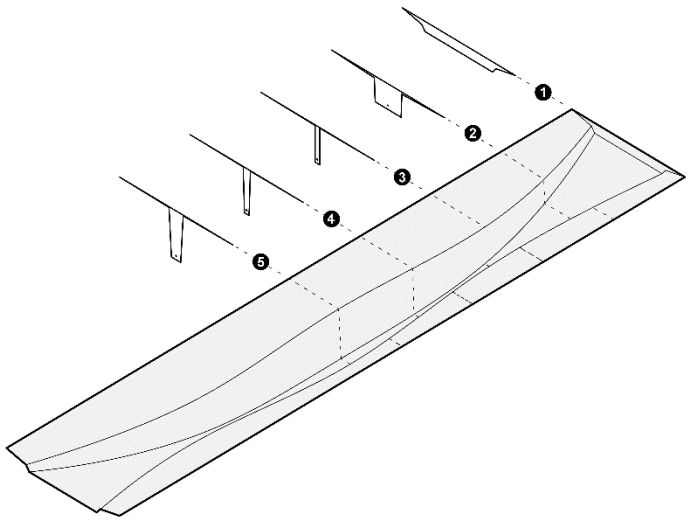

Figure 55 Sample element used to test shear capacity calculations

Table 5 summarizes an analysis of the above element's concrete shear capacity using all three methods. The table shows that the shear capacity is smallest according to IS 456, which is highly conservative. Therefore, this strategy uses IS 456 to calculate the shear capacity of the concrete elements during the optimization process.

Table 5 Concrete shear capacity calculated along the length of sample element

Section	ACI 318 (kN)	IS 456 (kN)	CFP (kN)
1	71.6	20.3	∞
2	43.8	21.3	37.1
3	11.6	9.5	11.7
4	14.2	10.9	11.3
5	30.3	17.4	13.9

The optimization can either be carried out assuming no transverse reinforcing, designing the concrete shear capacity, V_c, to meet the shear envelope, or it can be carried out with a fixed shear reinforcement capacity, V_s, using Equation 42 below:

$$V_n = V_c + V_s \tag{42}$$

6.2.1.5. Constraint 4 | Flange thickness

Similar to the flexural capacity constraint discussed in Section 6.2.1.3, a constraint is necessary to ensure that the slab's flange is deep enough to carry the necessary load in the transverse direction. To accomplish this, a constraint is placed on the flange thickness, t_f, based on a transverse model of the slab (see Figure 56). The model assumes that the flange behaves as a fixed cantilever with a span of half the slab's width. The cantilever is loaded with a uniform distributed load of 200kg/m^2 and a concentrated load of 200kg to simulate a person standing on its edge. This ensures that the flange is deep enough to transfer the required load to the web.

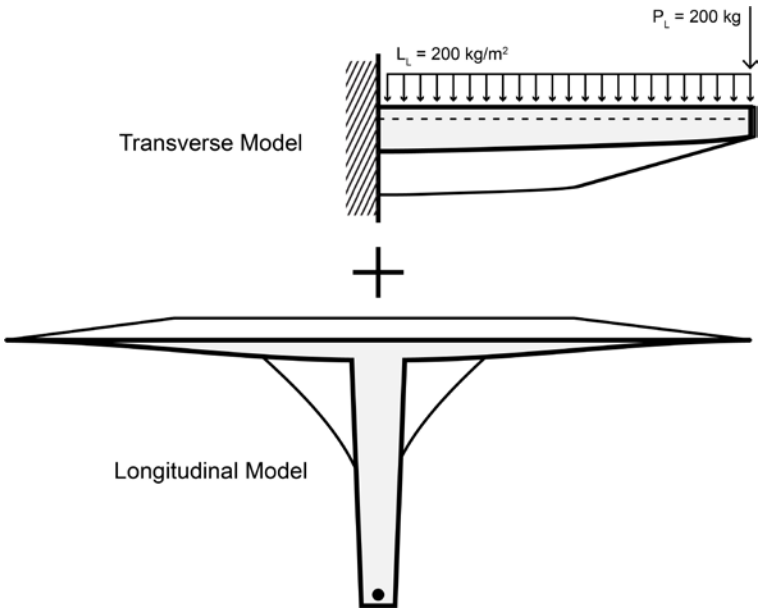

Figure 56 Superimposed transverse model of slab's flange

6.2.1.6. Constraint 5 | Effective flange width

In concrete design codes, there is often a specification for the effective flange width to be within a certain distance. This ensures that the entire flange is uniformly stressed, allowing it to be assessed as part of the shaped slab rather than as a separate slab spanning between beams. This strategy carries out a calculation of the effective flange width and makes sure that the overall slab width, b, does not go beyond the width defined in Equation 43:

$$b \leq 16t_f + b_w \tag{43}$$

6.2.1.7. Constraint 6 | Clear cover

A final check is carried out to ensure that the longitudinal reinforcing has a clear cover that is called for by code, 15mm for a slab. This is done using Grasshopper's inbuilt geometry components to check for intersection between the slab's exterior and a clear cover radius surrounding the steel. Figure 57 shows what an intersection between the clear cover radius and the section's geometry would look like

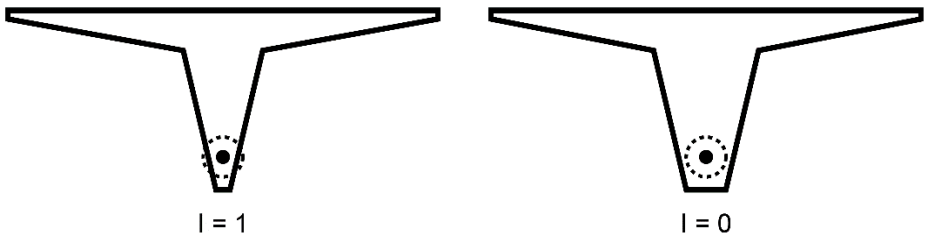

Figure 57 Clear cover check, where I is a Boolean expression for intersection; clear cover shown in dotted line

6.2.2. Performance | Embodied energy calculation

In this strategy, the embodied energy of the structure is selected as the objective "cost" and determined by multiplying the masses of concrete and steel by their unit embodied energies. The embodied energy of a reinforced concrete element can be found using the formula below:

$$EE = EEC_{concrete} * Vol_{concrete} * \gamma_{concrete} + EEC_{steel} * Vol_{steel} * \gamma_{steel} \quad (44)$$

The embodied energy coefficients, EEC, are found in literature specific to India [12] as their values will range depending on time and context. In this thesis, these values are set to 1MJ/kg for concrete and 42MJ/kg for steel.

As the flange width can also be variable, the optimization can be carried out over a given space rather than as a single element. The total embodied energy is then equal to the number slabs of a variable width needed to cover a given distance. An example design optimized across a 5m x 5m space is shown in Figure 58.

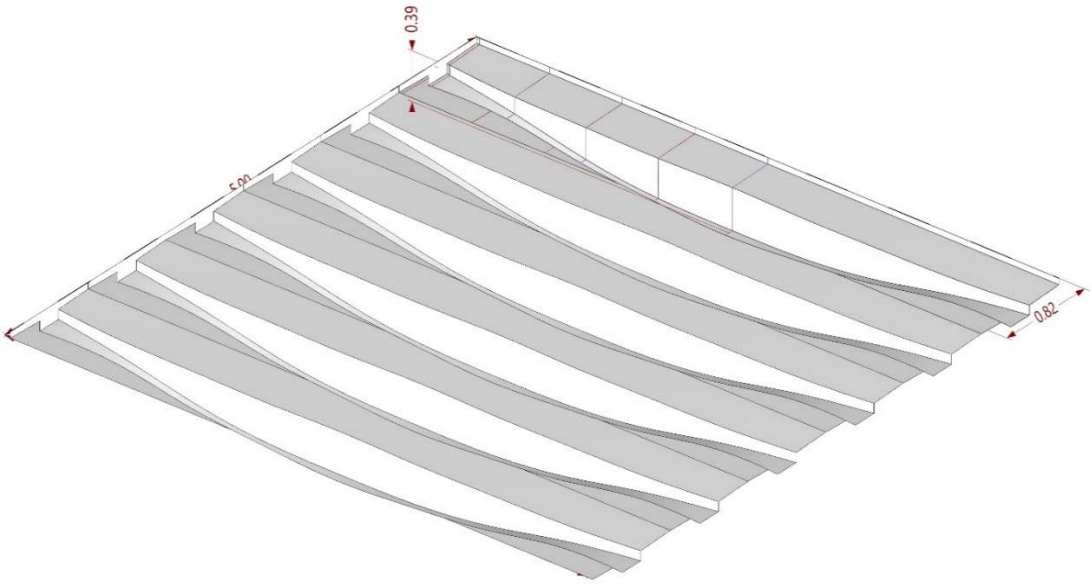

Figure 58 Example of a shaped slab for a 5mx 5m room with a 58 percent EE reduction compared to a flat slab

6.3. Geometric construction of a shaped slab

The digital geometry of an element is assembled using the process shown in Figure 59. First, the boundary conditions and span are defined. Subsequently, a number of planes are cut across the length, points defining the slab's geometry are defined at each plane, and the points are mirrored and lofted to form the final three-dimensional slab. This process is carried out using Grasshopper's geometry components. The following sections detail how the variables are arranged, bounded, and related to the final geometry of a shaped slab.

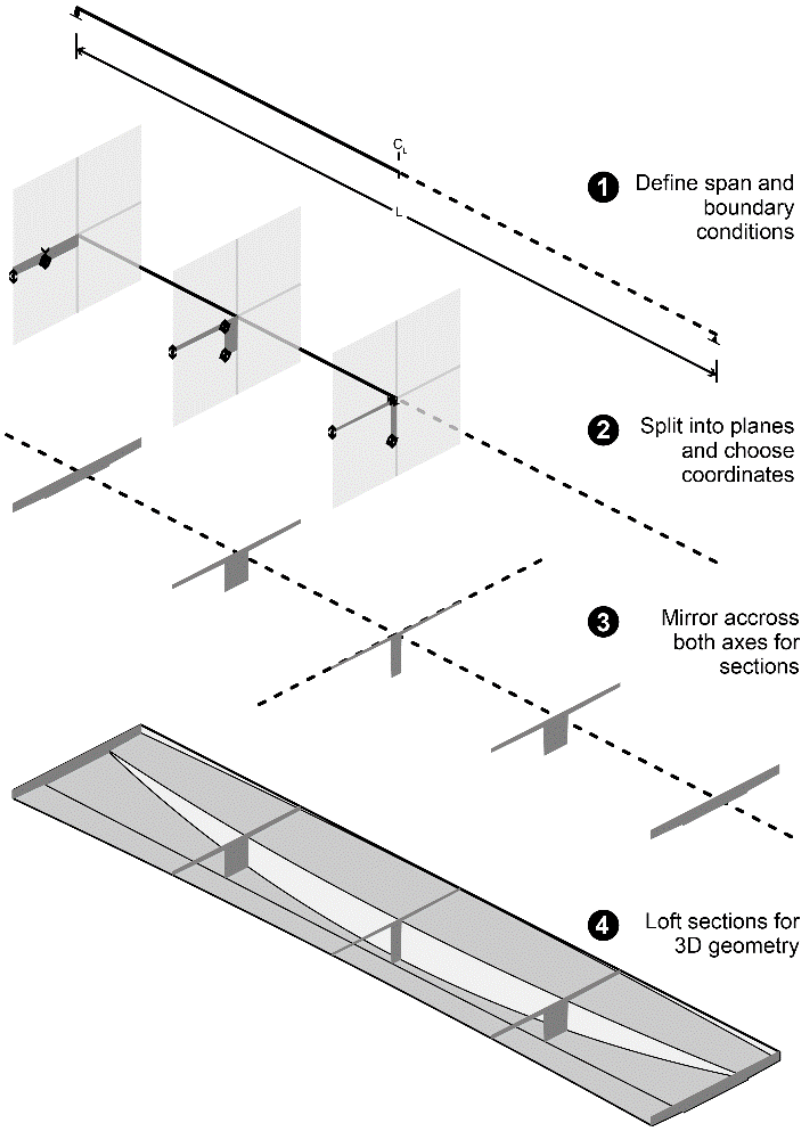

Figure 59 Procedure for digitally constructing shaped slab

6.3.1. Variable definition

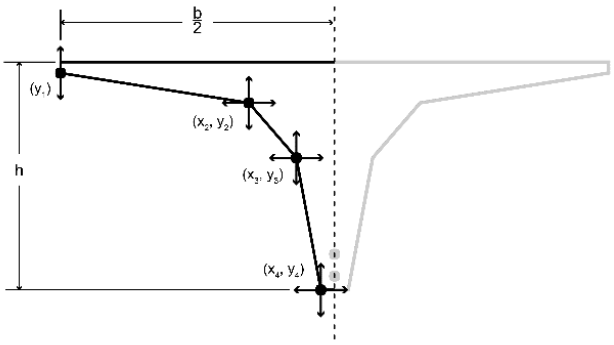

Coordinates	Bounds
x_2, x_3, x_4	$0.015\frac{b}{2} \leq x \leq 0.95\frac{b}{2}$
y_1, y_2, y_3	$0.015\text{h} \leq y \leq 0.95\text{h}$
y_4	$0.03 \text{ meters} \leq y \leq 1.00 \text{ meters}$

Figure 60 Shaped slab control points and their associated bounds

The points that control the slab's geometry are shown in Figure 60, along with a table of their bounds. The horizontal coordinates are bound by the variable dimension, b, while the vertical coordinates are bound by the variable dimension, h. Consequently, the variables for optimization are not the coordinates, but the coefficients that manipulate the coordinates as a function of their bounds. This relationship is demonstrated by the following set of equations:

$$x_2 = \frac{a_1 b}{2} \tag{45}$$

$$x_3 = \frac{a_2 b}{2} \tag{46}$$

$$x_4 = \frac{a_3 b}{2} \tag{47}$$

$$y_1 = a_4 h \tag{48}$$

$$y_2 = ((1 - a_4)a_5 + a_4)h = a_5^* h \tag{49}$$

$$y_3 = ((1 - a_5^*)a_6 + a_5^*)h = a_6^* h \tag{50}$$

$$y_4 = h \tag{51}$$

where $0.05 \leq a_i \leq 0.95$ to prevent overlapping coordinates and avoid lofting errors in Grasshopper.

As a result of these relationships, the design vector of variables for the constrained optimization is made up of the coefficients, the maximum width of the slab, and the maximum height at each section:

$$\boldsymbol{x} = \begin{bmatrix} a_1 \\ a_2 \\ a_3 \\ a_4 \\ a_5 \\ a_6 \\ b \\ h \end{bmatrix} \tag{52}$$

6.3.2. Translation from points to slab

The translation of coordinates to 3-dimensional geometry must be considered carefully, as a number of issues can occur in the analytical analysis of an element when the geometry is formed incorrectly. For instance, the type of interpolation between points is important. Figure 61 shows an example of how the same points can result in a section that is impossible to analyze when the type of interpolation between them changes from linear to cubic.

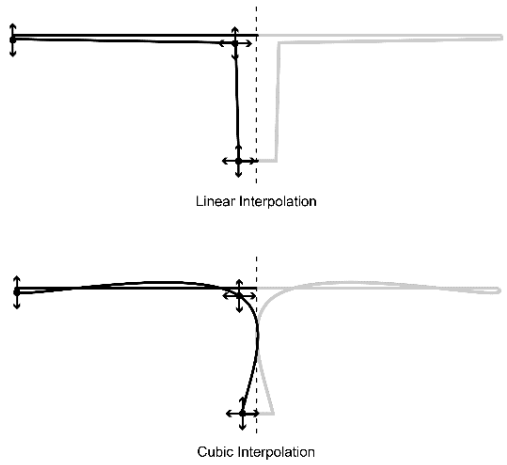

Figure 61 Effect of interpolation degree on resultant geometry from similar points

In order to bypass this issue, the points are interpolated longitudinally rather than transversely, as shown in Figure 62. This geometry is then rotated about the x- and y- axis and closed to create a solid element that can be assessed as explained in Section 6.2.1. The sections are lofted together using Grasshopper's built-in components, lofting longitudinally to ensure a smooth geometry. A smooth geometry helps avoid shear concentrations from sudden changes in section [24].

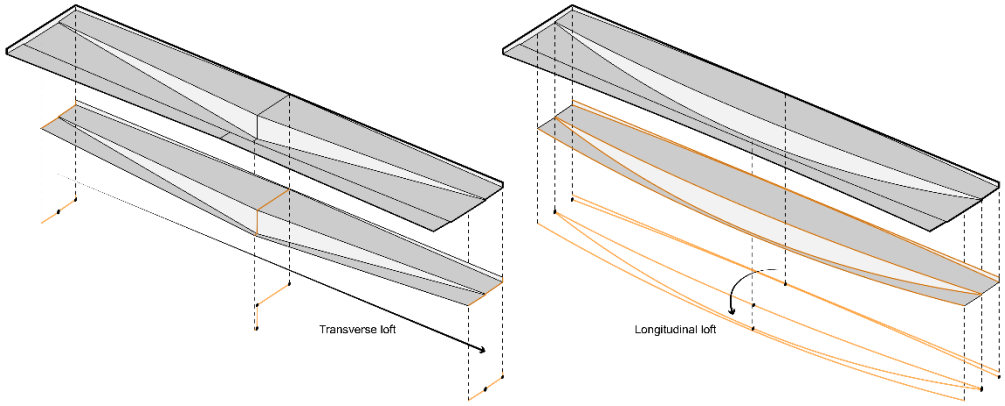

Figure 62 Effect of lofting direction on resultant geometry from the same points

6.4. Constrained optimization problem

In summary, the methodology discussed above results in a constrained optimization problem that can be defined as follows:

minimize $EE(\boldsymbol{x})$

subject to $V_n > V_u$

$M_n > M_u$

$\rho_{max} > \rho > \rho_{min}$

$b \leq 16t_f + b_w$

$I = 0$

This constrained optimization is carried out using the COBYLA algorithm, or Constrained Optimization by Linear Approximation [59]. This is an optimization algorithm that can be carried out using Radical, a tool in the Design Space Exploration plugin [57] specifically developed to carry out constrained optimization. The optimization is stopped when either a maximum number of iterations has been completed, or the objective is no longer changing beyond a set tolerance. In this strategy, the maximum number of iterations is set to 1000, and the tolerance is 0.001.

6.4.1. Optimization problem controls

The initial framework for the optimization problem is made up of a number of controls that can be altered: the number of planes for geometry construction, the number of points and their degrees of freedom, the

number of sections for analysis, and more. This section will discuss the impact of those controls on the optimization performance and expediency. These controls are summarized in Table 6 below.

Table 6 Optimization controls and tested ranges

Optimization controls	Range
Number of construction planes	**2-5**
Sections for analysis	5
Constraints per section	4
Subdivisions for integration	10
Variable points per plane	3
Degrees of freedom per plane	**3-5**
Total section variables	**6-25**
Total constraints	25

Nine test runs are conducted to explore the impact of these controls on the final results and computational time. The controls highlighted in bold text are manipulated during these runs and the results of each test are discussed in the following section.

6.4.1.1. Optimization control testing

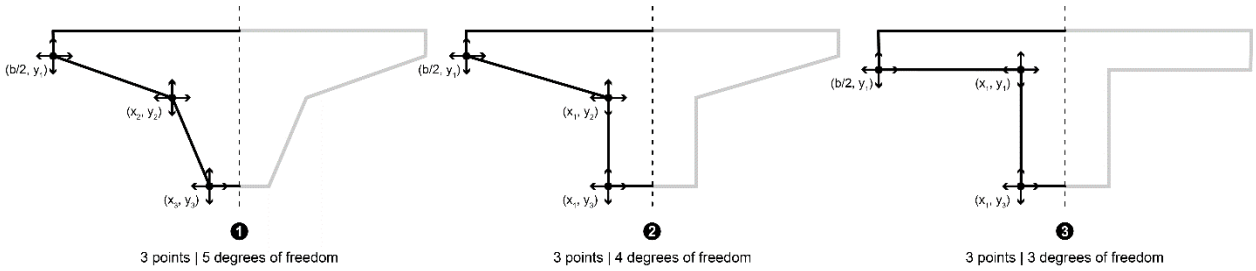

Figure 63 Variable degrees of freedom for optimization test runs

The setup of each test run is shown in Figure 63 and summarized in Table 7. Each run explores a combination of two variable controls: the number of construction planes and the degrees of freedom (DoF) of three points on each plane. The diagram above shows the impact of the DoF on the section's construction; this is repeated on each plane resulting in a total number of section variables that is the product of the number of planes and DoF.

Table 7 Optimization controls manipulated for each test run

Run	Planes	DoF	Section Variables
1	5	5	25
2	3	5	15
3	2	5	10
4	5	4	20
5	3	4	12
6	2	4	8
7	5	3	15
8	3	3	9
9	2	3	6

The resulting designs of each test run are shown in Appendix D, and their embodied energy reductions and optimization times are summarized in Table 8 below.

Table 8 Final embodied energy (EE) reduction, optimization time, and iterations for each test run

Run	%EE Reduction	Time (s)	Iterations
1	58%	397	630
2	64%	258	555
3	61%	78	188
4	63%	284	525
5	61%	184	305
6	62%	89	152
7	62%	199	331
8	64%	202	326
9	64%	96	167

The test runs suggest that the various arrangements of the optimization controls had little impact on the final results. The optimization was often completed within 1-8min and yielded an embodied energy reduction of 58-64% percent. This suggests that increasing the number of variables adds more time to the optimization but ultimately does not impact the EE reductions very much.

It is important to note that these controls can be adjusted for various fabrication constraints. The degrees of freedom, number of construction planes, and relationship between variable coordinates can mark the

difference between a doubly-curved geometry reliant on subtractive manufacturing and a singly-curved geometry that can be approximated with bent sheet materials.

6.5. Prototype design

To test the results of this strategy, a small-scale slab with a span of 1.25m and width of 0.25m is designed for fabrication and load testing. The resultant design is shown in Figure 65. The slab is designed for a distributed load of 19.7kN/m resulting in a maximum imposed moment of 3.86kN-m at midspan. For ease of construction, the slab is designed with a fixed tensile reinforcement of 9.5mm diameter, 415MPa strength steel.

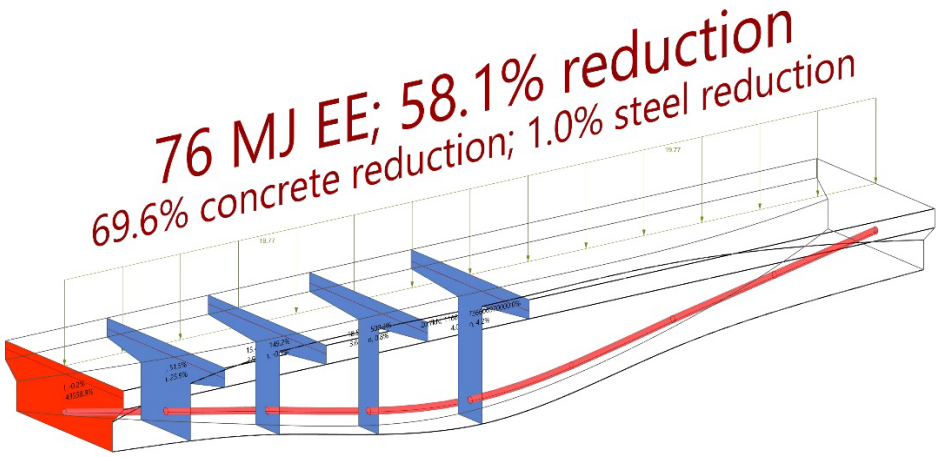

Figure 64 Chosen design for fabrication with Grasshopper visualization; section planes show points of analysis where red means a constraint is not met

The first step is the design of an optimized flat slab undergoing the same loads, minimizing its embodied energy by adjusting its depth. The result is a flat slab of 196mm depth, with a total embodied energy of 177MJ. The next step is the design of an optimized slab using this strategy. The slab shown in Figure 65 is designed with 12 variables: four degrees of freedom on three section planes. The material and embodied energy savings of the resultant designs are summarized in Table 9. As the longitudinal steel volume remains fixed, the entirety of the embodied energy reduction occurs in the concrete.

Table 9 Material volumes and EE of control and optimized slab

	Control Slab	Resultant Design	% reduction
Volume of Concrete (m^3)	6.13E-02	1.90E-02	69%
Volume of Steel (m^3)	8.90E-05	8.90E-05	0%
EE (MJ)	177	76	57%

6.6. Fabrication

As in previous strategies, two small-scale slabs are fabricated using a plywood box and a CNC-milled foam insert (see Figure 67).

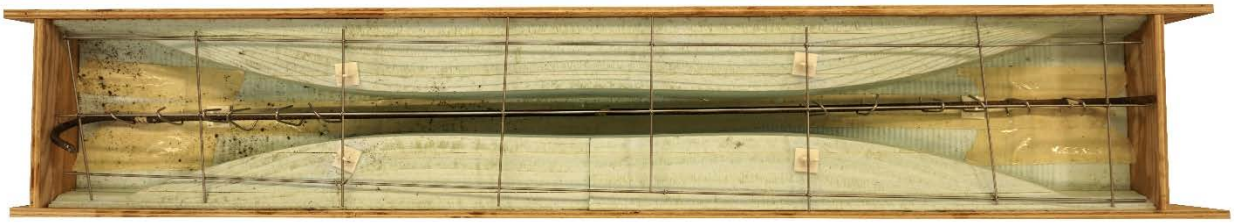

Figure 65 Milled CNC foam and plywood box used for optimized slab fabrication

The slab is reinforced with a single 9.5mm longitudinal reinforcing bar with a yield stress of 415MPa and 3.2mm mild-steel transverse reinforcing wire with a yield stress of 345MPa. To simplify assembly and hold the transverse steel in place a mesh of 3.2mm wire, arranged as in Figure 67a, and 3D printed rebar chairs are used.

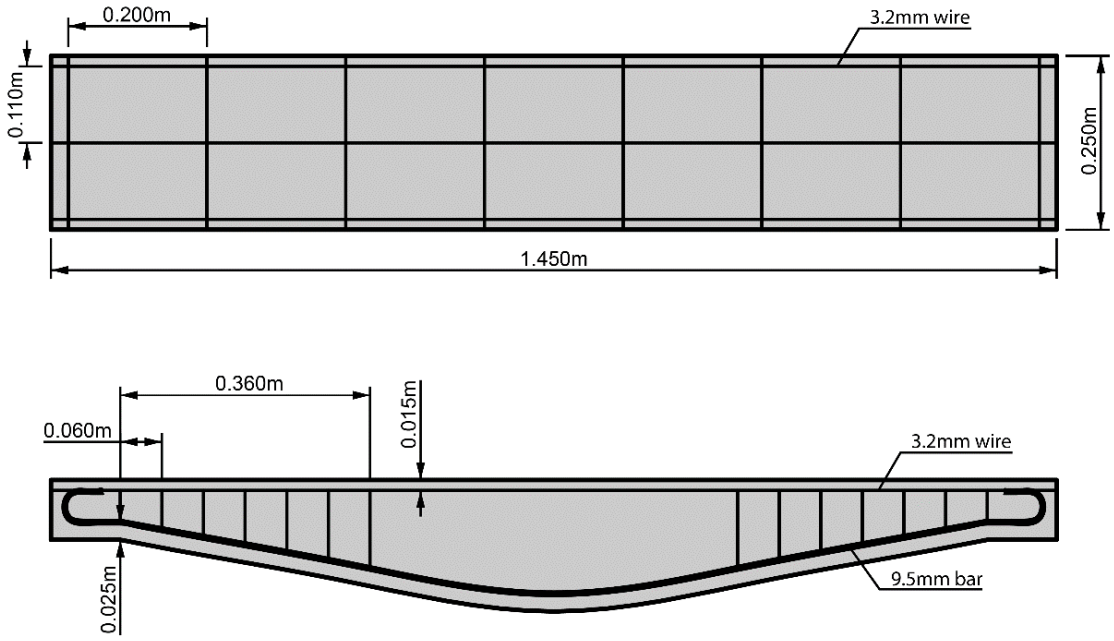

Figure 66 a) Top view of flange mesh and b) Longitudinal section of transverse and longitudinal reinforcing

The longitudinal reinforcement is bent using a Hitachi VB16Y Rebar Cutter/Bender, which allows for specific angles to be bent. Nonetheless, a simplified rebar profile is used which reduces the central curvature to a

single angle. Figure 68 shows that this results in a small error in the rebar's location, but not too substantial at the scale of the slab.

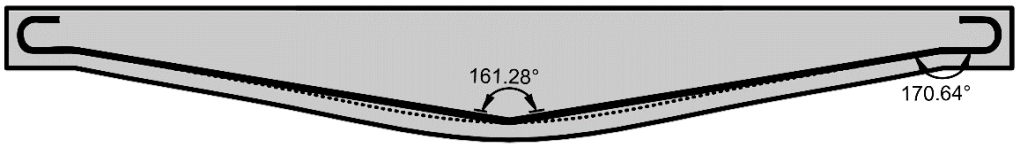

Figure 67 Final longitudinal rebar profile, original design profile shown in dotted black line

In addition to the CNC milled foam, an approximation of the slab is fabricated using singly-curved plywood. This is a method commonly used in furniture fabrication, and provides a proxy for common methods of building with sheet metal in India. This results in a similar mold design with one main different: the flange is now a single thickness, adding more material for the ease of fabrication. An image of the form is shown in Figure 68. Further information on the fabrication of this formwork can be found in [60].

Figure 68 Bent wood form and plywood box for approximated slab fabrication

6.7. Load testing

Load testing is carried out with four points of loading, approximating the uniform loading that the slab was designed for. With the loading conditions shown in Figure 69 below, it is estimated that the design will withstand 6kN at each point, or 24kN in total.

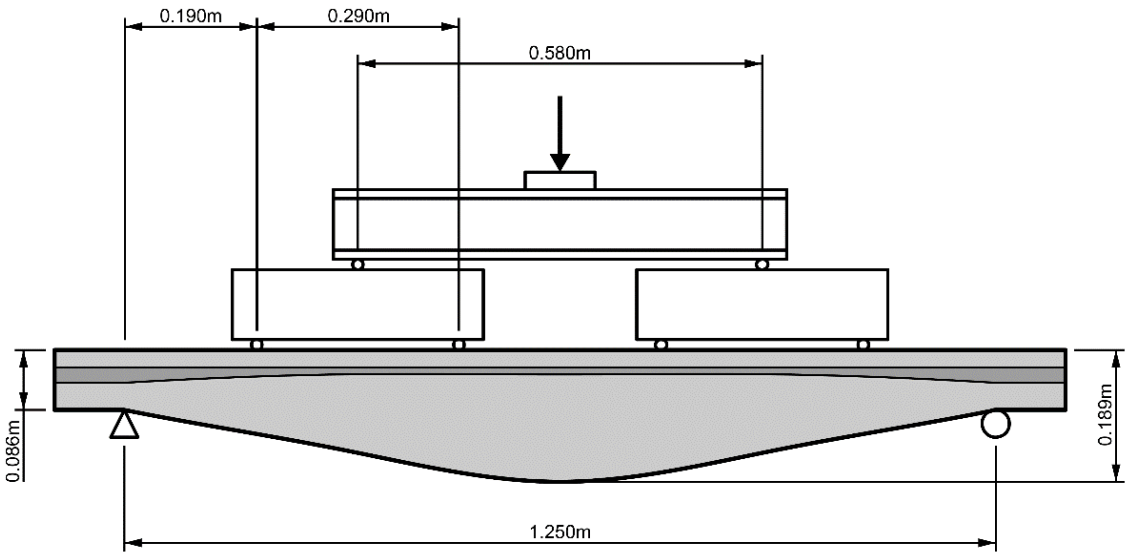

Figure 69 Setup for load testing with four points of concentrated loading

The slab mid-span deflections are collected using a linear variable differential transformer (LVDT) mounted to measure deflections from the slab's supports and disregard deflections of the testing machinery. An image of the testing setup is shown in Figure 70 below.

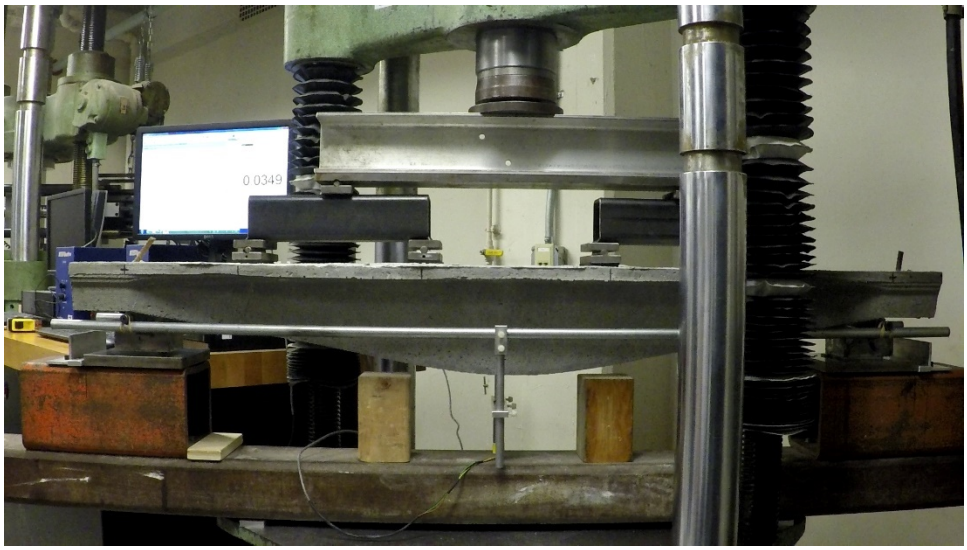

Figure 70 Fixture for load testing slabs, LVDT is mounted below beam for deflection measurements

6.8. Results and Discussion

This strategy results in an EE reduction of 55-70 percent in the design of a shaped slab. The result varies depending on the span, loading conditions, and bounds placed on the optimization procedure. This saving

is accomplished through the constrained optimization of a shaped concrete slab, designed to minimize the embodied energy while meeting constraints of ductility, flexural resistance, shear resistance, flange thickness, flange width, and clear cover.

Three slabs were cast and tested, two built with CNC milled forms and one with bent plywood, each with their own concrete mix. The mix design is adjusted after the first mix to increase workability without reducing the strength of the mix. This is accomplished by increasing the cement paste/aggregate ratio while keeping the water/cement ratio (w/c) consistent, as shown in Table 10.

Table 10 Mix designs for each slab

Material	Slab 1	Slab 2	Slab 3
Cement (kg)	26.6	30.9	25.2
Sand (kg)	102.7	96.1	104.1
Water (kg)	14.4	16.7	14.4
Plasticizer (ml)	890.0	620.0	21.5
1.5% sand (kg)	1.5	1.4	1.6
Total (kg)	145.3	145.2	145.3
w/c	0.54	0.54	0.57
paste/aggregate	0.40	0.50	0.38

As a result of the varied mixes, six cylinders are cast and tested to determine the concrete strength for each prototype slab. The results of the cylinder tests are summarized in Table 11.

Table 11 Uniaxial compression test results for each slab

Cylinder	Mix 1 Stress (MPa)	Mix 2 Stress (MPa)	Mix 2 Stress (MPa)
1	22.8	36.2	17.1
2	22.3	36.9	18.0
3	19.5	35.7	N/A
Average	**21.6**	**36.3**	**17.5**

Additionally, the slabs are weighed to identify how much concrete is added when simplifying the flange thickness to a single dimension in the bent wood formwork of Slab 3. These weights and percent differences are summarized in the table below.

Table 12 Weight and % difference for prototype slabs

Slab	Construction	Weight (kgs)	%Weight change
1	CNC Foam	43.8	0%
2	CNC Foam	43.8	0%
3	Bent Wood	54.0	23%

The results of the cylinder tests shown in Table 11 show that the two mixes result in substantially different strengths. The mix used for Slab 1 is 28 percent weaker than the design strength of 30MPa, the mix for Slab 2 is 21 percent stronger, and the mix for Slab 3 is over 40 percent weaker. This may explain the subsequent difference in performance shown in Figure 71, where Slab 1 fails at a load of 23.3kN, Slab 2 fails at a load of 30.1kN, and Slab 3 fails at 25.3kN.

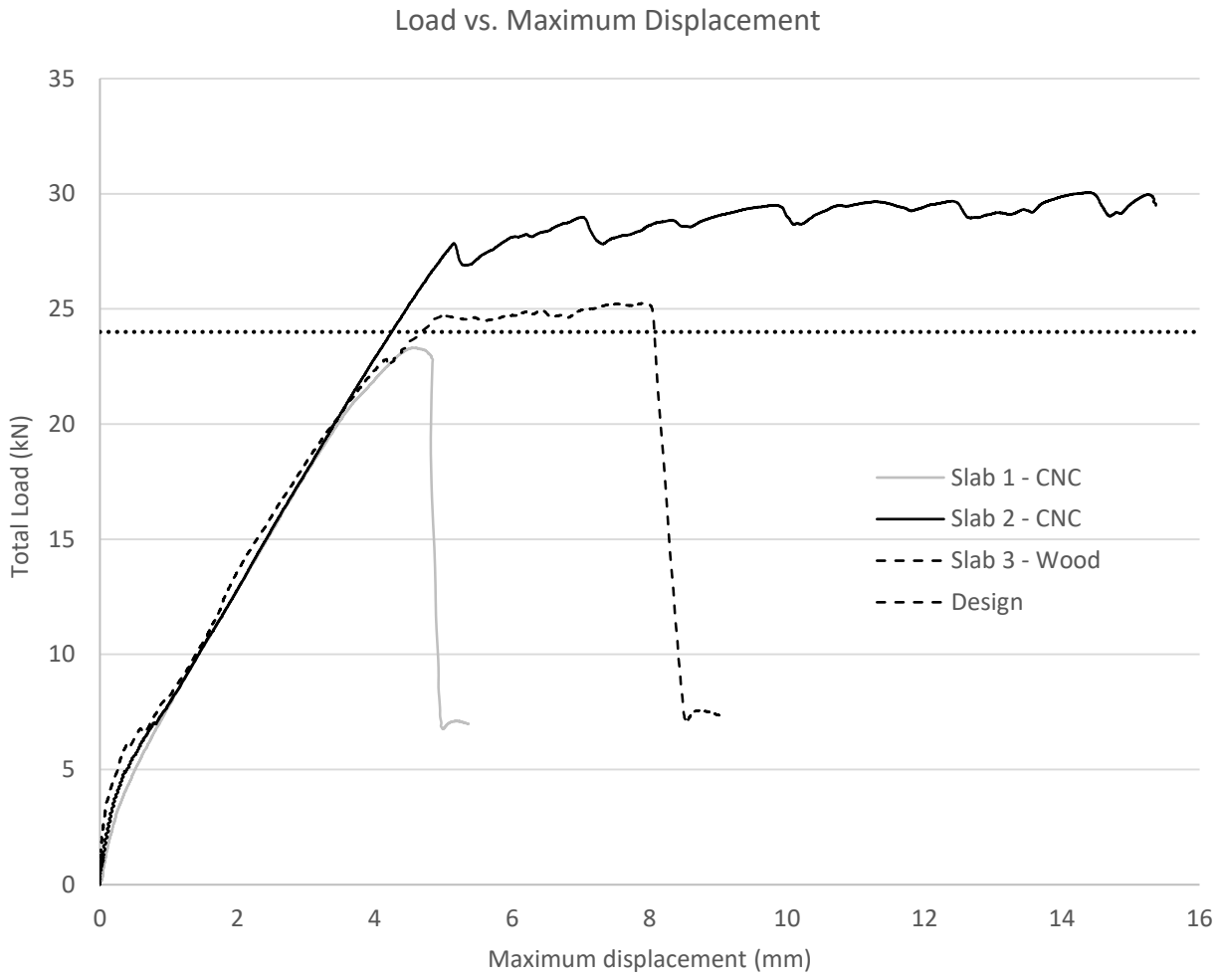

Figure 71 Test results of optimized slabs undergoing four concentrated point loads

Slab 1 is three percent weaker than the design strength of 24kN, failing in a sudden brittle manner due to a shear crack going through the support. Slab 2 reaches an ultimate strength 25 percent stronger than the design load, and fails in a desirable ductile manner (see Figure 72). Slab 3, despite the far weaker mix design, surpasses the design load by 5 percent. This may be due to the additional material in the simplified flange These results suggest that this strategy can provide substantial material reductions, but it is sensitive to errors in mix design and fabrication. Although these results are promising, further tests are required to verify them further.

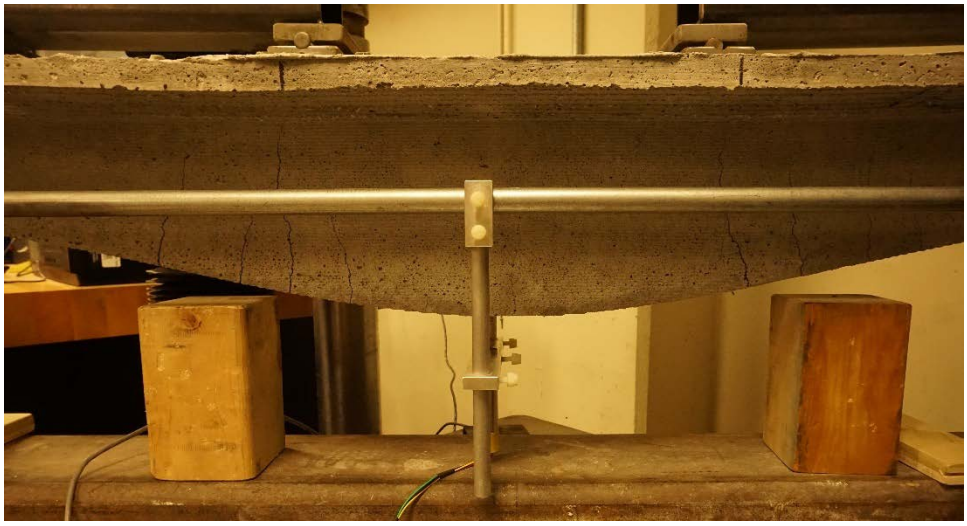

Figure 72 Close up of Slab 2 after loading shows flexural cracks near midspan

6.9. Full-scale prototype

A 5m prototype was built with local partners in New Delhi to test the viability of this strategy at full-scale. Working with the Society for Technology and Action for Rural Advancement (TARA), the fabrication and testing took place in New Delhi. This experiment also explored the market feasibility of the technology for presentation to potential stakeholders in India. The result of this exploration is a 5m x 1m shaped slab designed with a 47 percent reduction in embodied energy, 30 percent reduction in concrete, and 68 percent reduction in longitudinal steel when compared to a flat slab of similar dimensions. The slab is designed to carry a uniform floor load of 200 kg/m^2 and its own dead load as discussed in Section 6.2.1.

6.9.1. Design and fabrication

At the start of this process, the design shown in Figure 73 was presented to the local partner. The design has an embodied energy reduction of 60 percent and required 50 percent less concrete and 75 percent less steel than an equivalent flat slab.

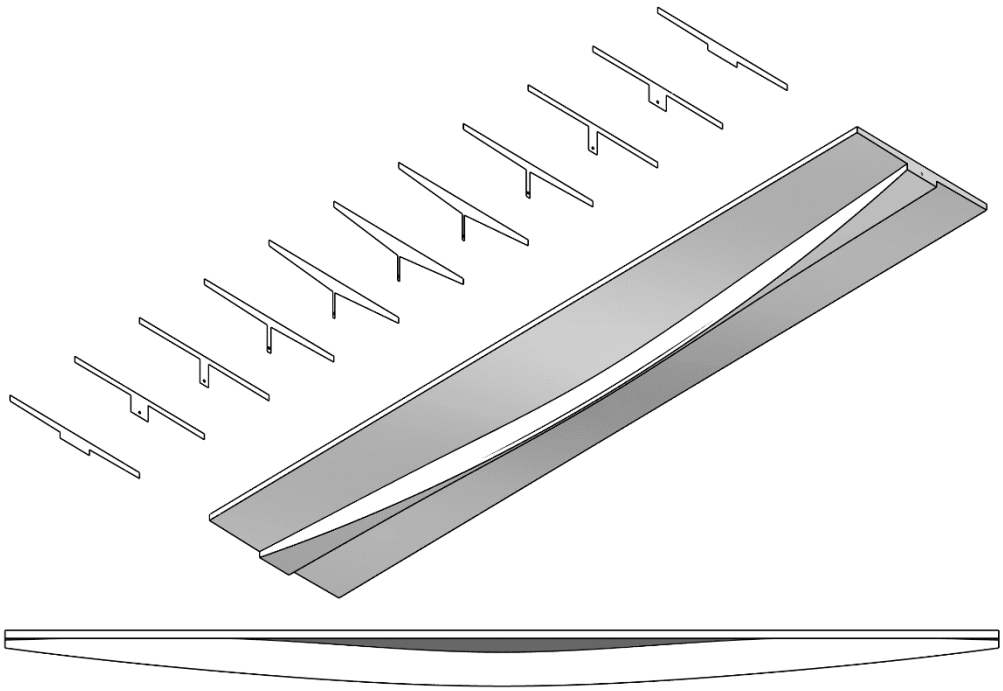

Figure 73 Original design of 5m x 1m slab for fabrication and testing in India

The expectation was that the slab would be built using CNC-milled extruded polystyrene foam, using subtractive manufacturing to build a doubly-curved geometry. However, the local engineers could not find foam blocks in the required quantity and proposed using CNC-milled steel blocks several centimeters thick. As this would have resulted in an impractical excess of weight, waste, embodied carbon, and cost it was decided that an alternative design would be necessary. The partners had extensive experience with sheet metal and welding, so the design algorithm was adjusted for single-curved surfaces that could be built from laser-cut sheet metal (see Figure 74). This was done remotely and accomplished relatively quickly, providing the local partners with a new design within two hours.

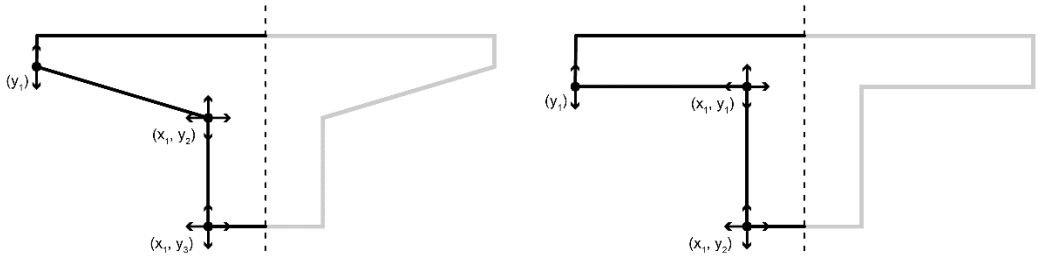

Figure 74 Degrees of freedom resulting in a) doubly curved geometry or b) singly curved surfaces

The local engineers were also uncomfortable with how thin the flange was getting, so the slab was redesigned with a minimum flange thickness of 6cm to ease their concerns. This added approximately 10 percent more concrete to the original optimized design, highlighting the impact of the flange thickness on the material efficiency of the slab. The updated design has an embodied energy reduction of 47 percent and uses 30 percent less concrete and 68 percent less steel than an equivalent flat slab. The final design provided for fabrication is shown in Figure 75 below.

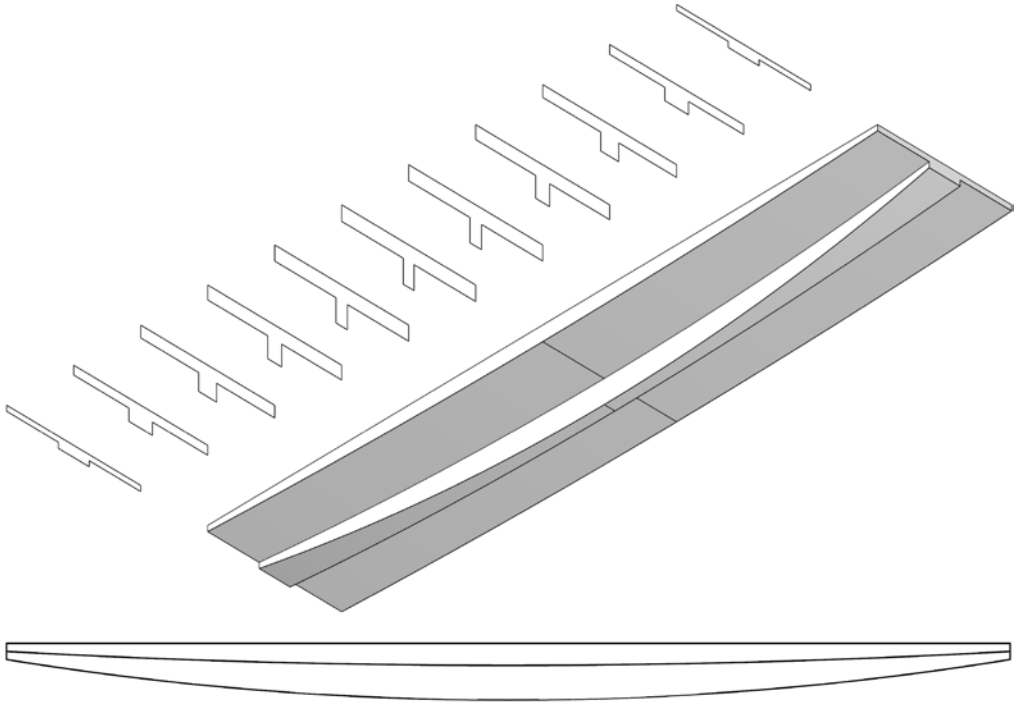

Figure 75 Updated design of 5m x 1m slab for sheet metal mold

The slab was fabricated using a sheet metal mold, assembled from laser-cut 3mm steel, and built for simple disassembly for future use (see Figure 76). The design of the mold was carried out by the local partner and their in-house engineers. The slab was reinforced with a 16mm bar for tensile reinforcement, 6mm steel bars for shear reinforcement, and a mesh of 6mm bars to reinforce the flange (see Figure 76 through Figure 82). As of this writing the slab has been cast and cured and it will be load tested in a Delhi-based testing lab to assess its structural capacity and behavior during failure.

Figure 76 Half of curved sheet metal formwork for full-scale prototype

Figure 77 Close up of sheet metal formwork showing manually welded joints

Figure 78 Partnering engineer overseeing fabrication of sheet metal form

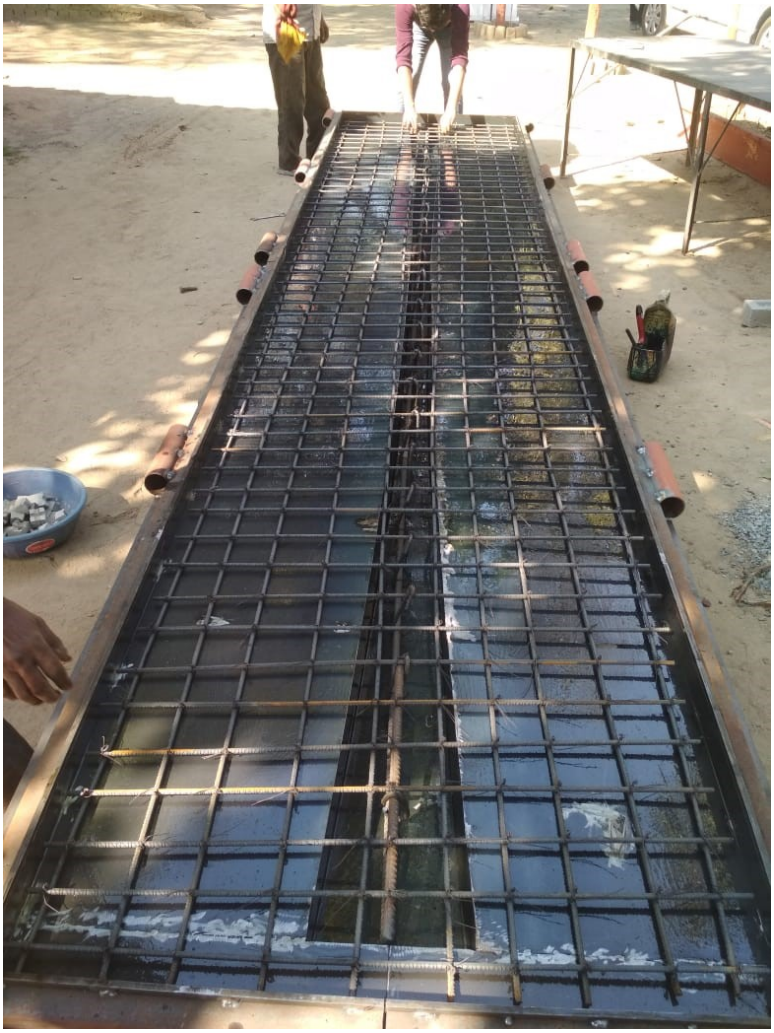

Figure 79 Rebar placement within prototype mold

Figure 80 Concrete casting and finishing

Figure 81 Demolded slab with parts of reusable formwork lying beside it

Figure 82 Cured shaped slab prepared for load testing

6.9.2. Cost assessment

This prototype provides valuable insight into the cost and obstacles to building a shaped slab within the Indian context. A table detailing the costs of the slab construction is shown below.

Table 13 Cost breakdown of full-scale slab fabrication

M40 Grade of Concrete

Raw Materials (RM)	Quantity (In kg)	Rate (INR/kg)	Total RM cost (INR)	% of total cost
Sand	376	1.28	480.65	
Aggregate (10mm)	394	1.35	532.42	
OPC 43 Grade	277	6.5	1800.8	
Water	116	0.2	23.265	
Total Quantity	**1163**	**Total Cost**	**2837.1**	**29%**

Steel

Raw Materials (RM)	Quantity (In kg)	Rate (INR/kg)	Total RM cost (INR)	% of total cost
16mm steel	48	48.3	2318.4	
6mm steel	30	50.5	1515	
Winding wire	2	65	130	
Total Quantity	**80**	**Total Cost**	**3963.4**	**40%**

Labor

Raw Materials (RM)	Quantity (In kg)	Rate (INR/kg)	Total RM cost (INR)	% of total cost
Steel rod cutting and bending	1 master-craftsman	700 per master-craftsman	1200	
	1 helper	500 per helper		
Concrete casting	1 expert mason	800 per expert mason	1800	
	2 helpers	500 per helper		
Total			**3000**	**31%**
Grand Total (In Rs.)			**9800.5**	

This table details the costs of a one-off prototype, suggesting that further savings could be made if this were carried out on a larger scale. For instance, the local partners suggest that labor costs, which currently constitute 31 percent of the slab's cost, would further decrease with large-scale manufacturing of steel elements and mechanized concrete mixing. Additionally, the steel makes up 40 percent of the cost, but this could go down through careful design of the shear and flange reinforcement. As it stands, the slab's flange and web are over-reinforced due to fabrication oversight.

CHAPTER 7 CONCLUSION

The three strategies each present varied methods in the design of material efficient horizontal spanning concrete elements. Strategy 1 uses a method similar to the uniform-strength beam designs of early mechanics, designing for flexural demand and then reinforcing against shear forces. Strategy 2 uses a combination of shape optimization and ULS beam design to remove material between the tensile steel and compression frame, ultimately designing a Vierendeel truss-like beam. Strategy 3 uses a constrained optimization that expands upon Strategy 1 by simultaneously manipulating multiple dimensions of a slab while checking the slab against numerous structural constraints. As discussed in the following sections, these strategies each rely on a combination of manual labor and digital fabrication and provide different levels of material efficiency.

7.1. Results and discussion

New and emerging methods of fabrication enable designers to realize increasingly complex designs and processes. Subsequently, digital fabrication provides a pathway to constructing and testing the oft-complex results of structural optimization. Working between the vast opportunities of digital fabrication and the bounds of scalable construction in India, all three strategies use digital fabrication to realize their final results. Nonetheless, the complexity of fabrication ranges in each strategy and call for varying levels of skill.

Strategy 1, the variable-width beam, uses the simplest form of digital fabrication in the mold construction. An insert is placed in an otherwise regular prismatic form, showing how material efficiency can be achieved through relatively simple means. This strategy uses an insert made of CNC-milled extruded polystyrene foam, but this could be replaced by materials like plywood, thermo-formed plastic, and sheet metal. The design of the steel reinforcement presents another opportunity for material efficiency through digital

fabrication. As mentioned before, sufficient transverse reinforcement is key in enabling a ductile failure for a variable-width beam. Typically, to simplify construction, designers will choose one size and spacing of transverse reinforcement that satisfies the most extreme shear requirement. This is over-structured and calls for more steel than necessary. This strategy presents two methods—CNC-bent wire and rebar or CNC-waterjet plate steel—that overcome this limitation and allow for a more minute control of the volume of reinforcing steel in a variable-width beam. When scaled up to residential construction, these methods could make shaped structures increasingly viable and competitive in material constrained markets.

Strategy 2, the cavity beam, uses CNC-milled foam as the primary formwork to hold the plastic bottles in place for casting. Additional exploration may result in alternative methods for fabrication, including a way to suspend the bottles in the desired locations and rotations without restricting the width of the beams to the width of the bottles. CNC-bent reinforcement could also pair well with this method, potentially designing supports for the bottles within the reinforcing cage, reinforcing against the shear forces that were neglected in the original tests.

Strategy 3, the shaped slab, utilizes a similar approach to strategy 1 by placing an insert that could fit within standard slab formwork. This strategy uses CNC-milled foam, but it could also be done by approximating the geometry in bent steel plates or thin sheets of wood. As demonstrated, the design methodology can be adjusted to utilize only singly-curved surfaces resulting in a form that can be built from elastically bent materials. This would be more time and material efficient than common methods of subtractive manufacturing. The steel reinforcement for a shaped slab presents unique challenges that have been explored in previous literature [39], [46] and studied briefly in this thesis. In this strategy, the longitudinal reinforcement is bent using an industry standard automated rebar bender, but further research could include the use of industrial-scale CNC rebar bending for more precise profiles and increased design freedom.

With each strategy, the goal is the reduction of material consumption in meeting a structural demand. As discussed in Chapter 1, material efficiency can be quantified by mass reduction, cost reduction, embodied energy reduction, and more depending on the priority of the designer. For this thesis, material efficiency is first looked at through concrete and mass reduction, and then extended to include steel reduction in the optimization of embodied energy. Each of the strategies achieve various levels of material efficiency (see Figure 83), and their results are summarized in Table 14.

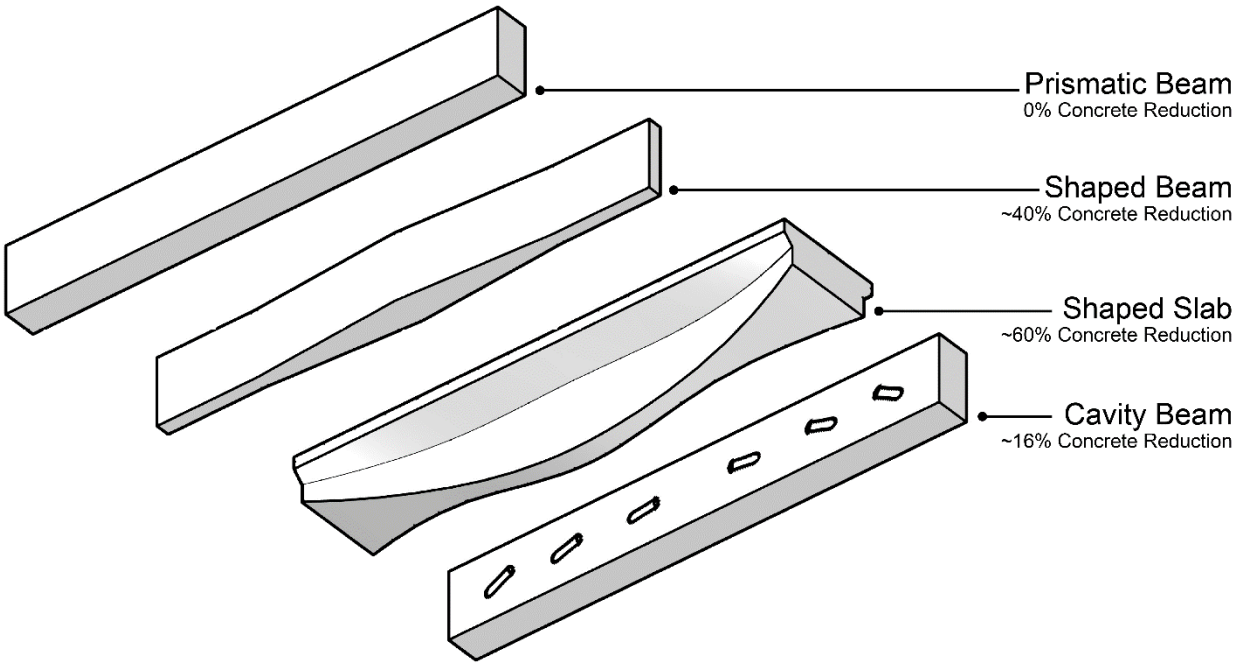

Figure 83 Three strategies for material efficient concrete elements explored in this thesis

Table 14 Summary of stategies and material reductions

Strategy	% concrete reduction	% steel reduction	% EE reduction
1 | Variable-width beam	40	0	34
2 | Cavity Beam	16	0	12
3 | Shaped slab	40-70	0-80	55-70

7.2. Summary of contributions

This thesis presents three strategies for the design of material efficient horizontal spanning concrete elements for residential construction in India. The strategies all follow a methodology of computational structural design, digital fabrication, and structural load testing to verify their feasibility for use in construction. The thesis references historic approaches to the design of efficient concrete structures while applying digital structural design and fabrication methods that reconcile them with modern-day construction practices.

Historic practices in material efficient concrete construction were often reserved for exclusive and significant architectural projects. They often relied upon non-rigorous rules-of-thumb, physical testing experience, or simplified models of concrete mechanics. Today, the advent of computational optimization

and digital fabrication allows designers to push those practices further with increased precision and fabrication potential. This thesis applies this new-found design and fabrication freedom to the wide-spread problems of housing insecurity in Indian cities.

This thesis also applies an understanding of concrete mechanics to existing methods of structural optimization. As discussed in Chapter 2, structural optimization is a long-existing practice but it historically neglects the material complexity of materials like reinforced concrete. Recent attempts to utilize structural optimization in the design of efficient concrete elements either idealize it through the use of fiber reinforcing and non-standard mix designs or by designing them as largely compressive structures. While viable to some contexts, these approaches are not yet realistic in India's urban construction context. Thus, this thesis presents a pragmatic and promising methodology to the optimization of concrete horizontal spanning elements.

At the building scale, structural elements typically account for 50 percent of the mass and embodied energy. As a building exceeds 10 stories, the horizontal spanning elements can account for over 80 percent of the structure's mass and embodied energy [21]. By removing 60 percent of the mass of horizontal spanning elements, as this thesis proposes, the structural weight can be reduced by nearly 50 percent. This does not include the secondary effects of reducing the dead load on vertical elements, which in turn decreases the demand on building foundations. Additionally, lateral loads like seismic activity can be reduced proportional to a reduction in the weight of a building's mass.

Not only can these practices curb the ecological costs of concrete in India, they can also help curb the ecological costs of concrete worldwide. Cement is the source of up to 8 percent of global carbon emissions and, as concrete remains the most widely produced and used construction material in the world, there is a strong desire to reduce the ecological impact of concrete construction. If the Paris agreement on climate change is to be met, countries need to reduce their cement-related emissions by 16 percent in 2030 [61]. This thesis proffers that structural design and digital fabrication may help meet this goal.

7.3. Limitations and future work

The scope of this thesis was the design of one-way horizontal span reinforced concrete elements built for the modular spans of Indian residential construction. The elements were designed for simply-supported boundary conditions and static residential loads, considering flexural and shear stresses. Additionally, the third strategy considers the impact of fabrication upon the design process, giving flexibility to designers to

adjust the optimization method to suit their fabrication limits and opportunities. That being said, there are a number of ways this research could expand with future work.

Further analysis and subsequent design improvements can be made for dynamic loading conditions like seismic activity. The scope can also be expanded to include the design and optimization of vertical elements. This would increase the material savings by looking at the entire built structure, from the roof to the foundations. While stiffness is assessed in the load testing results, more work can be done to calculate deflections before testing and to design for stiffness constraints. This is difficult for irregular sections and multi-material systems like reinforced concrete, but numerical methods such as Finite Element Analysis could be used to analyze complex shaped structures for their expected deflections.

As discussed in each strategy, laboratory limitations on prototype scale presents various fabrication and load test restrictions. Nonetheless, their promising results show that further full-scale testing is worth pursuing. Full-scale testing is essential to proving that the strategies are reliable and would demonstrate their viability to stakeholders in India's residential construction.

There is also room for an economic evaluation of these strategies. It is typically difficult to assess the market feasibility of a new technology in construction without long-term commitment and research outside the scope of this thesis. Through further market analysis and exploration with local partners, the strategies can include the costs of complex formwork and guide designers towards economic means of structural efficiency. This can lead to a techno-economic model that considers the capital investment and eventual return on investment for each of the strategies.

Finally, factors beyond structural behavior can be considered in the design of concrete horizontal elements. Future work can look into the implementation of thermal transmissivity, thermal insulation, mechanical systems, daylighting, and more with the structural design of concrete floor and roof elements. Often in practice the sizing of structural elements in residential construction can be controlled by non-structural factors such as acoustic transmission and fire resistance. The methodology of this thesis can be expanded to consider these factors through performative shaping or the addition of lightweight materials that provide better performance. This work can dissuade designers from relying on "more" concrete to deal with all of these issues and promote a more informed and nuanced use of material.

7.4. Concluding remarks

There is an immense demand for housing in India's cities, and Indian builders need to build efficiently and quickly to meet this demand. The majority of new housing construction in India's cities will be built from concrete and, as material costs contribute to the bulk of construction costs, new practices are needed for material efficient concrete structures. Furthermore, these concerns are echoed in cities worldwide in rapidly urbanizing LEDCs. The strategies presented in this thesis show that structural optimization and digital fabrication can help in the construction of affordable housing and low-carbon concrete construction. This thesis proposes that efficient structural elements, appropriately designed for the context and local construction practices, could and should be used anywhere a flat concrete slab would be used. If scaled up to mass-produced residential construction, these strategies can enrich the architectural design process and abate the economic and environmental costs of construction.

APPENDICES

APPENDIX A | STRATEGY 1 SCRIPT

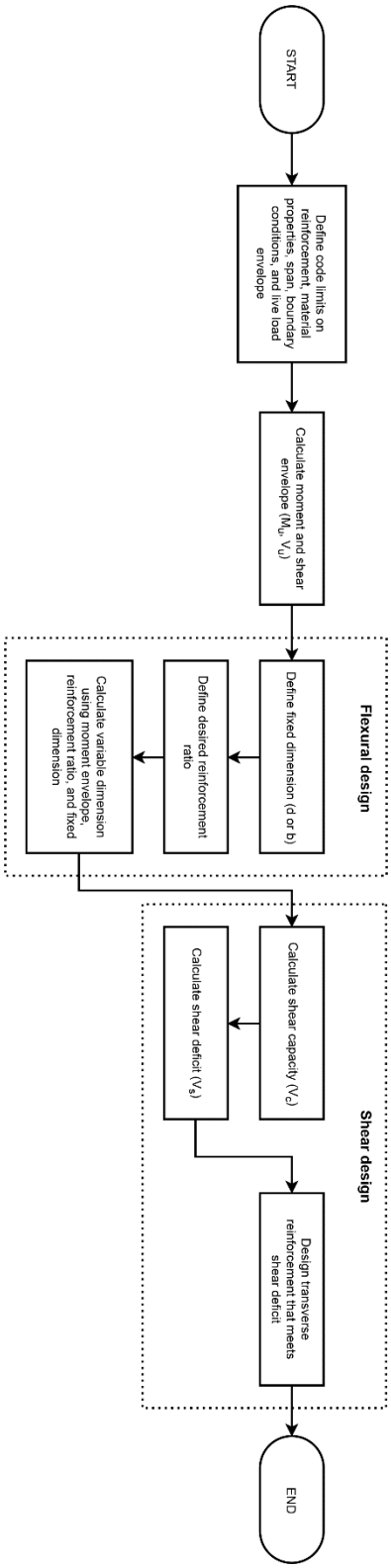

APPENDIX B | STRATEGY 2 SCRIPT

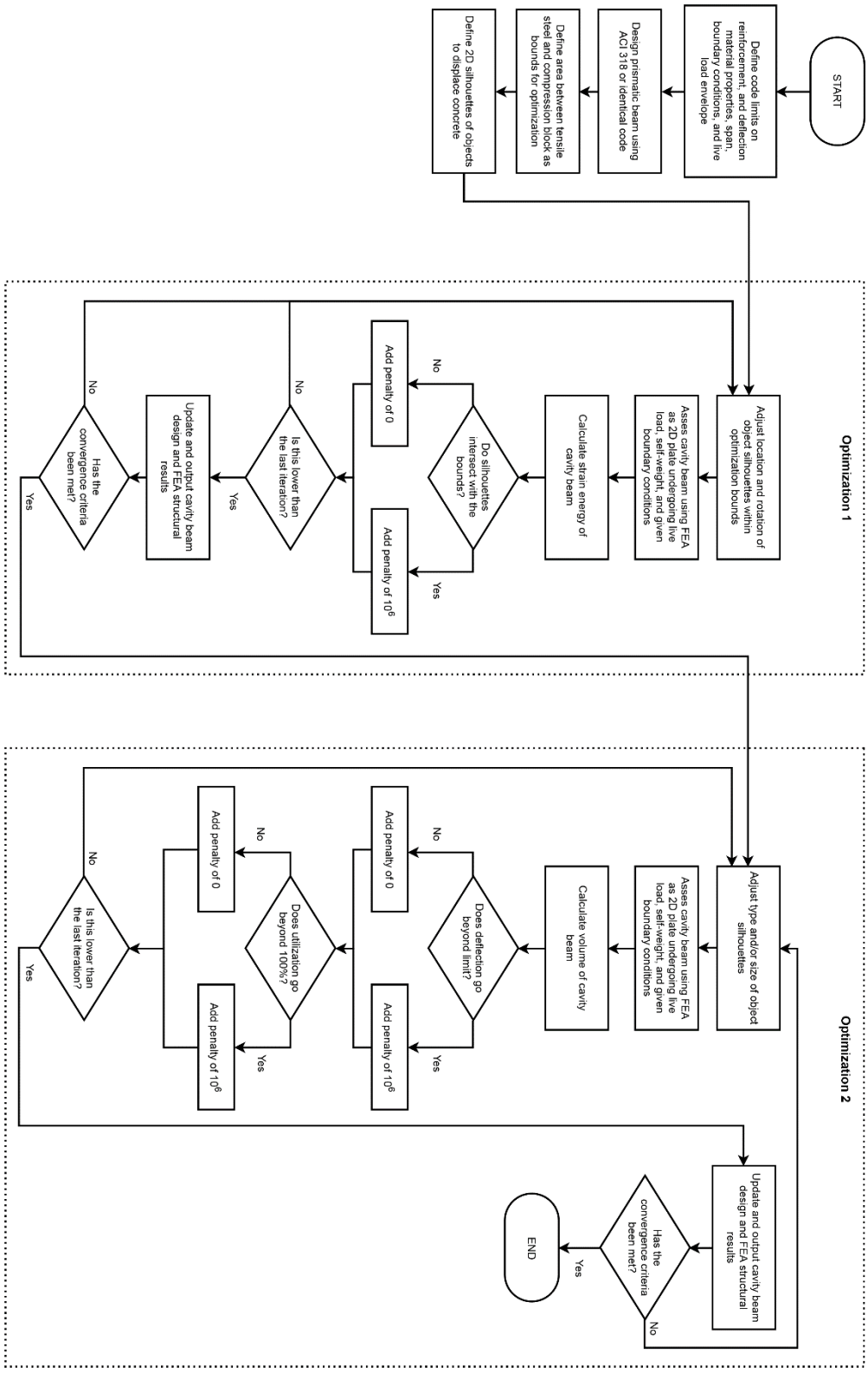

APPENDIX C | STRATEGY 3 SCRIPT

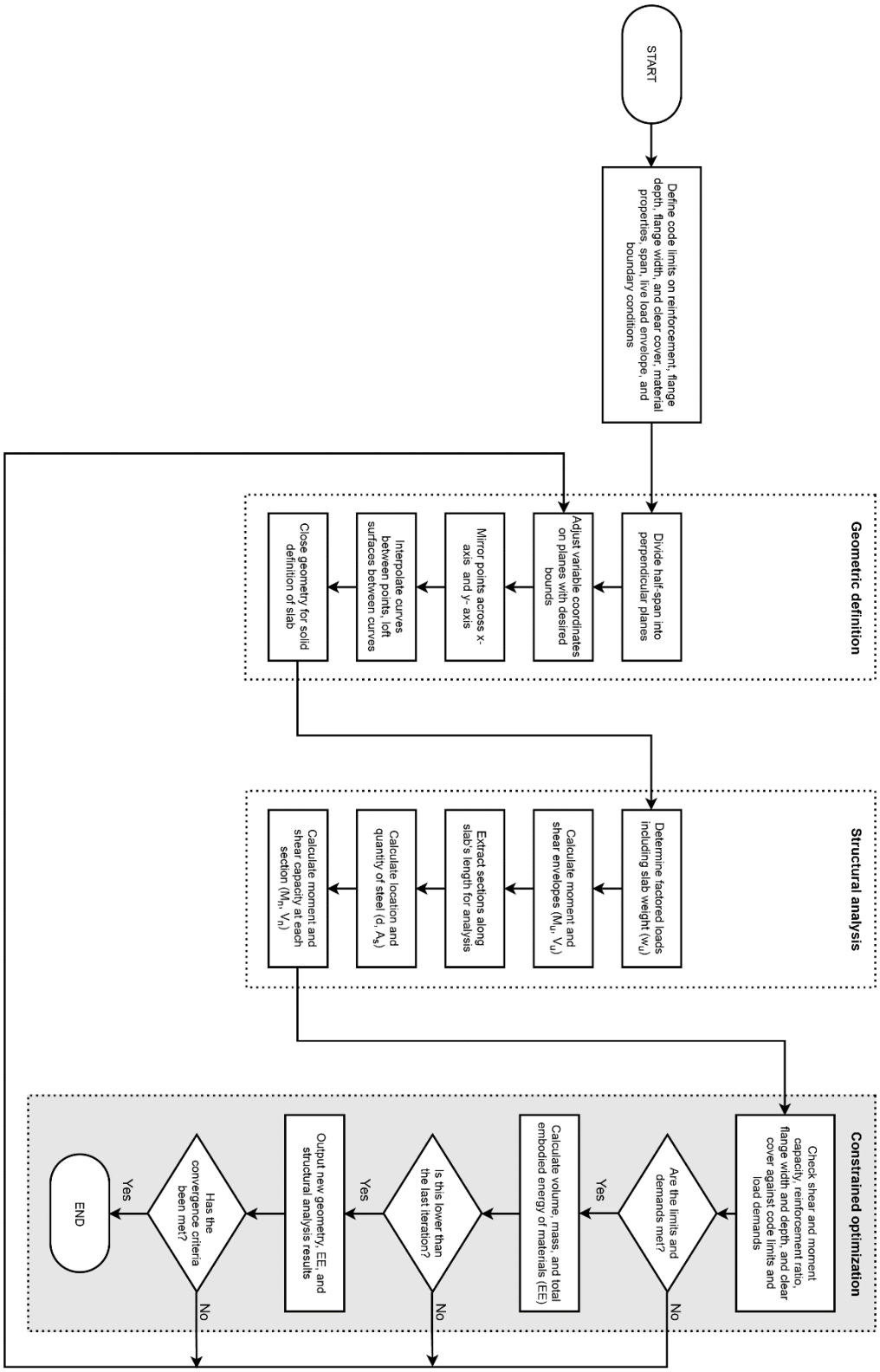

APPENDIX D | OPTIMIZATION TEST RESULTS

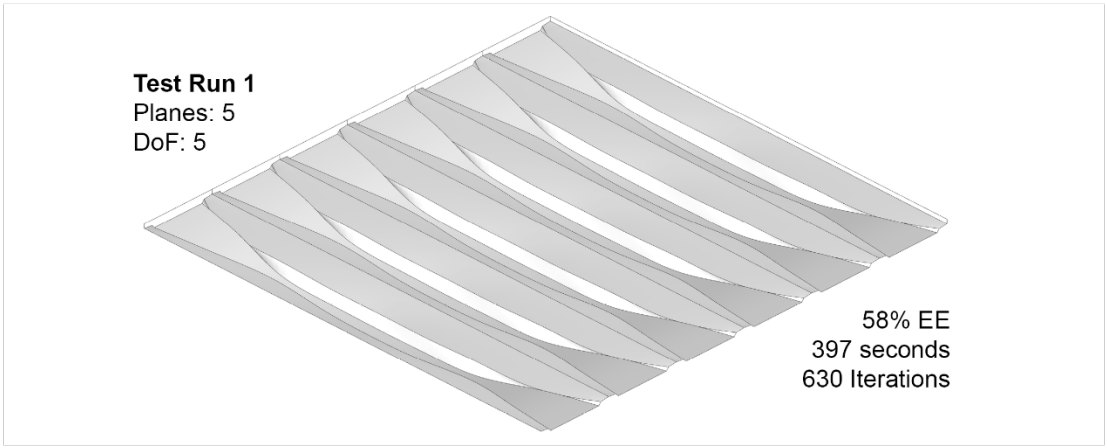

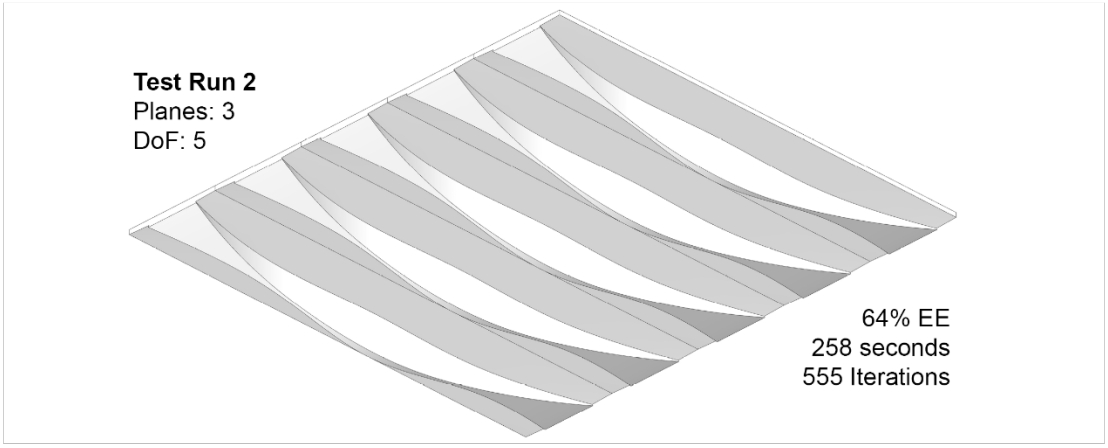

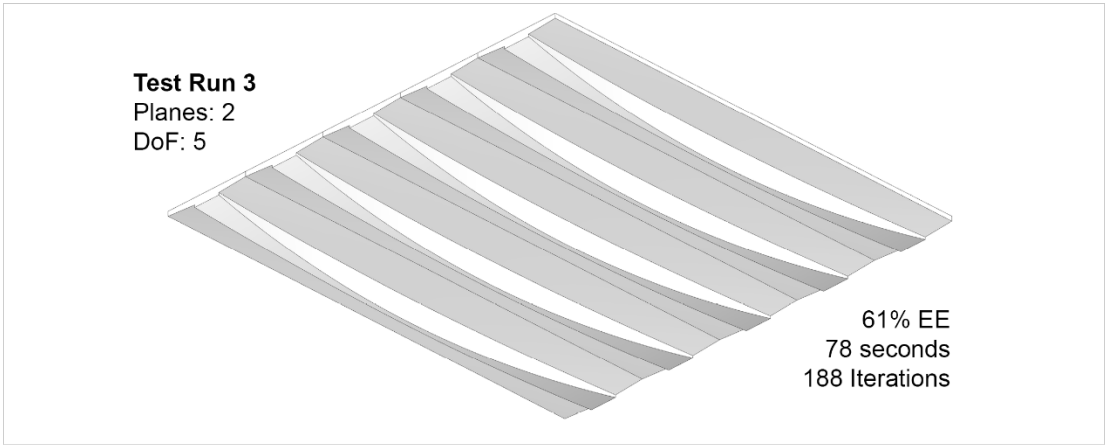


Test Run 4
Planes: 5
DoF: 4
63% EE
284 seconds
525 Iterations

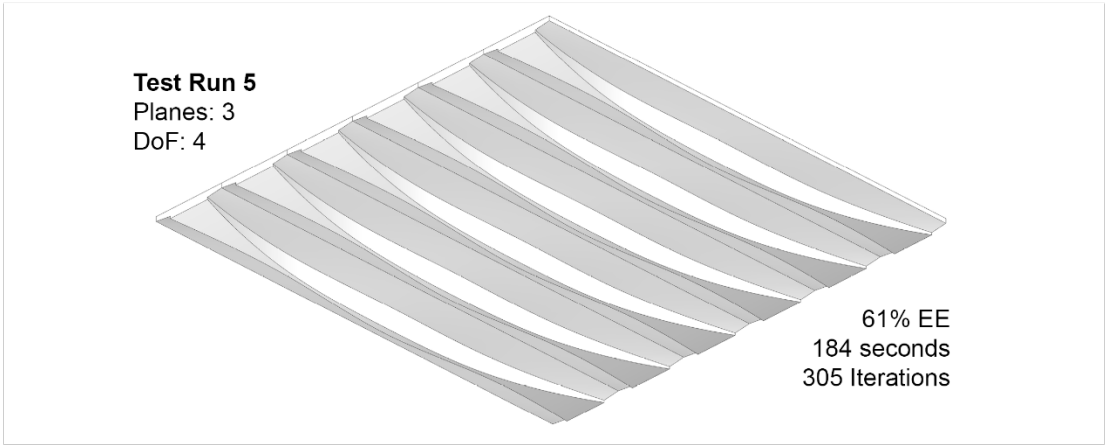
Test Run 5
Planes: 3
DoF: 4
61% EE
184 seconds
305 Iterations

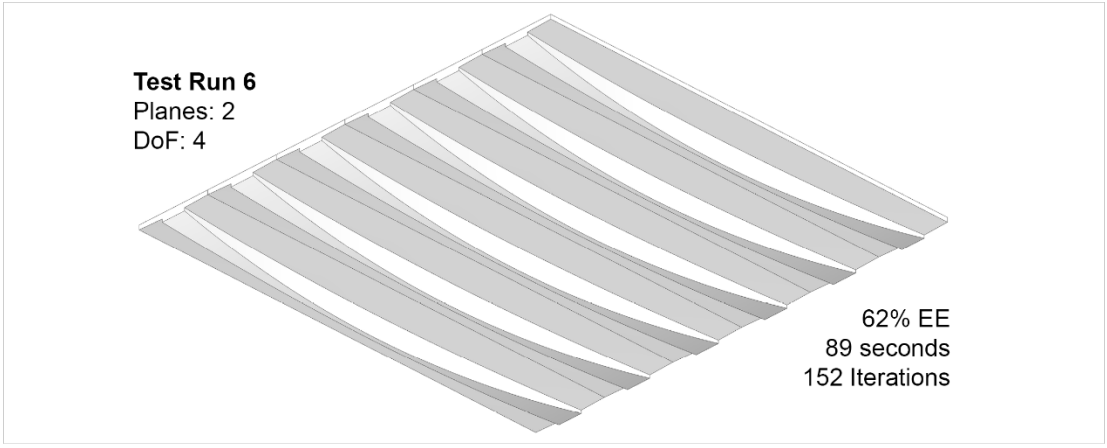
Test Run 6
Planes: 2
DoF: 4
62% EE
89 seconds
152 Iterations

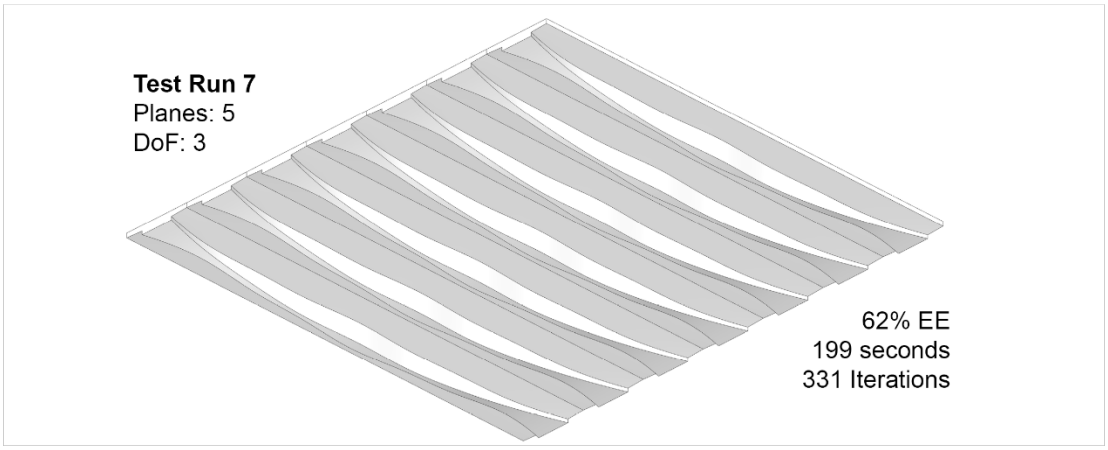
Test Run 7
Planes: 5
DoF: 3
62% EE
199 seconds
331 Iterations

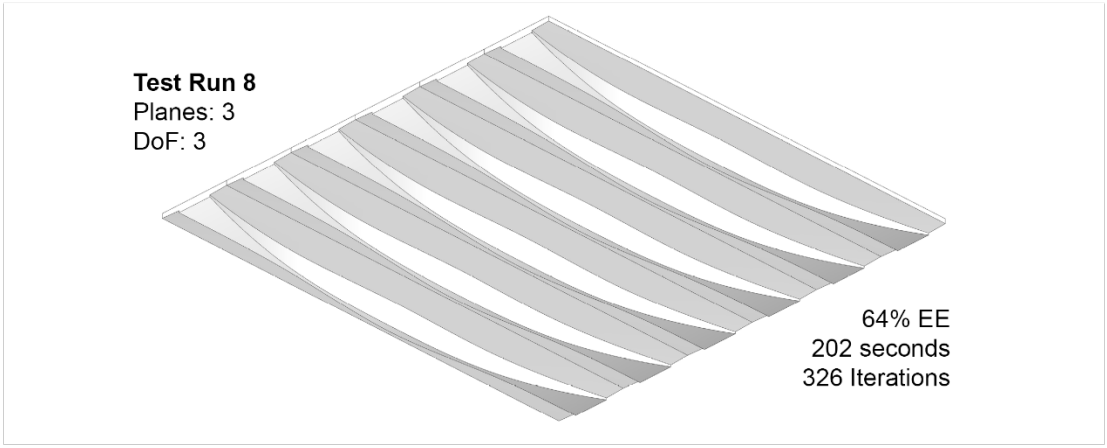
Test Run 8
Planes: 3
DoF: 3
64% EE
202 seconds
326 Iterations

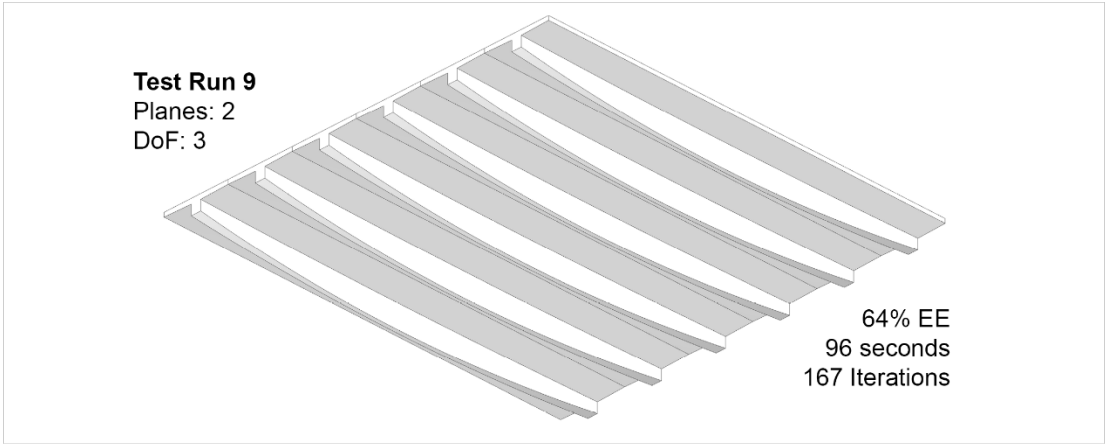
Test Run 9
Planes: 2
DoF: 3
64% EE
96 seconds
167 Iterations

APPENDIX E | FABRICATION IMAGES

Figure 84 Fabrication of plywood box for cavity beam

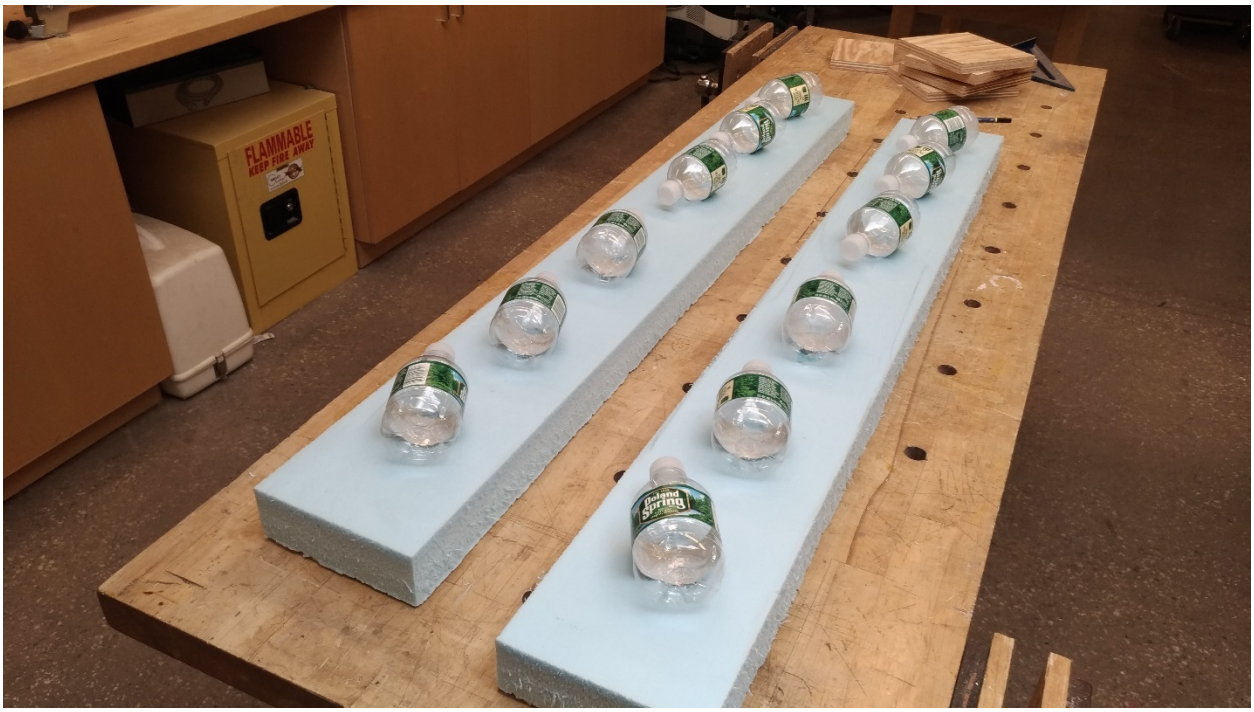

Figure 85 Bottles secured to CNC milled foam formwork

Figure 86 Casting of cavity beams

Figure 87 Comparison between cavity beam and prismatic control beam

Figure 88 Three-point load test of cavity beam

Figure 89 Cavity beam after load testing showing shear failure mode

Figure 90 Close up photo of reinforcing cage for CNC bent wire reinforcement

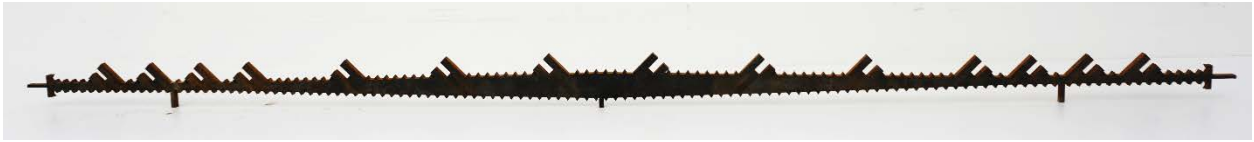

Figure 91 Individual elements of CNC waterjet steel plate reinforcement

Figure 92 Close up view of CNC waterjet plate reinforcement, connection between transverse and longitudinal steel

Figure 93 CNC milled foam and plywood boxes for shaped beams

Figure 94 Casting of shaped beam, checking concrete cover on vibrating table

Figure 95 Resultant shaped beams and prismatic control beam

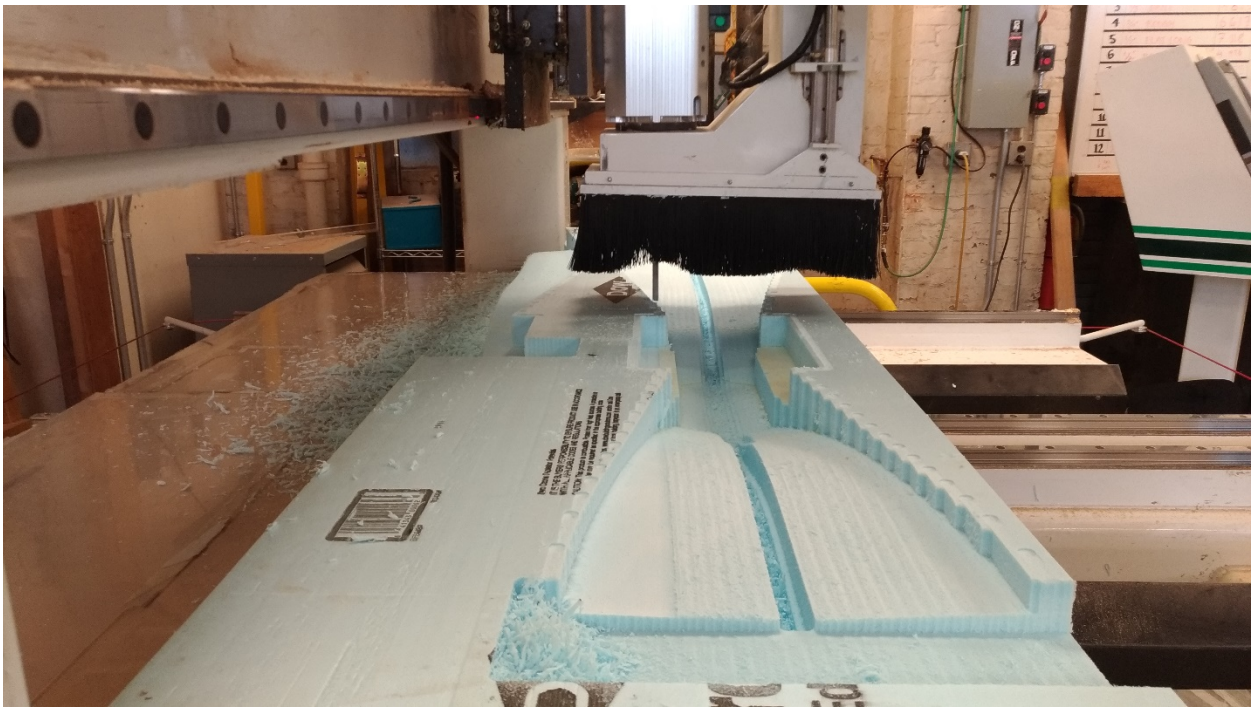

Figure 96 CNC milling of shaped slab foam formwork

Figure 97 CNC milled foam, plywood box, and steel reinforcement of shaped slab prototype

Figure 98 Bent wood and steel reinforcement for shaped slab prototype

Figure 99 Resultant prototype slabs cast using CNC milled foam, hanging fabric, and bent plywood

Figure 100 Close up of CNC milled foam formed shaped slabs

Figure 101 Close up of bent wood formed shaped slabs

APPENDIX F | CONSTRUCTION PRACTICE

Figure 102 Imported formwork for flat-slab construction, courtesy of Larsen & Toubro

Figure 103 Assembled formwork for flat concrete slab supported by steel poles

Figure 104 Layout of post-tensioning tendons and tensile reinforcement for long-spanning concrete slab

Figure 105 Auto-climbing system used in construction of vertical core

Figure 106 Manual concrete pouring at tower construction site, courtesy of Harsh Vardhan Jain Architects

Figure 107 Construction worker carting ready-mix concrete to pouring location

Figure 108 Residential neighborhood construction, Emerald Hills in New Delhi, courtesy of EMAAR

Figure 109 Cast-in-situ concrete columns and formwork for beams

Figure 110 Formwork for cast-in-situ flat slabs

Figure 111 Hybrid system of concrete beams and kiln-fired brick staircase

APPENDIX G | STATE OF THE ART IN INDIA

Figure 112 Jack arch and precast beam prototype, Roorkee, courtesy of Central Building Research Institute

Figure 113 Hybrid soil block and concrete beams, courtesy of Auroville Earth Institute (AVEI)

Figure 114 Auditorium with 15m-span conical vault, Pondicherry, courtesy of AVEI

Figure 115 Exterior of 15m-span conical vault, Pondicherry, courtesy of AVEI

Figure 116 Semi-circular ferro-cement channels, New Delhi, courtesy of Development Alternatives (DA)

Figure 117 Low concrete domes, courtesy of DA

Figure 118 One-way vault built from interlocking conical blocks, courtesy of Anupama Kundoo Architect

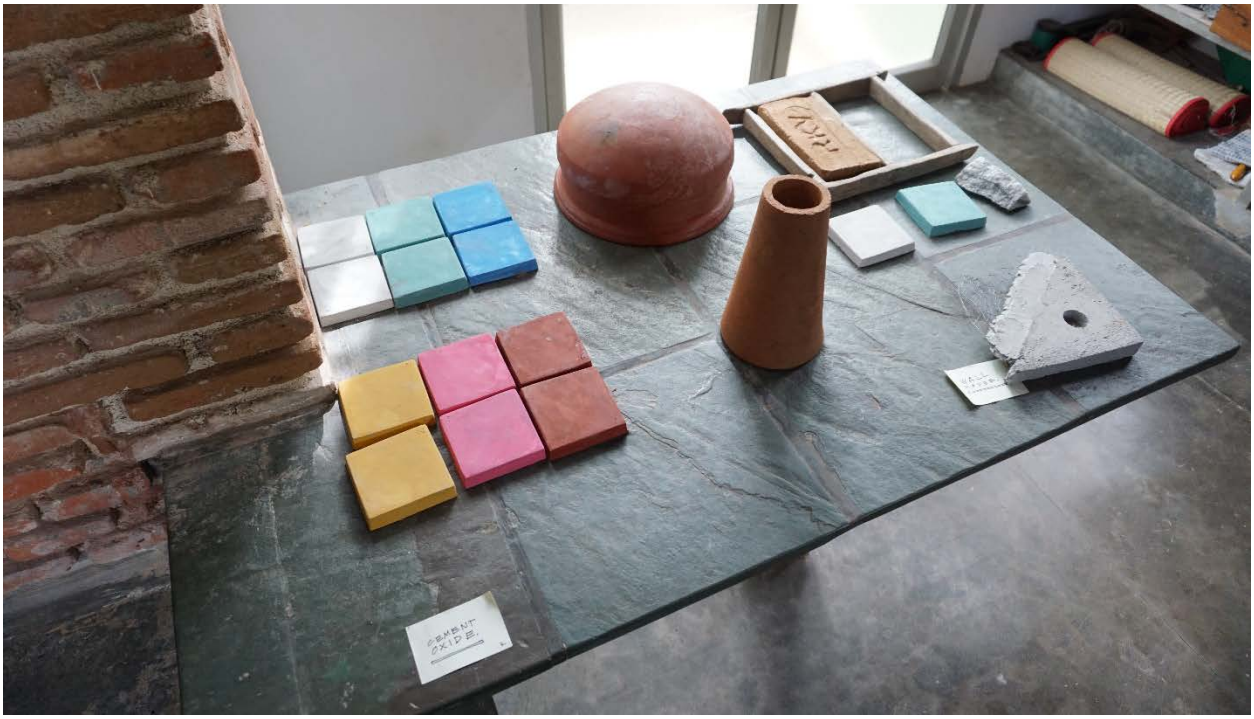

Figure 119 Colored tiles, pots for filler slabs, and conical blocks for vaults, courtesy of Anupama Kundoo Architect

Figure 120 Standard filler slab, courtesy of Indian Institute of Science (IISc)

Figure 121 Jack arch using construction waste and low-carbon concrete, courtesy of IISc

APPENDIX H | HISTORIC CONCRETE STRUCTURES

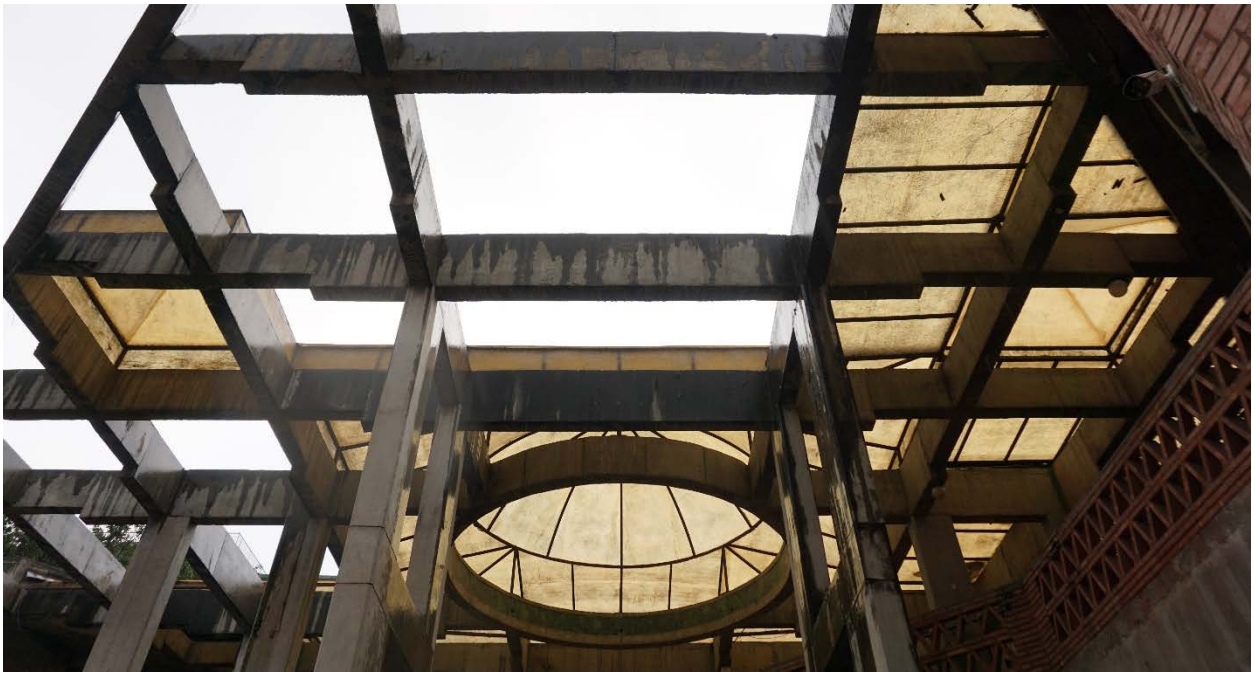

Figure 122 Shaped beams at Indian Habitat Centre by Joseph allen Stein and BV Doshi, New Delhi, 1993

Figure 123 Shaped two-way slab at Sri Ram Centre by Shivnath Prasad and Mahendra Raj, New Delhi, 1969

Figure 124 Suspended floors at State Trading Corporation by Raj Rewal and Mahendra Raj, New Delhi, 1988

Figure 125 Folded plates and beams at Municipal Stadium by Charles Correa and Mahendra Raj, Ahmedabad, 1960

Figure 126 Post tensioned leaning towers of NCDC by Kuldip Singh and Mahendra Raj, New Delhi, 1980

Figure 127 Folded plates and twisted columns of Tagore Hall by BV Doshi and Mahendra Raj, New Delhi, 1965

REFERENCES

[1] E. Koehn and M. Soni, "Prefabrication in Developing Countries: India," in *Creative Systems in Structural and Construction Engineering*, 2001, pp. 57–61.

[2] "India's urbanization: A closer look | McKinsey & Company." [Online]. Available: https://www.mckinsey.com/global-themes/urbanization/indias-urbanization-a-closer-look. [Accessed: 30-Jan-2018].

[3] A. Brown, "Strong growth for Indian construction industry," *KHL*, 18-Mar-2019. [Online]. Available: https://www.khl.com/international-construction/strong-growth-for-indian-construction-industry/137389.article. [Accessed: 19-Apr-2019].

[4] A. Desai, "Financing Affordable Housing for the Low-Income in Urban India," *Soc. Impact Res. Exp. SIRE*, Jan. 2014.

[5] S. Singh, "Building a house for everyone in India," 22-Mar-2019.

[6] KPMG, "Decoding Housing for all by 2022 | KPMG | IN," 2014. [Online]. Available: https://home.kpmg.com/in/en/home/insights/2014/09/decodinghousing.html. [Accessed: 28-Sep-2017].

[7] F. D. K. Ching, B. Onouye, and D. Zuberbuhler, *Building structures illustrated*, Second edition. Hoboken, New Jersey: Wiley, 2014.

[8] J. J. Salama *et al.*, *Reducing the cost of new housing construction in New York City: 2005 update*. New York: Furman Center for Real Estate and Urban Policy : New York University School of Law : Robert F. Wagner Graduate School of Public Service, 2005.

[9] CIDC, "Planning Commission: 11th Five Year Plan," 2012. [Online]. Available: http://www.cidc.in/new/activities7.html. [Accessed: 16-Oct-2017].

[10] C. E. L. De Wolf, "Low carbon pathways for structural design : embodied life cycle impacts of building structures," Thesis, Massachusetts Institute of Technology, 2017.

[11] T. Abergel, B. Dean, and J. Dulac, "Global Status Report 2017: Towards a zero-emission, efficient, and resilient buildings and construction sector," *U. N. Environ. Programme*, p. 48, 2017.

[12] B. V. Venkatarama Reddy and K. S. Jagadish, "Embodied energy of common and alternative building materials and technologies," *Energy Build.*, vol. 35, no. 2, pp. 129–137, Feb. 2003.

[13] H. Van Damme, "Concrete material science: Past, present, and future innovations," *Cem. Concr. Res.*, vol. 112, pp. 5–24, Oct. 2018.

[14] J. Watts, "Concrete: the most destructive material on Earth," *The Guardian*, 25-Feb-2019.

[15] S. Bardhan, "Embodied energy analysis of multi-storied residential buildings in urban India," in *WIT Transactions on Ecology and the Environment*, 2011, vol. 143, pp. 411–421.

[16] N. Huberman, D. Pearlmutter, E. Gal, and I. A. Meir, "Optimizing structural roof form for life-cycle energy efficiency," *Energy Build.*, vol. 104, no. Supplement C, pp. 336–349, Oct. 2015.

[17] P. Foraboschi, M. Mercanzin, and D. Trabucco, "Sustainable structural design of tall buildings based on embodied energy," *Energy Build.*, vol. 68, no. Part A, pp. 254–269, Jan. 2014.

[18] S. White, *Building in the garden: the architecture of joseph allen stein in india and california.* Other: Oxford Univ Press, 1994.

[19] G. Bhatia and Housing and Urban Development Corporation (India), *Laurie Baker: life, work, writings*. New Delhi; New York: Penguin Books, 1994.

[20] M. Raj, V. Mehta, R. R. Mehndiratta, and A. Huber, Eds., *The structure: works of Mahendra Raj*. Zurich: Park Books, 2016.

[21] P. Block and N. Paulson, “E4: Efficiency, Economy, Elegance, and Ecology,” in *Design - Tales of Science and Innovation*, Chronos Verlag, 2019, pp. 13–21.
[22] M. Bechthold, “On shells and blobs - Structural surfaces in the digital age,” *Harv. Des. Mag.*, vol. 19, 2003.
[23] S. Timoshenko, *History of strength of materials: with a brief account of the history of theory of elasticity and theory of structures*. New York: Dover Publications, 1953.
[24] S. Timoshenko, *Strength of materials*. Malabar, Fla.: Krieger Pub. Co., 1930.
[25] A. Muttoni, *The Art of Structures: Introduction to the Functioning of Structures in Architecture*. EPFL Press, 2011.
[26] I. Opatowski, “Cantilever beams of uniform strength,” *Q. Appl. Math.*, vol. 3, no. 1, pp. 76–81, Apr. 1945.
[27] J. P. Li and W. A. Gross, “Beams of Uniform Strength Subjected to Uniformly Distributed Load,” vol. 62, no. 1, p. 5, 1955.
[28] R. L. Barnett, “Minimum-Weight Design of Beams for Deflection,” *Trans. Am. Soc. Civ. Eng.*, vol. 128, no. 1, pp. 221–255, 1963.
[29] R. T. Haftka, Z. Gürdal, and M. P. Kamat, *Elements of Structural Optimization*. Dordrecht: Springer Netherlands, 1990.
[30] Jr. Haug E. J. and P. G. Kirmser, “Minimum Weight Design of Beams With Inequality Constraints on Stress and Deflection,” *J. Appl. Mech.*, vol. 34, no. 4, pp. 999–1004, Dec. 1967.
[31] A. B. Lall, “Development Alternatives World Headquarters,” 2015. [Online]. Available: https://www.ashokblallarchitects.com/Development-Alternatives-World-Headquarters. [Accessed: 03-May-2019].
[32] A. Frearson, “Anupama Kundoo uses ferrocement to create Lego-like house,” *Dezeen*, 07-Jun-2016. [Online]. Available: https://www.dezeen.com/2016/06/07/anupama-kundoo-full-fill-homes-ferrocement-house-model-arsenale-venice-architecture-biennale-2016/. [Accessed: 28-Jan-2019].
[33] L. K. Davis, M. Varma, and S. Maïni, “Sharanam: Case Study of a 15 Meter Span Earthen Conical Vault,” *Structures*, vol. 18, pp. 10–19, Apr. 2019.
[34] L. K. Davis and S. Maïni, “AVEI School of Earthen Architecture,” presented at the Terra Lyon, 2016, p. 10.
[35] F. Amtsberg, G. Parmann, A. Trummer, and S. Peters, “From Analysis to Production and Back Attempts and Results of Reusable Adaptive Freeform Production Strategies for Double Curved Concrete Construction Elements,” in *Robotic Fabrication in Architecture, Art and Design 2016*, D. Reinhardt, R. Saunders, and J. Burry, Eds. Cham: Springer International Publishing, 2016, pp. 304–315.
[36] D. Veenendaal and P. Block, “Design process for prototype concrete shells using a hybrid cable-net and fabric formwork,” *Eng. Struct.*, vol. 75, pp. 39–50, Sep. 2014.
[37] H. R. Schipper and S. Grünewald, “Efficient material use through smart flexible formwork method,” *ECO-Crete Int. Symp. Environ. Friendly Concr. Reyk. Icel. 13-15 August 2014*, 2014.
[38] M. West, *The Fabric Formwork Book: Methods for Building New Architectural and Structural Forms in Concrete*. Routledge, 2016.
[39] J. J. Orr, A. Darby, T. Ibell, and M. Evernden, “Design methods for flexibly formed concrete beams,” *Proc. Inst. Civ. Eng. - Struct. Build.*, vol. 167, no. 11, pp. 654–666, Nov. 2014.
[40] G. Morrow, “Fabric formwork - Bomnong L´Or Project, Cambodia,” *StructureMode*. .
[41] W. Hawkins, J. Orr, P. Shepherd, T. Ibell, and J. Bregulla, “Thin-shell textile-reinforced concrete floors for sustainable buildings,” 2017.
[42] D. L. López, D. Veenendaal, M. Akbarzadeh, and P. Block, “Prototype of an ultra-thin, concrete vaulted floor system,” in *Proceedings of the IASS-SLTE 2014 Symposium*, 2014.

[43] B. Dillenburger, R. Flatt, Joseph Schwartz, and M. A. Meibodi, “The Smart Slab - 3D-printed formwork for a radical new concrete aesthetic,” *dbt*. .
[44] D. Lowke, E. Dini, A. Perrot, D. Weger, C. Gehlen, and B. Dillenburger, “Particle-bed 3D printing in concrete construction – Possibilities and challenges,” *Cem. Concr. Res.*, vol. 112, pp. 50–65, Oct. 2018.
[45] R. A. Buswell, W. R. Leal de Silva, S. Z. Jones, and J. Dirrenberger, “3D printing using concrete extrusion: A roadmap for research,” *Cem. Concr. Res.*, vol. 112, pp. 37–49, Oct. 2018.
[46] E. Lloret Fritschi, “Smart Dynamic Casting - A digital fabrication method for non-standard concrete structures,” Doctoral Thesis, ETH Zurich, 2016.
[47] A. Forty, *Concrete and culture a material history*. London: Reaktion Books, 2013.
[48] G. Muller, G. I. B. Rankin, and HENNEBIQUE, “THE HENNEBIQUE SYSTEM: A RENAISSANCE?,” *Proc. Inst. Civ. Eng.*, vol. 90, no. 1, pp. 179–187, Feb. 1991.
[49] ACI Committee 318, ACI Committee 318, ACI Committee 318, and American Concrete Institute, *Building code requirements for structural concrete (ACI 318-14): an ACI standard ; Commentary on building code requirements for structural concrete (ACI 318R-14) : an ACI report*. 2016.
[50] J. Schlaich, K. Schafer, and M. Jennewein, “Toward a Consistent Design of Strucutral Concrete,” *PCI J.*, vol. 32, no. 3, pp. 74–150, 1987.
[51] M. D. Kotsovos and M. N. Pavlović, *Ultimate limit-state design of concrete structures: a new approach*. London: Thomas Telford, 1999.
[52] Jorg Schlaich, Kurt Shafer, Mattias Jennewein, and Michael D. Kotsovos, “Toward a Consistent Design of Structural Concrete - Comments,” *PCI J.*, vol. 32, no. 3, pp. 74–150, 1987.
[53] J. J. Orr, T. J. Ibell, A. P. Darby, and M. Evernden, “Shear behaviour of non-prismatic steel reinforced concrete beams,” *Eng. Struct.*, vol. 71, pp. 48–59, Jul. 2014.
[54] P. A. Claisse, *Civil engineering materials*. Amsterdam Boston Heidelberg: Butterworth-Heinemann, an imprint of Elsevier, 2016.
[55] C. Presinger and Bollinger+Grohmann, *Karamba*. .
[56] “Rechenraum e.U. - goat,” 2018. [Online]. Available: https://www.rechenraum.com/en/goat.html. [Accessed: 06-May-2018].
[57] N. Brown, J. Felipe, R. Danhaive, and C. Mueller, *Design Space Exploration*. Digital Structures, 2018.
[58] D. A. Fanella and S. K. Ghosh, Eds., *Simplified design: reinforced concrete buildings of moderate size and height*, 2nd ed. Skokie, Ill: Portland Cement Association, 1993.
[59] M. J. D. Powell, “A view of algorithms for optimization without derivatives,” *Camb. Univ. Tech. Rep. DAMTP*, p. 12, 2007.
[60] A. M. Anderson, “Fabrication and construction Methods for Low-Cost, Low-Carbon Structural Components for Housing in India,” Massachusetts Institute of Technology, 2019.
[61] L. Rodgers, “The massive CO2 emitter you may not know about,” 17-Dec-2018.